Effect of binder on electrochemical performance of Silicon/Graphene anodes for Lithium ion batteries

A Thesis

Presented to the Faculty of the Graduate School

of Cornell University

In Partial Fulfillment of the Requirements for the Degree of

Master of Science

by

Avinash Umasankaran

August 2020

ABSTRACT

The sun is not always shining, and the wind is not always blowing, hence energy storage becomes an essential part of human life. Among the energy storage technologies, batteries are touted to be the front runners, especially Lithium-ion batteries (LIBs) with their existing infrastructure offer solutions to the current barriers in this field. The era of battery powered vehicles has made the need for growth in LIB's even more evident, as more and more vehicles are deployed every year. However, current LIB's lie far behind gasoline powered vehicles owing to their low energy density. Range anxiety has been a major hindrance to the deployment of electric vehicles (EVs). To tackle this issue, researchers have transitioned from traditional graphite anode to different chemistries. Silicon anodes, owing to their extremely high theoretical capacity and its high abundance has gained a lot of attention. However, silicon expands nearly 3 times its original size leading to issues like pulverization and delamination that cause severe capacity decay. This has been a major impediment to the commercialization of Si anodes. In this work, various strategies have been discussed to overcome these issues. The significance of properties in binders, a polymeric material used to bind the electrode components, and maintain the electrode integrity has been discussed. Moreover, the effect of silicon (active material) particle size on the electrochemical performance has been investigated.

The results demonstrate the significance of binder molecular weight, an important property that determines the coulombic efficiency and capacity retention. Further results show the importance of silicon size and the addition of electrode modifications that render a stable capacity over several cycles of deep discharge. The results show a successful demonstration of a scalable and economically feasible fabrication technique to mitigate volume expansion in silicon-based anodes.

BIOGRAPHICAL SKETCH:

Avinash Umasankaran was born in Chennai, India. Right from an early age, Avinash was extremely interested in science and math and this led him to pursue his Bachelor of Technology in Chemical Engineering at SSN College of Engineering, Anna University. His enthusiasm for science grew during his undergrad, where he explored various research domains by working on multiple projects - from polymer science to nanotechnology. To pursue his newly ignited passion for research, Avinash decided to do his Master of Science (M.S.) degree in the Chemical and Biomolecular Engineering department at Cornell University in 2018. The courses he took in his first semester led to a newfound fascination for renewables and sustainability which in turn sparked his interest in energy storage. He has always wanted to bring about a positive change in society and realized that he could accomplish that through his work in this field. He found Prof. Yong L. Joo's research to be analogous with his goals and decided to work under him. The present dissertation is the result of his research in the Joo lab on developing advanced polymer binders for the next generation of lithium-ion battery anodes.

Outside of academics, Avinash was actively involved in club activities at Cornell. He was the director of Energy Day Programming in the Cornell Energy Systems Club. He also was a part of the fundraising committee at Asha Cornell, a non-profit organization striving to make a difference in society by promoting the education of underprivileged children in India. He plans to join the battery industry and become an integral part of a community that believes in and works tirelessly to drive sustainability forward.

ACKNOWLEDGEMENTS:

I am so grateful to have met so many people who made my life in Ithaca more enjoyable. First off, I would like to thank my thesis advisor, Prof. Yong L. Joo for believing in me, encouraging me constantly, and pushing me onwards to become a better researcher. He was always available with his lucid solutions whenever I approached him with an issue. This combined with his regular feedback kept me on track during my thesis.

I would also like to thank my committee member, Prof. Jin Suntivich for his constructive feedback and insightful comments. I would also like to express my special gratitude to Prof. Héctor D. Abruña and Prof. Suntivich for teaching me the fundamentals of Electrochemistry which proved to be invaluable for my thesis.

I gratefully acknowledge my funding from Hyundai for making this work possible. Special thanks to Cornell Centre for Materials Research and Cornell Energy Systems Institute for their advanced equipment and extremely supportive staff members, especially Malcolm Thomas, Philip Carubia, and Steve Kriske for training me on instruments and being extremely patient with me.

My sincere thanks to Dr. Somayeh Zamani, Dr. Mohammed AlAmer, Christopher Klaassen, and for teaching me experimental skills from fabrication to analysis. Their guidance helped me complete my thesis. Special thanks to Yash Joshi and Caspar Yi for providing critical research advice and for their interesting conversations. I am thankful for all the past and present Joo group members who have helped me along the way in this research and maintained a friendly work environment. Despite all the chaos caused by Covid-19 over the past few months, they continued to encourage me through virtual meetings and activities.

I would like to thank my beloved friend Abhaiguru who has accompanied me through all my ups and downs over the past six years. I would also like to thank my friends Aishwarya, Arvind, and Anirudh for providing me with their constant advice and support. In addition to this, I would like to that all my friends from my home country who constantly kept motivating me throughout my Master's.

Last but not the least, I would like to thank my family. My father who is showering his blessings from the sky, my mother for constantly providing the mental support and my brother for being there whenever I wanted him. I thank them for carrying me throughout my life and being my support system.

TABLE OF CONTENTS

LIST OF FIGURES

LIST OF TABLES

CHAPTER 1: INTRODUCTION

Energy is essential to all life and living organisms and exists in different forms. With technology developing at a rapid pace in all directions, the need for a cost-effective and reliable source of energy has gained a lot of importance. According to Enerdata yearbook, the consumption of energy worldwide has grown by nearly 3% in the year 2019. United States is the 2nd largest consumer of global energy of about 18% according to the Energy Information Administration (EIA) and ranks 2nd in the emission of CO_2 (5416 $MtCO_2$) below China, contributing nearly 15% of the worldwide emissions. Currently, 79% of the total energy consumption in the United States is sourced from fossil fuels (petroleum, coal, and natural gas) as reported by the EIA. Fossil fuels are not inexhaustible, and pollutants released by burning fossil fuels are wrecking the environment. This over-dependence on non-renewable resources leads to several negative issues that impact the planet and their living organisms. Reports from multiple sources suggest that the future of living organisms on this planet would be in danger if the trend continues. In the past decade, researchers all over the world have actively focused their attention towards alternate sources of energy. In recent years, there has been a forward movement towards renewable energy by various governments to make their citizens learn and fight global warming.

Energy resources that can be utilized repeatedly over a period of time are called renewable energy. Some examples of renewable energy are solar, wind, and biomass energy. But the common problem encountered with these renewable energy sources is the intermittency issue [1], [2]. These energy sources need some sort of storage technology to make themselves a reliable source that can provide energy to the grid when there is no generation (Example: Sun during the night, wind when not blowing). Therefore, this transition from harvesting energy from renewable resources towards storing it opens a new avenue for energy storage technology [3], [4]. To penetrate the market of

renewables, the cost and reliability of energy storage are the most important characteristics. In recent years, batteries have gained a lot of attention and are tipped to be the front runner among energy storage technologies [5]. Batteries are already a part of the everyday life of human beings through the various electronic devices we use [6], [7]. The working of a battery is very simple. It consists of two electrodes at different potentials in an ionically conductive electrolyte. When the electrodes are connected externally by a device, the ions flow through the electrolyte from the positive to the negative electrode with the electrons flowing in the reverse. This operation results in the storing of electrical energy by the external circuit [8,9,10]. Batteries have various chemistries, the most prominent and the commercial ones are Lithium-ion batteries (LIBs). In recent years, LIBs have emerged as the most prominent battery choice in electronics and transportation sectors. This is mainly due to the high energy and high power density offered by LIBs compared to the other commercial technologies[11].

Since its commercialization in 1991 by Sony Corporation, Lithium-ion batteries are widely used in small, portable electronic devices due to high energy density, high power discharge capability, and long cycle life. Currently, graphite and lithium metal oxides (like $LiCoO_2$) are used as negative and positive electrodes for commercial high volume manufacturing of LIBs [8], [12]. Automobile companies like Tesla, Nissan, etc., in the past few years, have performed various modifications (like geometry, separators[13], and electrolyte materials[14]) to the conventional electrodes and have successfully produced pure electric vehicles. However, all the modifications involve the same chemistry as lithium-ion batteries and hence limit their practical capacities[15]. The electric vehicles market is encountering a major barrier in application due to range anxiety. Range anxiety is the fear that a vehicle has insufficient range to reach its destination thereby stranding the vehicle's occupants. Range anxiety is primarily used in reference to battery electric

vehicles (BEVs) and is considered to be a major barrier to large scale adoption of electric vehicles [16], [17]. To cure the range anxiety issue, there has to be a dramatic increase in the energy density and power density of Li-ion batteries for electric vehicle applications[15].

To produce batteries that have higher energy densities and capacities, a change in the chemistry of the electrode (anode/cathode) is necessary. Since its inception and commercialization, carbon material has always been used as the anode as opposed to the cathode material that has undergone various changes [3], [18]. Over the past few years, researchers have directed their attention towards finding different viable chemistries for Li-ion anodes. There are 3 prominent chemistries in Li-ion anode that started gaining attention, namely intercalation, conversion, and alloying chemistry.

Chemistries in Li-ion batteries:

Intercalation/de-intercalation: The first class of chemistry is intercalation chemistry, the most popular one. The mainly studied intercalation anodes involve graphite and Lithium titanium oxide $Li_4Ti_5O_{12}$ (LTO) [11], [12]. Intercalation refers to the reversible insertion and extraction of Li into a solid host which can have different structures like layered/spinel etc. In both LTO and graphite, the lithium ions intercalate into the structure of these materials during charging and de-intercalate during discharge. For example, graphite has a layered structure held together by van der Waals forces and lithium intercalates between carbon layers upon charge/discharge. The maximum concentration of Li in graphite is one Li per six carbon atoms (LiC_6), and the theoretical capacity of graphite anodes is 372 mAh/g [19]. The volume change in graphite anodes when lithium intercalates is less than 10%. Whereas, LTO on the other hand undergoes a highly reversible, stress-free intercalation process. LTO has various advantages like favorable Li potential (1.5V), fast cycling because of its high reduction voltage, and prolonged cycle life. However, LTO is

inferior to graphite due to its poor energy density (low specific capacity - 160 mAh/g). Hence, graphite has gained more attention among the intercalation chemistries and has shown good cycling and rate capability characteristics [20].

Conversion: The second class of chemistry is the materials involving conversion chemistry. In this chemistry, the electrodes are made up of nanoparticles of transition metal oxides like cobalt oxide, nickel oxide, and copper oxide, as well as certain phosphides and fluorides that undergo reduction reaction with Li-ions leading to the formation Li_2O. It can be depicted as follows:

$$Li + M_aX_b \rightleftharpoons aM + bLi_nX$$

Here, M is often a transition metal and X represents the anion, which is oxygen in the case of anodes. This chemistry has proved to be better in terms of the capacities when compared to the intercalation chemistries with almost twice (700 mAh/g) the capacities of intercalation anodes [21], [22]. However, these anodes have various issues that limit their commercialization. The major issues involving conversion chemistry-based anodes are their operation at higher temperatures, high volume changes during cycling (charge & discharge), unstable solid electrolyte interface (SEI), and low first cycle coulombic efficiency/initial coulombic efficiency (ICE) [22].

Alloying/de-alloying: The third class of the family of anode materials is the materials that undergo an alloying mechanism. Common materials belonging to this class are Tin, Germanium, Gallium, and Silicon [23],[24]. Different from the intercalation species, lithium is not stored between carbon layers but forms alloys with metallic elements. The mechanism can be depicted as follows:

$$M + yLi \rightleftharpoons Li_yM$$

Intermetallic materials were also used as negative electrode materials owing to their relatively high capacities. Silicon and Tin lithiated up to 4.4 Lithium ions for each atom of their own resulting in high specific capacities of 4200 mAh/g and 900 mAh/g respectively [18], [25], [26].

Among the alloying chemistry, Silicon has recently gained a lot of interest owing to its extremely high theoretical capacity of 4200 mAh/g which is almost 10 times that of current commercial graphite electrodes (372 mAh/g). Typically, Si alloys formed are Li_2Si, $Li_{15}Si_4$, $Li_{21}Si_8$, $Li_{22}Si_{15}$ which means for every Si atoms up to 4.4 Li-ions [27] can be stored compared to one Li atom per six C atoms in graphite(LiC_6) [28]. In addition to the high capacity, various other factors support the increasing research in Silicon anodes. Silicon shows beneficial intrinsic properties, like low delithiation potential vs Li/Li^+ at 0.4V when compared to the other anode materials, and are less likely to form dendritic growth at high current densities [29]. The formation of dendrites and their growth is a major problem in graphitic anodes and can lead to short circuits, ignitions/explosions [30]. Since the potential is higher than that of graphite (0.05V vs Li/Li^+), Si is less likely to form dendrites alleviating the safety concerns. In addition to this Silicon is the 2nd most abundant material on the earth's crust and is eco-friendly and non-toxic making it a much safer alternative. Moreover, the growth of the semiconductor industry has laid a mature infrastructure for the processing of Silicon [31], [32]. However, the commercial application of this high capacity silicon has been hindered due to their poor electrical conductivity and their large volume variation (around 300%) during the charging/discharging [33], [34]. This results in capacity fading during cycling and cell failure due to the following three main effects:

Pulverization: Pulverization is the cracking of anode material due to the stress-induced by volume change during lithiation and de-lithiation. Because of its inherent ability to store a large number of lithium ions, a huge amount of stress is generated. This leads to loss of electric contact among the active material (Silicon) which further leads to capacity fading upon cycling [35], [36].

Delamination: Delamination is a result of structural modification upon the cycling of the electrode. During lithiation/delithiation, the Silicon particles expand/contract volumetrically and

exert force on each other. This causes loss of contact between the active material and the electrode collector (Cu foil). The loss of active material drives down the utilization of silicon which in turn drives down the capacity and eventually causes cell failure [4], [37].

Unstable Solid-Electrolyte Interface (SEI): The Solid-Electrolyte Interface (SEI) is a thin interfacial layer formed on anode surfaces as a result of electrolyte decomposition at low potentials outside the electrolyte's electrochemical stability window [38], [39]. The instability in SEI can be attributed to the irreversible consumption of Lithium ions due to their reduction on the electrode surface and thus the buildup of SEI. Generally, the SEI layer is conductive for Li and covers the active material, preventing the further buildup of SEI and results in a smooth and thin SEI layer (Graphite anodes). However, the iterative volume change of Si excess amount of stress and breaks the SEI layer, leading to the formation of an additional SEI layer on the freshly exposed Si surface. This process continuously consumes Li-ions as well as the electrolyte and thus an increasingly high resistance is formed impairing the Coulombic efficiency every cycle and ultimately causing electrode failure [37], [40].

Over the past decade, multiple approaches have been used to tackle the above-mentioned issues. The main goals are to accommodate the large volume change of Si during cycling, facilitate the electrochemical reactions by providing quick lithium-ion diffusion pathways, improve the electrical conductivity of the system, and to ensure a smooth, thin and a stable formation of SEI. There have been various modifications done in the past decade to solve these issues involving the synthesis of nanosized silicon and tuning their geometries (0D [6], 1D [10], 2D [41] and 3D [10]), designing composite electrodes using complex carbonaceous materials[42–46] to alleviate the stress generated and also provide a conductive pathway, coating different materials to counter the

stress generated during volume expansion and creating porous electrode structure to accommodate the excess room for silicon expansion during lithiation.

Binders for silicon anodes:

Consequently, attention is increasingly moving beyond the active component of the electrode, to optimizing the overall electrode structure. Slowly, researchers have realized the potential of binder and have started to probe into their research [47], [48]. In this arena, it is becoming clear that the optimization of the binder component is the key to the realization of high capacity retention silicon anodes. A binder is a component of the electrode that is used to bond the active materials and the conductive additives together on to the current collector during the lithiation/de-lithiation process. Binders, though present in minimal amounts in the electrode, plays a crucial role in the electrode stability over multiple cycles. The main role of the binder is to maintain the physical integrity of the whole electrode system. Especially in silicon-based anodes, the binder comprises nearly 10% weight of the composite electrodes and serves multiple functions, including maintaining the mechanical integrity of the electrode, suppressing pulverization of silicon in the electrode, and preventing the delamination of active material from the copper current collector [49], [50]. Therefore, for a binder to be used in a silicon-based anode system for LIBs, must possess the following functional roles [11], [51], [52], [53], [54]:

1) **Maintain the mechanical integrity**: Bind the particles together with the current collector through chemical/mechanical mechanism with a high degree of reversibility upon cycling.
2) **Form homogenous slurry:** Form a homogenous slurry mixture enabling better dispersion of electrode components in the final electrode structure.

3) **Weak interactions with electrolyte:** Avoid swelling characteristics and alteration in mechanical properties when in contact with the electrolyte, thereby prevention additional electrolyte degradation.
4) **Binding interaction with electrode components:** Provide suitable binding interactions with both the active material (silicon) and conductive additive (graphene) forming stable electrical pathways.
5) **Electrochemically stable:** Must be electrochemically stable in the required electrochemical potential window.
6) **Low cost and eco-friendly**: Must not cost additional amounts to the battery components, must be environmentally benign, and enable facile processing of the electrode.

Binding Mechanism: It is important to understand the mechanism of a binder before dealing with the intricacies in their application. An effective binding process is divided into three main steps:

a) Diffusion/penetration step – In this step, the binder wets the substrate surface and penetrates through the pores present in the electrode material.

b) Interlocking step – In this step, the binders harden on the substrate surface through different reaction mechanisms leading to the interlocking effect.

c) Interfacial forces – In this step, the binder interacts with the active material. This interaction between the binder and active material decides the binding strength of the composite electrode.

Fig 1.1 a), b) and c) shows the 3 steps involved in the binding mechanism.

There are generally 3 different states associated with an active material – binder composite: the bonded layer, the fixed layer, and the excess layer of polymer. The excess layer is the free layer of the polymer surrounding the fixed layer. The properties of fixed and excess layers are mostly

dependent on the intrinsic properties (electrical/ionic conductivity, mechanical properties, porosity, etc.) of the polymer. Whereas the bonded polymer layer is the immediate layer surrounding the active material and is the reason for the interfacial reactions (supramolecular, covalent, etc.) between the polymer and active material. As the layers go far away from the active material, their strength decreases. For example, the strength of the fixed layer is higher than that of the excess layer due to their interaction with the bonded layer. Fig 1.1 d) shows the polymer states in the bonding system.

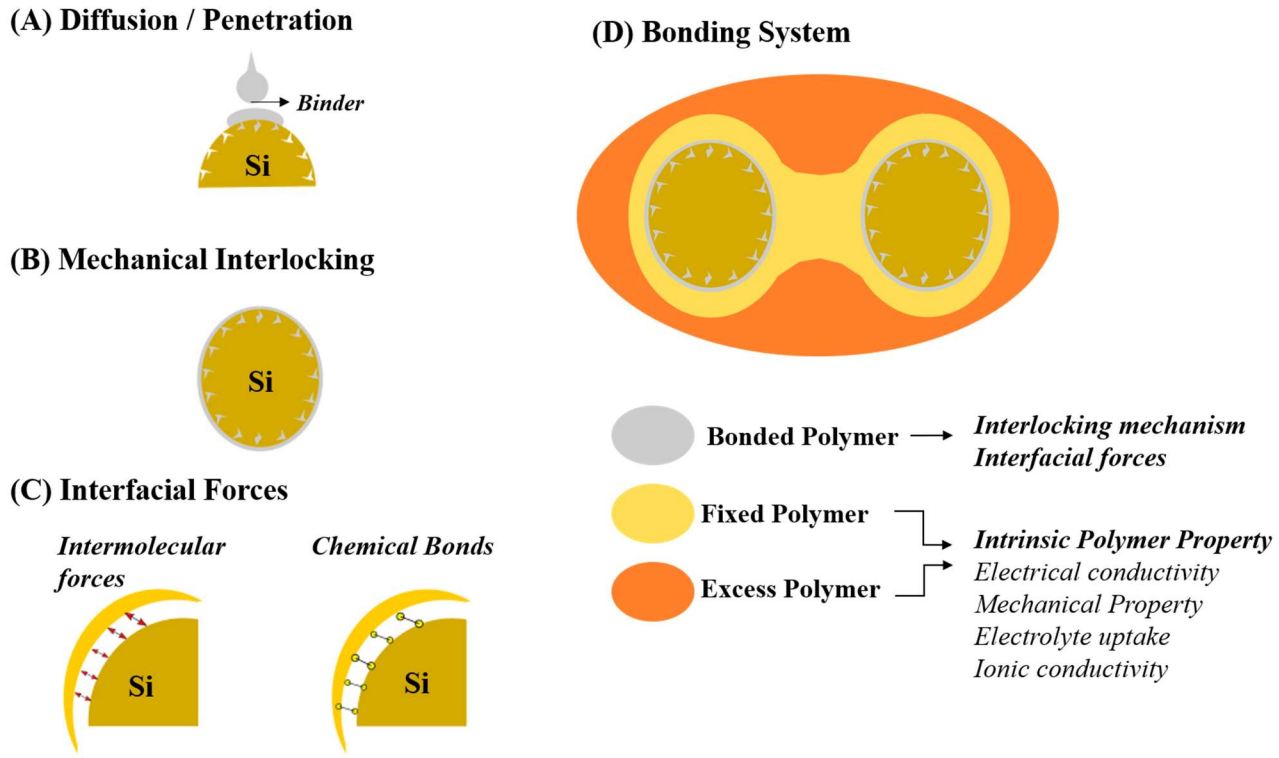

Fig 1.1 Schematic representation of binding mechanism a) Diffusion, b) Mechanical Interlocking, c) Interfacial forces and d) Polymer states in a bonding system

Binders are polymeric materials with varying properties. The application of binders differs from one another based on their adhesion strength, their polymer architecture, and their elasticity.

1) **Impact of polymer interactions**

It is well known that the role of a binder is to maintain the cohesion of electrode components and their adhesion to the current collector during the working of the cell [55]. Therefore, the binder is expected to play a pivotal role in maintaining the mechanical stability of the electrodes during long-term cycling. The adhesion strength of the polymers is very closely associated with their chemical nature. Based on their bond strength and reversibility, they can be classified into 3 categories: weak supramolecular interactions [53], strong supramolecular interactions [56], and covalent interactions [57].

Each of these three categories responds differently to mechanical stress. Supramolecular interactions inherently have a reversible binding nature, but covalent bonds do not. This reversibility nature of a bond depends on the strength of supramolecular interactions. For example, weak supramolecular interactions involve the van der Waals force that dissociates easily even under small stress. The driving force for recovery in these interactions is also weak. On the other hand, strong supramolecular interactions involve hydrogen bonding and ion-dipole interactions where the bonds are much stronger, and the recovery characteristics are much better than weak supramolecular interactions. Lastly, the covalent bonds are those that have high bond strengths but does not have the recovery ability and undergoes a plastic rupture. Covalent bonds can form a stiff network and suppress detachment of active Si particles, but their inherent irreversible nature eventually leads to the failure of the electrode [58].

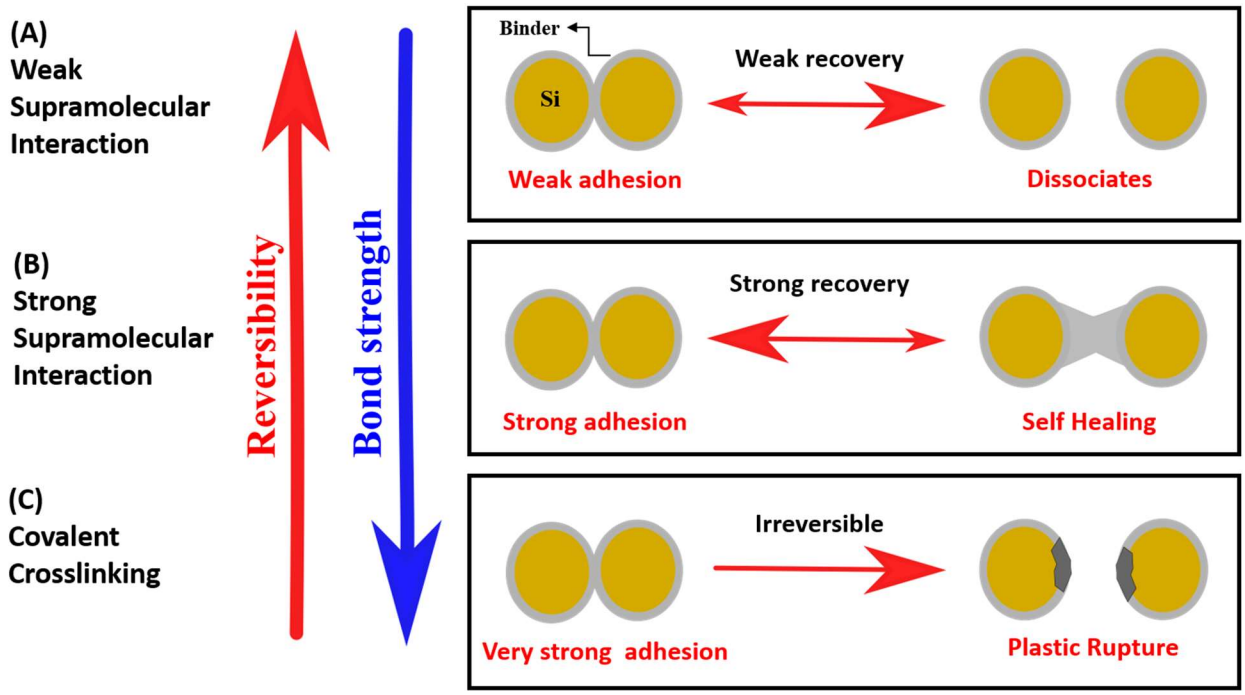

Fig 1.2 Classification of binders based on the impact of polymer interaction

2) Impact of polymer architecture

While the bond strength determines their extent of interactions at each anchoring point between the binder and silicon, the polymer architecture affects the adhesion by a different mechanism. The effect of polymer architecture demonstrates the mechanism of how mechanical forces exerted during charge/discharge can be distributed to the branched chains reducing the stress on the anchoring points. Based on their architecture, polymers can be classified into two types, linear and branched-chain polymers. A linear polymer is a one-dimensional (1D) polymer [59] that does not have any branching other than the monomer groups. On the other hand, a branched polymer has a 3D architecture with branching points connected by other polymers (star, graft, dendrimers, etc.) chains [29], [53], [59].

In Silicon anodes, the role of the polymeric binder is to dissipate the mechanical stress caused due to the volume change of Si due to the repeated charge and discharge cycles. Every anchoring point has maximum stress it can endure, beyond which it breaks, and adhesion is lost. In linear polymers, the anchoring point is a single node which receives the stress directly and subsequently detaches under high mechanical strengths. In contrast, for branched-chain polymers, the mechanical stress can be distributed to the branched chains through branching points (multiple nodes) which substantially reduces the stress applied to each anchoring point (node) [61]. In addition to this, the maximum stress each anchoring point can endure is higher as all the polymer chains co-operatively resist the force caused by the volume expansion through intrachain cohesion. Such multidimensional interactions make them strongly adhesive and immobile on the Silicon surface, thereby restraining their movement and extending the cycle life of batteries [62].

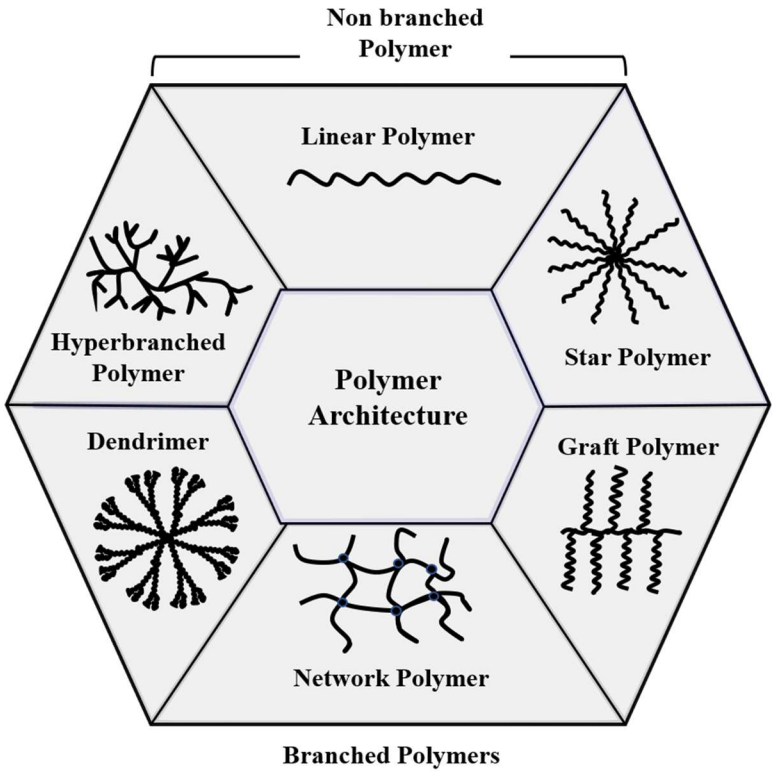

Fig 1.3 Classification of polymers in terms of their architecture

3) Elasticity of the binder

The first attempts made on addressing the poor mechanical stability and irreversible loss in capacity mainly focused on improving the elasticity of the polymer binder [63]. This area was mainly focused based on the fact that the binder undergoes large strains to accommodate the volume expansion of silicon particles. Therefore, the more elastic the binder is better it is to accommodate volume changes in the electrodes.

Over the past few years, research in polymer binders is growing constantly as they can potentially address the capacity loss due to cracking by maintaining cohesion between various materials in the electrode system. In this section, we would like to describe the various molecular design approaches that have been tested to address the instabilities that arise in silicon anodes.

Classification of binders based on properties:

1. Elastic polymer binders

One of the earliest approaches to address this poor mechanical stability and irreversible capacity loss in silicon anodes focused on the improvement of polymer elasticity. This idea is intuitively very attractive as the binder undergoes large strains to accommodate the volume changes in Silicon particles. PVDF, the commercial binder used failed miserably in Silicon anodes. Researchers improved its elasticity by making a complex binder named poly-vinylidene fluoride–tetrafluoroethylene–propylene) PVDF-TFE-P [64], [65]. PVDF could only sustain an elongation of 10% whereas the complex sustained up to 100% elongation and outperformed PVDF in electrochemical tests [54], [66]. Other examples of elastic binders include the use of Styrene-butadiene (SBR) [67], polyacrylamide [68], [69]. However, after multiple research publications, researchers concluded that elasticity may not be the most important factor in the choice of a binder. In fact, the polymer adhesion ability is more sought after. For example, stiff networks like CMC

performed better when compared to SBR, etc. Therefore, researchers have often combined an elastic binder with a non-elastic binder/stiff network to render characteristics of both the binders [44], [56], [70]. A recent study demonstrated the use of Polyacrylic acid (PAA) with Polyrotaxanes (PR) together [71]. Here, the molecular rings present in polyrotaxanes mechanically interlocked with PAA enabling a highly elastic material that can sustain up to 200% of the strain. This study is noteworthy as it demonstrated that elasticity may indeed be a vital design property in combination with other polymer binder properties.

2) Adhesive polymer binders

Strong adhesion between the binder, silicon, and other electrode components help silicon anodes prevent isolation of Si, delamination from the collector, and loss of conductive pathways. Usually strong adhesion to silicon particles have been achieved by polymers that contain -COOH, -OH,-COO and -NH_2 groups that bind directly with the Si surface [25], [53], [62]. Several studies attributed the success of CMC binder to its strong adhesive nature with Si. CMC is a non-elastic polymer that performed way more superior than other elastic alternatives[72]–[75]. Recent studies revealed that CMC and Si had hydrogen bonding interactions which rendered better stability and cyclic performance. Poly (acrylic) acid (PAA) and lithium substituted PAA (LiPAA) are additional examples of strongly adhesive polymer binder materials. Similar to CMC, PAA also showed excellent adhesion ability with silicon and also showed excellent capacities[61], [76], [77]. Other water-soluble polymers with strong adhesion capability include Poly(vinyl alcohol) (PVA) [78], [79] , Catechol polymers [56], Chitosan [80][81], Alginate[51], [82], Nafion[83]–[85] and polyacrylamide [86]. All these studies demonstrate that a strong adhesion capability with silicon is an important design parameter for producing high capacity stable silicon anodes.

3) Self-healing polymer binders

Self-healing polymer binders have received the most attention in recent times. Several studies have implemented these binders, with the hypothesis that the reversibility aspect in self-healing binders will be able to accommodate large volume changes in silicon without permanent fracture. Wang et.al [56], [87] researched a self-healing polymer binder to form a 3 D network, which could repair the damage caused by the silicon during cycling. It has been identified that crosslinking polymers is another effective way to prepare a self-healing binder. PAA has been commonly used to yield cross-linking self-healing polymer binder. Researchers have used PAA and PVA to prepare a waterborne PAA-PVA crosslinked binder for Si anodes [88]. This crosslinked polymer binder could effectively restrain the volume change of Silicon anodes during cycling leading to high cyclic stability and high efficiencies even at high currents. Thus, PAA binders and neutralized PAA binders are worthy to study deeper and could very well become one of the most promising candidates for commercial applications.

In this thesis, efforts have been made to tackle the failure modes associated with silicon-based anodes for LIB's with a special emphasis on the binders and their properties. We hypothesize the major failure mode for silicon-based anodes is the very high volume expansion that Silicon possesses during charge/discharge. Hence, we have aimed to explore multiple material based strategies to combat the volume expansion problem. Additionally, all the material processing methods are made in such a way that the whole process is robust, scalable, and environmentally friendly for larger single-step manufacturing efforts.

Air-Controlled Electrospray:

In this thesis, we use a unique facile mode for coating the anode. Air controlled electrospraying is used as the process for designing our electrodes. In electrospraying, the solution injected in the

nozzle is subjected to a sufficient voltage source and is drawn out of the jet needle at the desired flow rate. This liquid droplets now travel a certain distance and solidifies as it reaches the collector to form the desired electrode. Several researchers have used electrospinning to fabricate composite silicon anodes owing to its simplicity and environmentally nature of manufacturing [89, 90]. One small problem with electrospraying is its time consuming and gives us a lower volumetric energy density of the electrode. To counter this, we used Air controlled electrospray, which makes the process much faster because of the addition of air pressure and also addresses the problem of energy density [91]. The mechanism of air controlled electrospraying is pretty simple. The applied voltage source breaks up the solution into small jets of spray in the inner nozzle and these jets are further broken into smaller particles by the additional air pressure that drives these particles and deposits them on the collector placed at a certain distance. During this process, four factors are always modifiable, those are the distances (cm), flowrates (ml/min), pressure (psi), and the voltage (kV). Before any of the electrodes are prepared, the spray pattern is checked to make sure the spray is homogenous and does not cause any lumping.

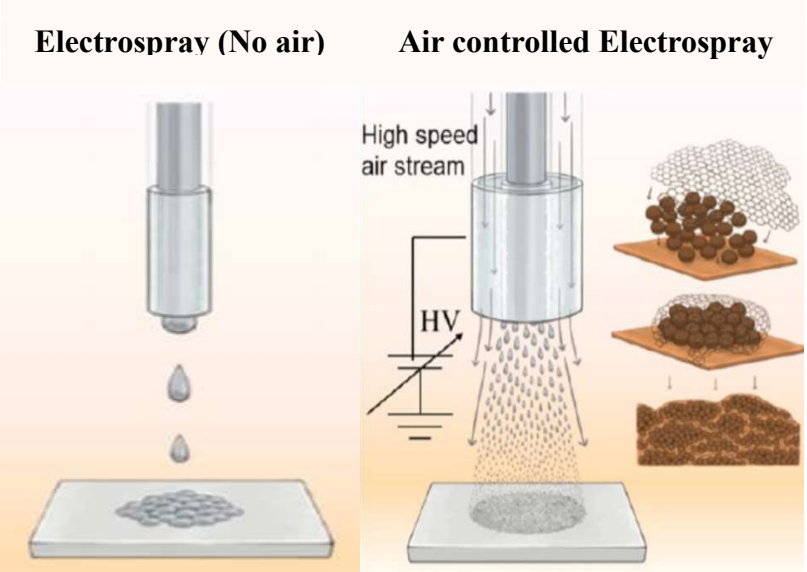

Fig 1.4 Schematic illustration of Conventional Electrospraying and Air-Assisted electrospraying for Silicon-Graphene based anodes

In chapter 1 of this work, the fundamental aspects of the application of silicon anodes in Lithium-ion batteries were discussed. The current challenge that Silicon anodes are facing and the possible ways to mitigate them were also discussed. Detailed literature revealed that proper design and application of binders could emerge as a potential counter to the volume expansion problem. Therefore, the properties of binders and characteristics of binders that make them suitable for the system were addressed. Finally, we discussed the commonly researched binders for Si anodes and the potential binders which could mitigate the problem of volume expansion.

In chapter 2 of this work, poly(acrylic) acid was used as the binder in a system comprising of Silicon nanoparticles and graphene. After the initial literature review, it was evident that additional research was needed towards PAA before its application in Si-based anodes. Researchers made several attempts to incorporate PAA as the binder, but there has been no

research regarding the key properties and optimal molecular weight of the binder. It is well known that the molecular weight of the polymer varies the intrinsic properties of the polymer and could well render different attributes. Most of the researchers working on PAA as a binder worked in low molecular weight ranges (Mw - 90,000 and 450,000). In chapter 2 of the thesis, we aim to study the effect of higher molecular weights of PAA (1.25 million and 3 million) and their effect in Silicon Graphene composite anodes.

In chapter 3 of this thesis, a different approach was used to address the same volume expansion problem in silicon anodes. Here we decided to study the effect of different sizes of silicon nanoparticles and their effect on electrochemical performance.

The work done in this thesis is of very high relevance to the current industrial problem (volume expansion) that we are facing. Both Chapter 2 and Chapter 3 are genuine attempts made to tackle the volume expansion problems with a different perspective.

References:

[1] N. Yuca, O. S. Taskin, and E. Arici, "An overview on efforts to enhance the Si electrode stability for lithium ion batteries," Energy Storage, vol. 2, no. 1, pp. 1–15, 2020, doi: 10.1002/est2.94.

[2] M. Gu, Y. He, J. Zheng, and C. Wang, "Nanoscale silicon as anode for Li-ion batteries: The fundamentals, promises, and challenges," Nano Energy, vol. 17, pp. 366–383, 2015, doi: 10.1016/j.nanoen.2015.08.025.

[3] C. P. Opsel, B. Graeme, and P. G. Blake, "Silicon based high performance Anode Materials for Next Generation Li-Ion Batteries," pp. 1–13, [Online]. Available: http://fse.studenttheses.ub.rug.nl/17294/1/mNANO_2018_PopselC.pdf.

[4] J. Hou, S. Qu, M. Yang, and J. Zhang, "Materials and electrode engineering of high capacity anodes in lithium-ion batteries," J. Power Sources, vol. 450, no. December 2019, p. 227697, 2020, doi: 10.1016/j.jpowsour.2019.227697.

[5] T. Kim, W. Song, D. Y. Son, L. K. Ono, and Y. Qi, "Lithium-ion batteries: outlook on present, future, and hybridized technologies," J. Mater. Chem. A, vol. 7, no. 7, pp. 2942–2964, 2019, doi: 10.1039/C8TA10513H.

[6] J. Y. Li, Q. Xu, G. Li, Y. X. Yin, L. J. Wan, and Y. G. Guo, "Research progress regarding Si-based anode materials towards practical application in high energy density Li-ion batteries," Mater. Chem. Front., vol. 1, no. 9, pp. 1691–1708, 2017, doi: 10.1039/c6qm00302h.

[7] P. PbSO, N. Koh, -e -, V. Li Si, and S. LiX, "PbO 2 H 2 O H 2 SO 4 /H 2 O H + PbSO 4 SO 4 2-+-e-2.0 V Lead-acid Li 1-x CoO 2 LiPF 6 EC-DMC LiPF 6 EC-DMC Lithium ion Future batteries? Lithium ion based on nanomaterials Ionic liquids Lithium metal Lithium-air Lithium-based electrolytes," Nature, vol. 451, no. 7, pp. 652–657, 2008.

[8] J. O. Besenhard, "The electrochemical preparation and properties of ionic alkali metal-and NR4-graphite intercalation compounds in organic electrolytes," Carbon N. Y., vol. 14, no. 2, pp. 111–115, 1976, doi: 10.1016/0008-6223(76)90119-6.

[9] A. Casimir, H. Zhang, O. Ogoke, J. C. Amine, J. Lu, and G. Wu, "Silicon-based anodes for lithium-ion batteries: Effectiveness of materials synthesis and electrode preparation," Nano Energy, vol. 27, pp. 359–376, 2016, doi: 10.1016/j.nanoen.2016.07.023.

[10] X. Zuo, J. Zhu, P. Müller-Buschbaum, and Y. J. Cheng, "Silicon based lithium-ion battery

anodes: A chronicle perspective review," Nano Energy, vol. 31, no. October 2016, pp. 113–143, 2017, doi: 10.1016/j.nanoen.2016.11.013.

[11] V. Etacheri, R. Marom, R. Elazari, G. Salitra, and D. Aurbach, "Challenges in the development of advanced Li-ion batteries: A review," Energy Environ. Sci., vol. 4, no. 9, pp. 3243–3262, 2011, doi: 10.1039/c1ee01598b.

[12] M. Li, J. Lu, Z. Chen, and K. Amine, "30 Years of Lithium-Ion Batteries," Adv. Mater., vol. 30, no. 33, pp. 1–24, 2018, doi: 10.1002/adma.201800561.

[13] H. Lee, M. Yanilmaz, O. Toprakci, K. Fu, and X. Zhang, "A review of recent developments in membrane separators for rechargeable lithium-ion batteries," Energy Environ. Sci., vol. 7, no. 12, pp. 3857–3886, 2014, doi: 10.1039/c4ee01432d.

[14] L. Chen, K. Wang, X. Xie, and J. Xie, "Effect of vinylene carbonate (VC) as electrolyte additive on electrochemical performance of Si film anode for lithium ion batteries," J. Power Sources, vol. 174, no. 2, pp. 538–543, 2007, doi: 10.1016/j.jpowsour.2007.06.149.

[15] M. M. Thackeray, C. Wolverton, and E. D. Isaacs, "Electrical energy storage for transportation - Approaching the limits of, and going beyond, lithium-ion batteries," Energy Environ. Sci., vol. 5, no. 7, pp. 7854–7863, 2012, doi: 10.1039/c2ee21892e.

[16] N. Rauh, T. Franke, and J. F. Krems, "Understanding the impact of electric vehicle driving experience on range anxiety," Hum. Factors, vol. 57, no. 1, pp. 177–187, 2015, doi: 10.1177/0018720814546372.

[17] H. A. Bonges and A. C. Lusk, "Addressing electric vehicle (EV) sales and range anxiety through parking layout, policy and regulation," Transp. Res. Part A Policy Pract., vol. 83, pp. 63–73, 2016, doi: 10.1016/j.tra.2015.09.011.

[18] J. O. Besenhard, J. Yang, and M. Winter, "Will advanced lithium-alloy anodes have a chance in lithium-ion batteries?," J. Power Sources, vol. 68, no. 1, pp. 87–90, 1997, doi: 10.1016/S0378-7753(96)02547-5.

[19] Z. Karkar, D. Guyomard, L. Roué, and B. Lestriez, "A comparative study of polyacrylic acid (PAA) and carboxymethyl cellulose (CMC) binders for Si-based electrodes," Electrochim. Acta, vol. 258, pp. 453–466, 2017, doi: 10.1016/j.electacta.2017.11.082.

[20] Y. Sun et al., "Graphite-Encapsulated Li-Metal Hybrid Anodes for High-Capacity Li Batteries," Chem, vol. 1, no. 2, pp. 287–297, 2016, doi: 10.1016/j.chempr.2016.07.009.

[21] P. Poizot, S. Laruelle, S. Grugeon, L. Dupont, and J. Tarascon, "Nano-sizedtransition-

metaloxidesas negative-electrode materials for lithium-ion batteries," vol. 407, no. September, 2000.

[22] S. H. Yu, S. H. Lee, D. J. Lee, Y. E. Sung, and T. Hyeon, "Conversion Reaction-Based Oxide Nanomaterials for Lithium Ion Battery Anodes," Small, vol. 12, no. 16, pp. 2146–2172, 2016, doi: 10.1002/smll.201502299.

[23] J. Xu, "lnvestigation of the Critical Role of Polymeric Binders for Silicon Negative Electrodes in Lithium- lon Batteries," 2016.

[24] K. Feng et al., "Silicon-Based Anodes for Lithium-Ion Batteries: From Fundamentals to Practical Applications," Small, vol. 14, no. 8, 2018, doi: 10.1002/smll.201702737.

[25] W. J. Zhang, "A review of the electrochemical performance of alloy anodes for lithium-ion batteries," J. Power Sources, vol. 196, no. 1, pp. 13–24, 2011, doi: 10.1016/j.jpowsour.2010.07.020.

[26] J. B. Park, J. S. Ham, M. S. Shin, H. K. Park, Y. J. Lee, and S. M. Lee, "Synthesis and electrochemical characterization of anode material with titanium-silicon alloy solid core/nanoporous silicon shell structures for lithium rechargeable batteries," J. Power Sources, vol. 299, pp. 537–543, 2015, doi: 10.1016/j.jpowsour.2015.09.019.

[27] G. Zhang et al., "A Quadruple-Hydrogen-Bonded Supramolecular Binder for High-Performance Silicon Anodes in Lithium-Ion Batteries," Small, vol. 14, no. 29, pp. 1–10, 2018, doi: 10.1002/smll.201801189.

[28] T. Ohzuku, "Formation of Lithium-Graphite Intercalation Compounds in Nonaqueous Electrolytes and Their Application as a Negative Electrode for a Lithium Ion (Shuttlecock) Cell," J. Electrochem. Soc., vol. 140, no. 9, p. 2490, 1993, doi: 10.1149/1.2220849.

[29] T. W. Kwon, J. W. Choi, and A. Coskun, "The emerging era of supramolecular polymeric binders in silicon anodes," Chem. Soc. Rev., vol. 47, no. 6, pp. 2145–2164, 2018, doi: 10.1039/c7cs00858a.

[30] S. S. Zhang, K. Xu, and T. R. Jow, "Evaluation on a water-based binder for the graphite anode of Li-ion batteries," J. Power Sources, vol. 138, no. 1–2, pp. 226–231, 2004, doi: 10.1016/j.jpowsour.2004.05.056.

[31] L. Y. Beaulieu, K. W. Eberman, R. L. Turner, L. J. Krause, and J. R. Dahna, "Colossal reversible volume changes in lithium alloys," Electrochem. Solid-State Lett., vol. 4, no. 9, 2001, doi: 10.1149/1.1388178.

[32] X. Zuo, J. Zhu, P. Müller-Buschbaum, and Y.-J. Cheng, “Silicon based lithium-ion battery anodes,” Nano Energy, vol. 31, p. 113, 2017.

[33] V. G. Khomenko and V. Z. Barsukov, “Characterization of silicon- and carbon-based composite anodes for lithium-ion batteries,” Electrochim. Acta, vol. 52, no. 8 SPEC. ISS., pp. 2829–2840, 2007, doi: 10.1016/j.electacta.2006.11.006.

[34] M. K. Datta and P. N. Kumta, “Silicon and carbon based composite anodes for lithium ion batteries,” J. Power Sources, vol. 158, no. 1, pp. 557–563, 2006, doi: 10.1016/j.jpowsour.2005.09.016.

[35] J. H. Ryu, J. W. Kim, Y. E. Sung, and S. M. Oh, “Failure modes of silicon powder negative electrode in lithium secondary batteries,” Electrochem. Solid-State Lett., vol. 7, no. 10, 2004, doi: 10.1149/1.1792242.

[36] A. Miranda, K. Sarang, B. Gendensuren, E.-S. Oh, J. Lutkenhaus, and R. Verduzco, “Molecular design principles for polymeric binders in silicon anodes,” Mol. Syst. Des. Eng., 2020, doi: 10.1039/c9me00162j.

[37] H. Wu and Y. Cui, “Designing nanostructured Si anodes for high energy,” Nano Today, vol. 7, pp. 414–429, 2012.

[38] M. Zhang, T. Zhang, Y. Ma, and Y. Chen, “Latest development of nanostructured Si/C materials for lithium anode studies and applications,” Energy Storage Mater., vol. 4, pp. 1–14, 2016, doi: 10.1016/j.ensm.2016.02.001.

[39] E. Peled and S. Menkin, “Review—SEI: Past, Present and Future,” J. Electrochem. Soc., vol. 164, no. 7, pp. A1703–A1719, 2017, doi: 10.1149/2.1441707jes.

[40] Y. Oumellal et al., “The failure mechanism of nano-sized Si-based negative electrodes for lithium ion batteries,” J. Mater. Chem., vol. 21, no. 17, pp. 6201–6208, 2011, doi: 10.1039/c1jm10213c.

[41] X. Zhou, Y. X. Yin, L. J. Wan, and Y. G. Guo, “Self-assembled nanocomposite of silicon nanoparticles encapsulated in graphene through electrostatic attraction for lithium-ion batteries,” Adv. Energy Mater., vol. 2, no. 9, pp. 1086–1090, 2012, doi: 10.1002/aenm.201200158.

[42] X. Liu, X. Zhu, and D. Pan, “Solutions for the problems of silicon–carbon anode materials for lithium-ion batteries,” R. Soc. Open Sci., vol. 5, no. 6, 2018, doi: 10.1098/rsos.172370.

[43] X. Gao, J. Li, Y. Xie, D. Guan, and C. Yuan, “A multilayered silicon-reduced graphene

oxide electrode for high performance lithium-ion batteries," ACS Appl. Mater. Interfaces, vol. 7, no. 15, pp. 7855–7862, 2015, doi: 10.1021/acsami.5b01230.

[44] N. Li, S. Jin, Q. Liao, H. Cui, and C. X. Wang, "Encapsulated within graphene shell silicon nanoparticles anchored on vertically aligned graphene trees as lithium ion battery anodes," Nano Energy, vol. 5, pp. 105–115, 2014, doi: 10.1016/j.nanoen.2014.02.011.

[45] Q. Cheng, Y. Okamoto, N. Tamura, M. Tsuji, S. Maruyama, and Y. Matsuo, "Graphene-Like-Graphite as Fast-Chargeable and High-Capacity Anode Materials for Lithium Ion Batteries," Sci. Rep., vol. 7, no. 1, pp. 1–14, 2017, doi: 10.1038/s41598-017-14504-8.

[46] G. Wang, X. Shen, J. Yao, and J. Park, "Graphene nanosheets for enhanced lithium storage in lithium ion batteries," Carbon N. Y., vol. 47, no. 8, pp. 2049–2053, 2009, doi: 10.1016/j.carbon.2009.03.053.

[47] Y. Shi, X. Zhou, and G. Yu, "Material and Structural Design of Novel Binder Systems for High-Energy, High-Power Lithium-Ion Batteries," Acc. Chem. Res., vol. 50, no. 11, pp. 2642–2652, 2017, doi: 10.1021/acs.accounts.7b00402.

[48] H. Chen et al., "Exploring Chemical, Mechanical, and Electrical Functionalities of Binders for Advanced Energy-Storage Devices," Chem. Rev., vol. 118, no. 18, pp. 8936–8982, 2018, doi: 10.1021/acs.chemrev.8b00241.

[49] S. Jiang, B. Hu, Z. Shi, W. Chen, Z. Zhang, and L. Zhang, "Re-Engineering Poly(Acrylic Acid) Binder toward Optimized Electrochemical Performance for Silicon Lithium-Ion Batteries: Branching Architecture Leads to Balanced Properties of Polymeric Binders," Adv. Funct. Mater., vol. 30, no. 10, pp. 1–9, 2020, doi: 10.1002/adfm.201908558.

[50] X. Shen et al., "Research progress on silicon/carbon composite anode materials for lithium-ion battery," J. Energy Chem., vol. 27, no. 4, pp. 1067–1090, 2018, doi: 10.1016/j.jechem.2017.12.012.

[51] D. Bresser, D. Buchholz, A. Moretti, A. Varzi, and S. Passerini, "Alternative binders for sustainable electrochemical energy storage-the transition to aqueous electrode processing and bio-derived polymers," Energy Environ. Sci., vol. 11, no. 11, pp. 3096–3127, 2018, doi: 10.1039/c8ee00640g.

[52] G. G. Eshetu and E. Figgemeier, "Confronting the Challenges of Next-Generation Silicon Anode-Based Lithium-Ion Batteries: Role of Designer Electrolyte Additives and Polymeric Binders," ChemSusChem, vol. 12, no. 12, pp. 2515–2539, 2019, doi:

10.1002/cssc.201900209.

[53] J. T. Li et al., “Water Soluble Binder, an Electrochemical Performance Booster for Electrode Materials with High Energy Density,” Adv. Energy Mater., vol. 7, no. 24, pp. 1–30, 2017, doi: 10.1002/aenm.201701185.

[54] L. Chen, X. Xie, J. Xie, K. Wang, and J. Yang, “Binder effect on cycling performance of silicon/carbon composite anodes for lithium ion batteries,” J. Appl. Electrochem., vol. 36, no. 10, pp. 1099–1104, 2006, doi: 10.1007/s10800-006-9191-2.

[55] K. Kierzek, “Influence of Binder Adhesion Ability on the Performance of Silicon/Carbon Composite as Li-Ion Battery Anode,” J. Mater. Eng. Perform., vol. 25, no. 6, pp. 2326–2330, 2016, doi: 10.1007/s11665-016-2083-7.

[56] Y. K. Jeong and J. W. Choi, “Mussel-Inspired Self-Healing Metallopolymers for Silicon Nanoparticle Anodes,” ACS Nano, vol. 13, no. 7, pp. 8364–8373, 2019, doi: 10.1021/acsnano.9b03837.

[57] D. Mazouzi, B. Lestriez, L. Roué, and D. Guyomard, “Silicon composite electrode with high capacity and long cycle life,” Electrochem. Solid-State Lett., vol. 12, no. 11, 2009, doi: 10.1149/1.3212894.

[58] N. Shimoi, M. Komatsu, and Y. Tanaka, “Selection of optimum binder for silicon powder anode in lithium-ion batteries based on the impact of its molecular structure on charge-discharge behavior,” Coatings, vol. 9, no. 11, 2019, doi: 10.3390/coatings9110732.

[59] P. Parikh et al., “Role of Polyacrylic Acid (PAA) Binder on the Solid Electrolyte Interphase in Silicon Anodes,” Chem. Mater., vol. 31, no. 7, pp. 2535–2544, 2019, doi: 10.1021/acs.chemmater.8b05020.

[60] K. Min et al., “Grafting Functional Groups in Polymeric Binder toward Enhancing Structural Integrity of Li x SiO2 Anode during Electrochemical Cycling,” J. Phys. Chem. C, vol. 122, no. 30, pp. 17190–17196, 2018, doi: 10.1021/acs.jpcc.8b03625.

[61] R. Guo, S. Zhang, H. Ying, W. Yang, J. Wang, and W. Han, “Preparation of an Amorphous Cross-Linked Binder for Silicon Anodes,” ChemSusChem, vol. 12, no. 21, pp. 4838–4845, 2019, doi: 10.1002/cssc.201902079.

[62] S. Huang, J. Ren, R. Liu, M. Yue, Y. Huang, and G. Yuan, “The progress of novel binder as a non-ignorable part to improve the performance of Si-based anodes for Li-ion batteries,” Int. J. Energy Res., vol. 42, no. 3, pp. 919–935, 2018, doi: 10.1002/er.3826.

[63] D. Munao, J. W. M. Van Erven, M. Valvo, E. Garcia-Tamayo, and E. M. Kelder, "Role of the binder on the failure mechanism of Si nano-composite electrodes for Li-ion batteries," J. Power Sources, vol. 196, no. 16, pp. 6695–6702, 2011, doi: 10.1016/j.jpowsour.2010.11.072.

[64] Z. A. Ghazi et al., "Key Aspects of Lithium Metal Anodes for Lithium Metal Batteries," Small, vol. 15, no. 32, pp. 1–26, 2019, doi: 10.1002/smll.201900687.

[65] G. G. Eshetu et al., "In-Depth Interfacial Chemistry and Reactivity Focused Investigation of Lithium-Imide- and Lithium-Imidazole-Based Electrolytes," ACS Appl. Mater. Interfaces, vol. 8, no. 25, pp. 16087–16100, 2016, doi: 10.1021/acsami.6b04406.

[66] M. Wu et al., "Toward an ideal polymer binder design for high-capacity battery anodes," J. Am. Chem. Soc., vol. 135, no. 32, pp. 12048–12056, 2013, doi: 10.1021/ja4054465.

[67] T. Li, J. Y. Yang, and S. G. Lu, "Effect of modified elastomeric binders on the electrochemical properties of silicon anodes for lithium-ion batteries," Int. J. Miner. Metall. Mater., vol. 19, no. 8, pp. 752–756, 2012, doi: 10.1007/s12613-012-0623-1.

[68] X. Zhu et al., "A Highly Stretchable Cross-Linked Polyacrylamide Hydrogel as an Effective Binder for Silicon and Sulfur Electrodes toward Durable Lithium-Ion Storage," Adv. Funct. Mater., vol. 28, no. 11, pp. 1–12, 2018, doi: 10.1002/adfm.201705015.

[69] A. Miranda et al., "A Comprehensive Study of Hydrolyzed Polyacrylamide as a Binder for Silicon Anodes," ACS Appl. Mater. Interfaces, vol. 11, no. 47, pp. 44090–44100, 2019, doi: 10.1021/acsami.9b13257.

[70] D. Lee, H. Park, A. Goliaszewski, Y. K. Byeun, T. Song, and U. Paik, "In Situ Cross-linked Carboxymethyl Cellulose-Polyethylene Glycol Binder for Improving the Long-Term Cycle Life of Silicon Anodes in Li Ion Batteries," Ind. Eng. Chem. Res., vol. 58, no. 19, pp. 8123–8130, 2019, doi: 10.1021/acs.iecr.9b00870.

[71] S. Choi, T. woo Kwon, A. Coskun, and J. W. Choi, "Highly elastic binders integrating polyrotaxanes for silicon microparticle anodes in lithium ion batteries," Science (80-.)., vol. 357, no. 6348, pp. 279–283, 2017, doi: 10.1126/science.aal4373.

[72] K. L. Browning, R. L. Sacci, M. Doucet, J. F. Browning, J. R. Kim, and G. M. Veith, "The Study of the Binder Poly(acrylic acid) and Its Role in Concomitant Solid-Electrolyte Interphase Formation on Si Anodes," ACS Appl. Mater. Interfaces, vol. 12, no. 8, pp. 10018–10030, 2020, doi: 10.1021/acsami.9b22382.

[73] Q. Huang, C. Wan, M. Loveridge, and R. Bhagat, “Partially Neutralized Polyacrylic Acid/Poly(vinyl alcohol) Blends as Effective Binders for High-Performance Silicon Anodes in Lithium-Ion Batteries,” ACS Appl. Energy Mater., vol. 1, no. 12, pp. 6890–6898, 2018, doi: 10.1021/acsaem.8b01277.

[74] Y. Bie, J. Yang, X. Liu, J. Wang, Y. Nuli, and W. Lu, “Polydopamine wrapping silicon cross-linked with polyacrylic acid as high-performance anode for lithium-ion batteries,” ACS Appl. Mater. Interfaces, vol. 8, no. 5, pp. 2899–2904, 2016, doi: 10.1021/acsami.5b10616.

[75] A. Urbanski et al., “An Efficient Two-Polymer Binder for High-Performance Silicon Nanoparticle-Based Lithium-Ion Batteries: A Systematic Case Study with Commercial Polyacrylic Acid and Polyvinyl Butyral Polymers,” J. Electrochem. Soc., vol. 166, no. 3, pp. A5275–A5286, 2019, doi: 10.1149/2.0371903jes.

[76] Y. Park et al., “A photo-cross-linkable polymeric binder for silicon anodes in lithium ion batteries,” RSC Adv., vol. 3, no. 31, pp. 12625–12630, 2013, doi: 10.1039/c3ra42447b.

[77] P. Parikh et al., “Role of Polyacrylic Acid (PAA) Binder on the Solid Electrolyte Interphase in Silicon Anodes,” Chem. Mater., vol. 31, no. 7, pp. 2535–2544, 2019, doi: 10.1021/acs.chemmater.8b05020.

[78] H. K. Park, B. S. Kong, and E. S. Oh, “Effect of high adhesive polyvinyl alcohol binder on the anodes of lithium ion batteries,” Electrochem. commun., vol. 13, no. 10, pp. 1051–1053, 2011, doi: 10.1016/j.elecom.2011.06.034.

[79] Q. D. Nguyen and K. H. Chung, “Frictional properties of polymer binders for Li-ion batteries,” Appl. Phys. Lett., vol. 116, no. 6, 2020, doi: 10.1063/1.5141495.

[80] L. Yue, L. Zhang, and H. Zhong, “Carboxymethyl chitosan: A new water soluble binder for Si anode of Li-ion batteries,” J. Power Sources, vol. 247, pp. 327–331, 2014, doi: 10.1016/j.jpowsour.2013.08.073.

[81] H. Lu et al., “Lignin as a binder material for eco-friendly Li-ion batteries,” Materials (Basel)., vol. 9, no. 3, pp. 1–17, 2016, doi: 10.3390/ma9030127.

[82] Y. Wang, D. Dang, D. Li, J. Hu, and Y. T. Cheng, “Influence of polymeric binders on mechanical properties and microstructure evolution of silicon composite electrodes during electrochemical cycling,” J. Power Sources, vol. 425, no. January, pp. 170–178, 2019, doi: 10.1016/j.jpowsour.2019.04.006.

[83] J. Xu, Q. Zhang, and Y.-T. Cheng, “High Capacity Silicon Electrodes with Nafion as Binders for Lithium-Ion Batteries,” J. Electrochem. Soc., vol. 163, no. 3, pp. A401–A405, 2016, doi: 10.1149/2.0261603jes.

[84] R. R. Garsuch et al., “Studies of Lithium-Exchanged Nafion as an Electrode Binder for Alloy Negatives in Lithium-Ion Batteries,” J. Electrochem. Soc., vol. 155, no. 10, p. A721, 2008, doi: 10.1149/1.2956964.

[85] J. Xu, L. Zhang, Y. Wang, T. Chen, M. Al-Shroofy, and Y. T. Cheng, “Unveiling the critical role of polymeric binders for silicon negative electrodes in lithium-ion full cells,” ACS Appl. Mater. Interfaces, vol. 9, no. 4, pp. 3562–3569, 2017, doi: 10.1021/acsami.6b11121.

[86] R. You et al., “An environmental friendly cross-linked polysaccharide binder for silicon anode in lithium-ion batteries,” Ionics (Kiel)., vol. 25, no. 9, pp. 4109–4118, 2019, doi: 10.1007/s11581-019-02972-z.

[87] Z. Chen, C. Wang, J. Lopez, Z. Lu, Y. Cui, and Z. Bao, “High-areal-capacity silicon electrodes with low-cost silicon particles based on spatial control of self-healing binder,” Adv. Energy Mater., vol. 5, no. 8, pp. 1–8, 2015, doi: 10.1002/aenm.201401826.

[88] M. T. Jeena et al., “Multifunctional molecular design as an efficient polymeric binder for silicon anodes in lithium-ion batteries,” ACS Appl. Mater. Interfaces, vol. 6, no. 20, pp. 18001–18007, 2014, doi: 10.1021/am504854x.

[89] Z. M. Huang, Y. Z. Zhang, M. Kotaki, and S. Ramakrishna, “A review on polymer nanofibers by electrospinning and their applications in nanocomposites,” Compos. Sci. Technol., vol. 63, no. 15, pp. 2223–2253, 2003, doi: 10.1016/S0266-3538(03)00178-7.

[90] Y. Zhmayev et al., “Controlling the Placement of Spherical Nanoparticles in Electrically Driven Polymer Jets and its Application to Li-Ion Battery Anodes,” Small, vol. 12, no. 40, pp. 5543–5553, 2016, doi: 10.1002/smll.201601878.

[91] L. Fei et al., “Graphene Oxide Involved Air-Controlled Electrospray for Uniform, Fast, Instantly Dry, and Binder-Free Electrode Fabrication,” ACS Appl. Mater. Interfaces, vol. 9, no. 11, pp. 9738–9746, 2017, doi: 10.1021/acsami.7b00087.

CHAPTER 2 : EFFECT OF BINDER MOLECULAR WEIGHT ON SILICON ANODES FOR LITHIUM-ION BATTERIES

Introduction:

Batteries are currently gaining attention increasingly in diverse fields of application, from cars to microchips [1], [2]. Batteries are simple conceptually, and yet their development has progressed much slower when compared to the progress in other devices. As a result, they still form the heaviest, costliest components of any electronic device. This slow progress has hindered the deployment of electric vehicles (EV). The current EV market is stalled by the range anxiety issue. Range anxiety is the fear that a vehicle has insufficient range to reach its destination thereby stranding the vehicle's occupants [3]. Range anxiety is primarily used in reference to battery electric vehicles (BEVs) and is considered to be a major barrier to large scale adoption of electric vehicles [4]. The current lithium-ion technology is at its limit and thus there needs to be a significant upgrade in terms of volumetric and gravimetric energy density for their application in Electric vehicles [5], [6]. In recent times, silicon has emerged as one of the promising candidates for electrode materials due to its extremely high theoretical capacity (4200 mAh/g) which almost 10 times that of commercial graphite anodes (372 mAh/g) [7]–[10]. Additionally, silicon shows beneficial intrinsic properties, like low delithiation potential (vs Li/Li^+ at 0.4V), and are less likely to form dendrites at high current density [11]. Moreover, silicon is the 2^{nd} most abundant material on the earth's crust and is non-toxic making it a much safer choice of electrode material [12]. However, silicon undergoes huge volume expansion during charge/discharge because of its inherent ability to store a lot of lithium ions (4.4 Li ions per Si atom)[13]. This creates huge stress in the electrode and leads to the pulverization of the electrode material. Pulverization further leads to loss of electrical contact among active material contributing to the rapid capacity fading [6]. Moreover, the active materials undergo delamination from the electrode surface due to the repeated

volume expansion [14]. Additionally, the cracking of Si particles causes the formation of an unstable Solid Electrolyte Interphase (SEI) [15]. SEI is a thin passivating layer formed at the electrode-electrolyte interphase at low potentials (> 1V). Due to repeated volume changes, the SEI layer is broken down over multiple cycles resulting in a thicker passivating film which increases the impedance of the cell. All the above-mentioned problems synergistically lead to the rapid failure of silicon-based anodes. In addition to the above-mentioned issues, silicon inherently has a very low conductivity impeding its use in high power density applications.

The primary goal to tackle the above issues is to accommodate the large volume change during cycling, to facilitate the electrochemical reaction by providing fast Li-ion diffusion pathways and to improve the conductivity of the whole system. There have been various modifications to solve these issues mostly involving nano silicon and tweaking their geometries (0D [16], 1D [17], 2D[18] and 3D [17]), using graphene networks to act as a mechanical buffer against volume expansion and creating porous structures to accommodate volume expansion. Consequently, attention is moving beyond the active electrode components to the overall electrode structure. Researchers are slowly realizing the potential of binder and are optimizing the binder component. Binders are a key component, especially in silicon-based anodes to counter the high volume expansion by providing mechanical stability to the electrode [19]. For application in Si-based anodes, a binder must possess the following functional roles[12], [20]: (1) Maintain mechanical integrity, (2) Form homogeneous slurry, (3) Weak interactions with electrolyte, (4) Good binding capability with electrode components, (5) Must be electrochemically stable, low cost and eco-friendly.

Currently, Poly(vinylidene difluoride) (PVDF) [21] is the commercially used binder. Its application in batteries is mainly owing to its electrochemically stable nature, its binding

capability, and its ability to allow facile transportation of Li. However, PVDF uses toxic and expensive solvents, and hence there is a slow shift against its use in commercial applications [22], [23]. On the other hand, aqueous binders - due to their environmentally benign nature, are gaining more attention in this domain.

The earliest attempts to address the poor mechanical stability and irreversible capacity loss in silicon anodes focused on improving the elasticity of the binder [24]. This idea gained a lot of attention since it is the binder that endures a large amount of strain in Silicon anodes to accommodate volume expansion. Binders like Styrene-butadiene (SBR) [25], polyacrylamide [26] gained a lot of attention due to their elastic behavior. After numerous research publications, researchers concluded that elasticity may not be the single most important factor to control volume expansion [27]. The focus shifted towards binders that can produce a strong adhesion with silicon particles [28]. A good adhesion ability between Si and binder prevents the isolation and delamination of Si particles from the current collector [29]. Usually, these strong adhesion characteristics are exhibited by the binders that contain -COOH, -OH,-COO and -NH_2 groups. These groups bind directly with the Si surface [30], [31]. Carboxy-methyl cellulose (CMC) [32]–[36] binds with Si through hydrogen bonding which rendered better stability and performance compared to elastic binders. Poly(acrylic) acid (PAA) is also an example of a strongly adhesive polymer binder [37]. Researchers reported that these binders form covalent links to siloxy (SiOH) groups present at the surface of Silicon dioxide (SiO_2) layer around the active Si particles[38]. In this way, the Si particles remain linked to the binder thereby maintaining the cohesion despite large volume changes. Most of these polymers are commercial polymers developed for other applications and there is a gap in understanding of factors that affect the binder characteristics in this application. The PAA binders have several advantages like low cost and excellent binding

capability in addition to its water-soluble and green nature [33], [39]. However, some of the properties of the binders are still not understood. Despite its existence in several molecular weight, there is still no conclusive evidence on the optimal molecular weight of PAA for its application in battery materials [28]. It is well known that the molecular weight of a polymer is one of the most important factors that control their physiochemical properties like, strength [22], stiffness, adhesion [28], viscosity, etc. (Example: Fig 2.1 shows a clear difference in viscosities of the 3 binders just by visualizing the solutions). The development of such binders for application in Si-based anodes is hindered by the lack of knowledge of their mechanism and its characteristic properties. In this chapter of the thesis, we aim to study the effect of molecular weight of poly(acrylic)acid - PAA binder using 3 different molecular weights (450,000, 1.25 million, and 3 million) and its influence on the electrochemical performance of Silicon/Graphene anodes.

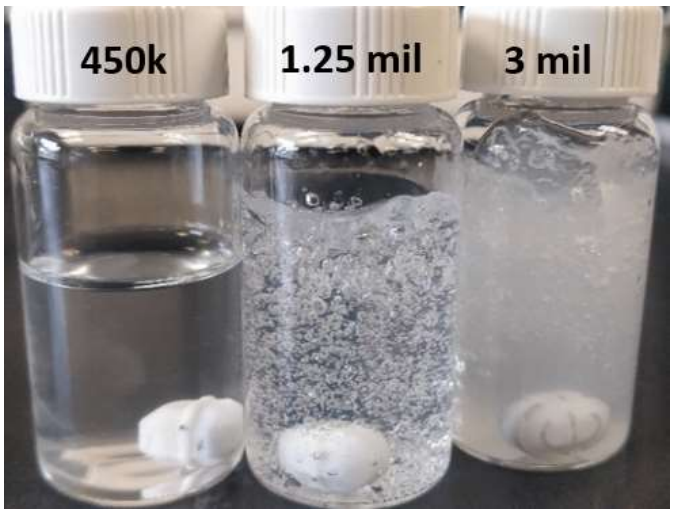

Fig 2.1 Visualization of difference in viscosities of 3 binder solutions

In this thesis, we use an air-controlled electrospray method to facilitate a scalable and an economic method of fabricating silicon anodes. Air controlled electrospraying involves the use of a voltage source to atomize a liquid solution in the syringe[41]–[43]. These liquid droplets are

driven to the collector by air pressure to quicken the process and remove further drying steps. Fig 2.2 shows the schematic representation of the process. The liquid solution comprising of silicon, graphene, and poly(acrylic) acid (PAA) was pumped through the nozzle under the influence of the electric field and high air pressure to obtain the desired silicon anode. High extensional forces imposed on the droplet by application of electric field and the high-pressure airflow ensures the formation of a uniform dispersion of the Si nanoparticles throughout the composite electrode. The resulting electrodes are stored in a dry vacuum over for 3 days until further electrode processing.

Experimental Section:

Preparation of electrospraying solution:

Preparation of Silicon/Graphene/450k PAA composite via Air-controlled Electrospray:

Initially, 0.4g of 450k poly(acrylic) acid (PAA, Sigma Aldrich) was dissolved in 10g of water and this mixture was left for stirring overnight. To a separate vial, 0.15g of Si (US Research Nanomaterials c.a. 30-70nm) was added to 3.6g of water and was stirred for 10 minutes. To this mixture, about 0.65g of the prepared PAA solution (4% wt) was added and was allowed to stir under room temperature for 4 hours. This mixture is then sonicated for 30 minutes and 2.7g of Graphene dispersion in water (5% wt, ACS) was added. This mixture was further allowed to stir for 4 hours and sonicated for 30 minutes. Then another 0.65g of PAA solution is added to the mixture and .allowed to stir for 30 minutes. The solution was then pumped from the syringe at a flow rate of 0.05ml/minute and sprayed on to a copper disk that was placed at a distance of 20cm away from the tip of the nozzle. To achieve good atomization of droplets and proper dispersion of the solution, a voltage of 20kV was supplied to the outer nozzle by the power supply in addition to the air pressure (25 psi) supplied through the inner nozzle. The resulting droplets from the spray

form a uniform dry layer of active material on the surface of the copper disk. This electrode was dried in a vacuum oven for 3 days before testing them in coin cells.

Preparation of Silicon/Graphene/1.25mil PAA composite via Air-controlled Electrospray:

Initially, 0.2g of 1.25million poly(acrylic) acid (PAA, Sigma Aldrich) was dissolved in 10g of water and this mixture was left for stirring overnight. To a separate vial, 0.2g of Si (US Research Nanomaterials c.a. 30-70nm) was added to 3.7g of water and was stirred for 10 minutes. To this mixture, about 1.6g of the prepared PAA solution (2% wt) was added and was allowed to stir under room temperature for 4 hours. This mixture is then sonicated for 30 minutes and 4.8g of Graphene dispersion in water (5% wt, ACS) was added. This mixture was further allowed to stir for 4 hours and sonicated for 30 minutes. Then another 1.6g of PAA solution is added to the mixture and allowed to stir for 30 minutes. The solution was then pumped from the syringe at a flow rate of 0.35ml/minute and sprayed on to a copper disk that was placed at a distance of 22cm away from the tip of the nozzle. To achieve good atomization of droplets and proper dispersion of the solution, a voltage of 25kV was supplied to the outer nozzle by the power supply in addition to the air pressure (25 psi) supplied through the inner nozzle. The resulting droplets from the spray form a uniform dry layer of active material on the surface of the copper disk. This electrode was dried in a vacuum oven for 3 days before testing them in coin cells.

Preparation of Silicon/Graphene/3 mil PAA composite via Air-controlled Electrospray:

Initially, 0.1g of 3 million poly(acrylic) acid (PAA, Sigma Aldrich) was dissolved in 10g of water and this mixture was left for stirring overnight. To a separate vial, 0.2g of Si (US Research Nanomaterials c.a. 30-70nm) was added to 1.5g of water and was stirred for 10 minutes. To this mixture, about 2.5g of the prepared PAA solution (1% wt) was added and was allowed to stir under

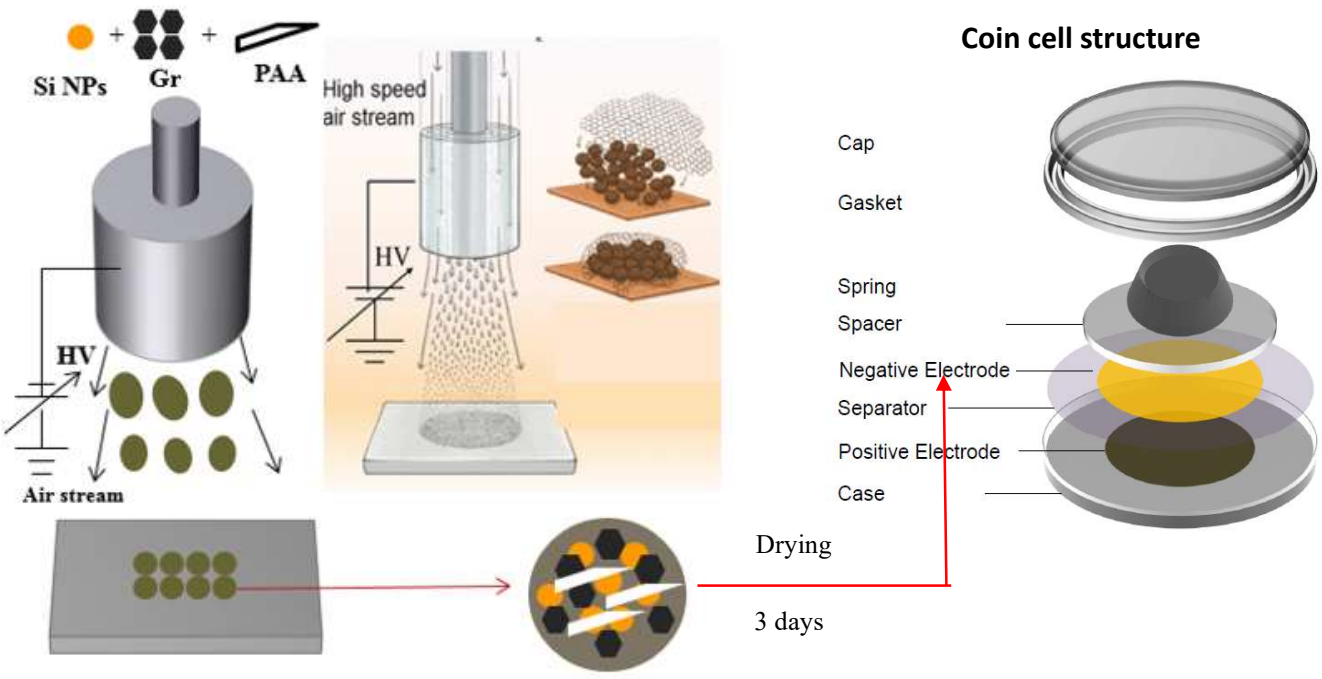

Fig 2.2: Schematic representation of electrode fabrication

room temperature for 4 hours. This mixture is then sonicated for 30 minutes and 3.4g of Graphene dispersion in water (5% wt, ACS) was added. This mixture was further allowed to stir for 4 hours and sonicated for 30 minutes. Then another 2.5g of PAA solution is added to the mixture and allowed to stir for 30 minutes. The solution was then pumped from the syringe at a flow rate of 0.25ml/minute and sprayed on to a copper disk that was placed at a distance of 25cm away from the tip of the nozzle. To achieve good atomization of droplets and proper dispersion of the solution, a voltage of 25kV was supplied to the outer nozzle by the power supply in addition to the air pressure (30 psi) supplied through the inner nozzle. The resulting droplets from the spray form a uniform dry layer of active material on the surface of the copper disk. This electrode was dried in a vacuum oven for 3 days before testing them in coin cells.

Material characterization of electrodes: The prepared composite electrodes were characterized by using Scanning Electron Microscope (SEM, Zeiss Gemini, and Tescan Mira-3) and Energy Dispersive Spectroscopy (Tescan Mira-3) to assess the morphology and component distribution of the electrode. Thermogravimetric analysis (TGA, TA instruments Q500) was used to characterize the composition (%) of the electrode. Thermogravimetric analysis was carried out over a temperature range from 20°C to 800°C at a ramp rate of 10°C/minute. Nitrogen and air flows are maintained at the flow rate of 40ml/min and 60ml/min, respectively.

Characterization of the polymer binder: The polymer binder strengths were analyzed using Dynamic Mechanical Analysis (DMA) (TA Instruments DMA Q800). Dynamical mechanical analysis (DMA) is the technique of applying a stress/strain to material and analyzing its response to the given stress. The polymer binder solutions were dropped cast into a mold and allowed to dry at room temperature. These films were then cut into the specified dimensions (15 x 3 x 0.1 mm). The cut films are then loaded into the two shafts of the DMA tool. A preload of 0.05N and a ramp rate of 0.5N/min were used to analyze the stress-strain curve of the polymer binders.

Battery fabrication and electrochemical measurements of Si/Graphene/PAA electrodes:

2032 type coin cells were made using the electrospray Silicon composite disks as the anode and lithium metal disc (MTI) was used as the counter electrode. A polythene material (Celgard) was used as the separator to test the performance of these half cells. A 1M $LiPF_6$ salt in ethylene carbonate, diethyl carbonate, and dimethyl carbonate in the ratio of 4:4:2 with 10% fluoroethylene carbonate were used as solvents inside half cells. All the capacities reported in this chapter were normalized by the total mass of active material (Silicon, Graphene, PAA) on the copper disk. Electrochemical properties of the cells were characterized by electrochemical impedance

spectroscopy (PARASAT 4000, Princeton Applied Research) and galvanostatic charge and discharge cycles (MTI). A voltage window of 0.01-1.5V Vs Li/Li^+ was applied to the half cells.

Results and discussion:

Characterization of Silicon-Graphene-PAA nanocomposite:

The air-controlled electrospraying process forms a dense coating with a uniform distribution of Silicon-Graphene and the binder (PAA) on the copper surface. The electrodes dry as soon as the droplets come into contact with the copper disk without additional drying steps. Graphene sheets act as conductive agents in our composite system improving the interconnectivity between the active materials in the electrode.

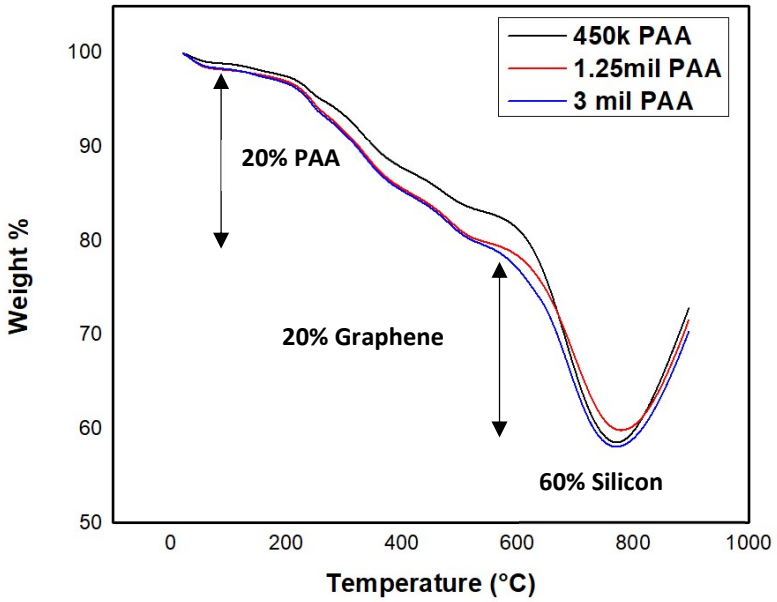

Fig 2.3: Thermogravimetric analysis (TGA) comparison of 3 binder systems

To compare different binder materials, it is essential to ensure all electrodes had the same composition of Silicon, Graphene, and PAA (60:20:20). Hence, they were subjected to thermogravimetric analysis (TGA). Fig 2.3 shows the comparison of TGA analysis for 450k, 1.25mil, and 3mil poly(acrylic) acid (PAA) with Silicon-Graphene composite. Fig 2.3 all the three

mixtures have a similar composition (60% Silicon, 20% Graphene, 20% PAA binder), thereby making a valid electrochemical comparison.

The morphology of the electrodes containing each binder was visualized using Scanning Electron Microscopy (SEM). Fig 2.4 a), b) and c) show the top view of electrodes containing 450k, 1.25 mil, and 3mil PAA binder along with Si-Graphene composite, respectively. All images are taken at a magnification of 20μm to make a valid comparison. It is apparent from the morphology images in Fig 2.4 that the binder molecular weight changes the morphology of the electrode. The morphological changes in the electrode show clear evidence that an increase in the molecular weight of the binder increases the aggregation of active materials. Fig 2.4 b) and c) (1.25 million and 3 million Mw PAA) show a significant aggregation when compared to that of Fig 2.4 a) (450k PAA). The morphology of these electrodes was observed at higher magnification (1 μm) to give a much clearer picture. Fig 2.5 a), b) and c) shows the higher magnification SEM images of Si-Graphene-Binder composite electrodes with different molecular weight binders. 450k PAA (Fig 2.5 a), shows an even distribution of Silicon and Graphene in the electrode. 1.25 million PAA (Fig 2.5 b), shows the uneven distribution of Si and Graphene, whereas 3 million PAA (Fig 2.5 c), shows clusters of Si particles with very high aggregation with very less graphene presence. This confirms the significant increase in aggregation as the molecular weight increases. This increased aggregation of active material in the electrodes could cause significant issues during the electrochemical cycling of the anodes.

Fig 2.6, 2.7, 2.8 shows the elemental distribution of Silicon, Graphene, and PAA through Energy Dispersive Spectroscopy (EDS). The images show the distribution of Si, C, and O corresponding to Silicon, Graphene, and poly(acrylic) acid. The images support our previous evidence exhibiting aggregation nature as the molecular weight of the polymer increases.

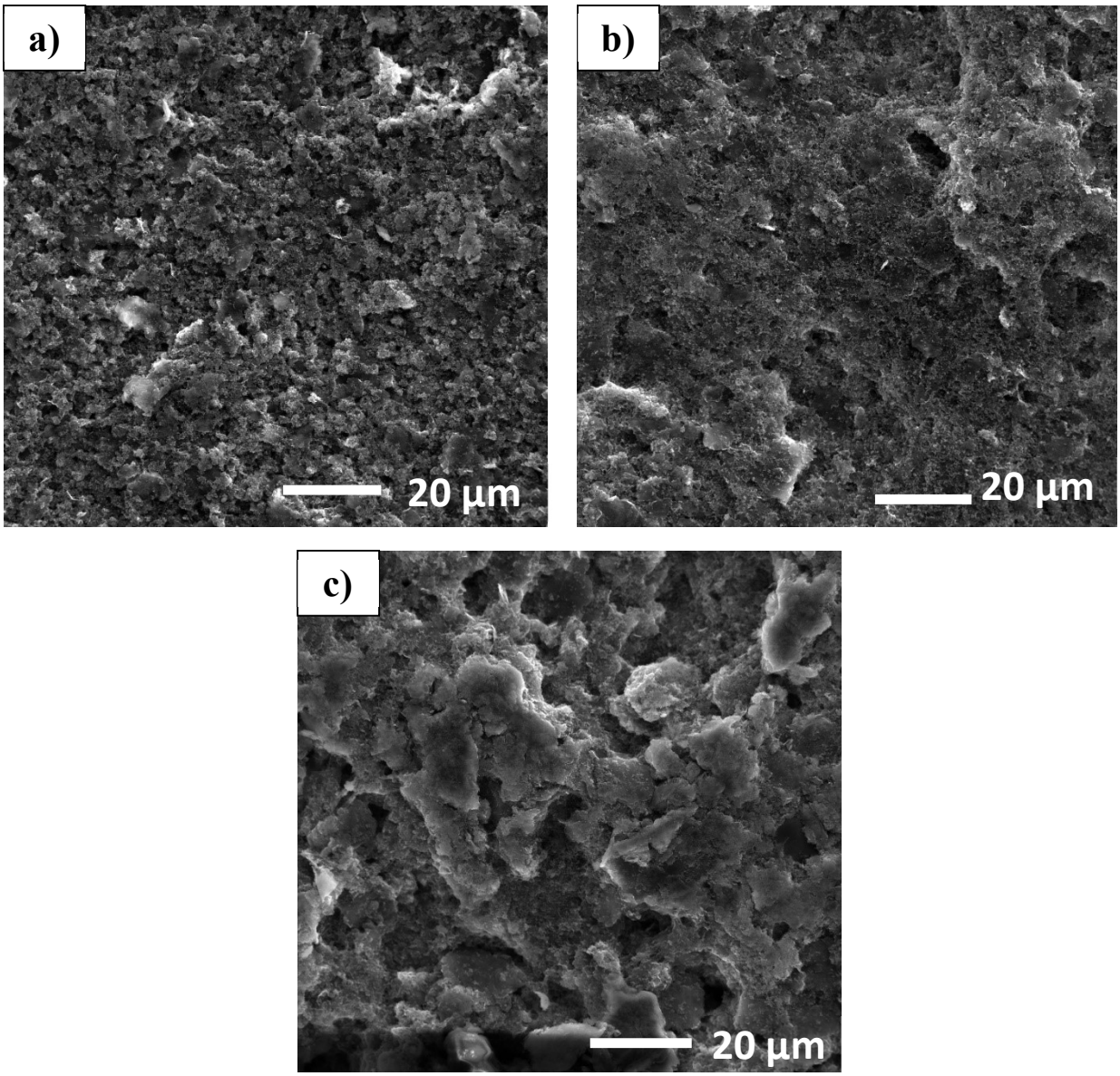

Fig 2.4 Low magnification (20 µm) SEM images of Si-Graphene-Binder electrode

a) 450k PAA b) 1.25million PAA c) 3million PAA

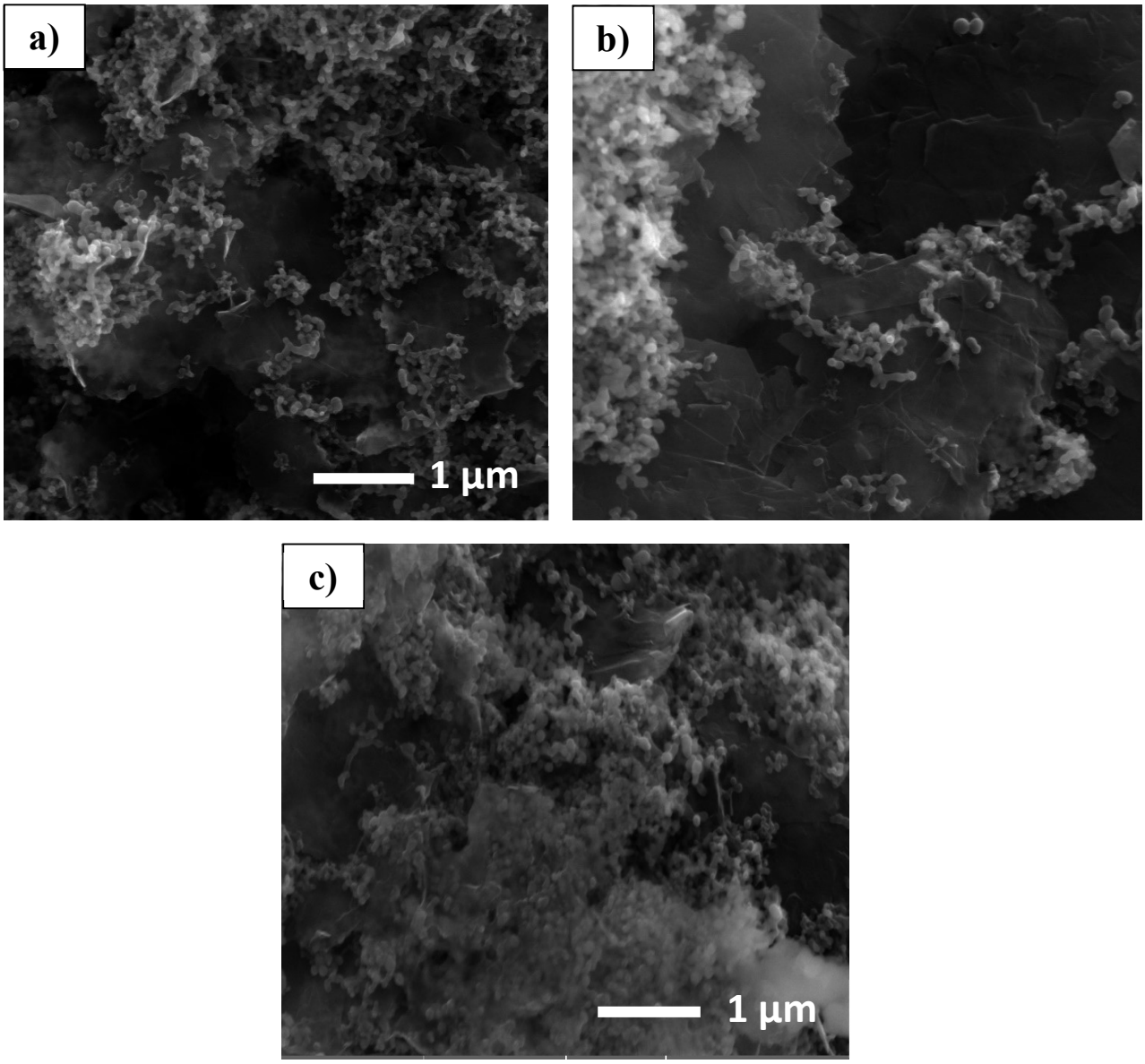

Fig 2.5 High magnification (1 µm) SEM images of Si-Graphene-Binder electrode a) 450k PAA b) 1.25million PAA c) 3million PAA

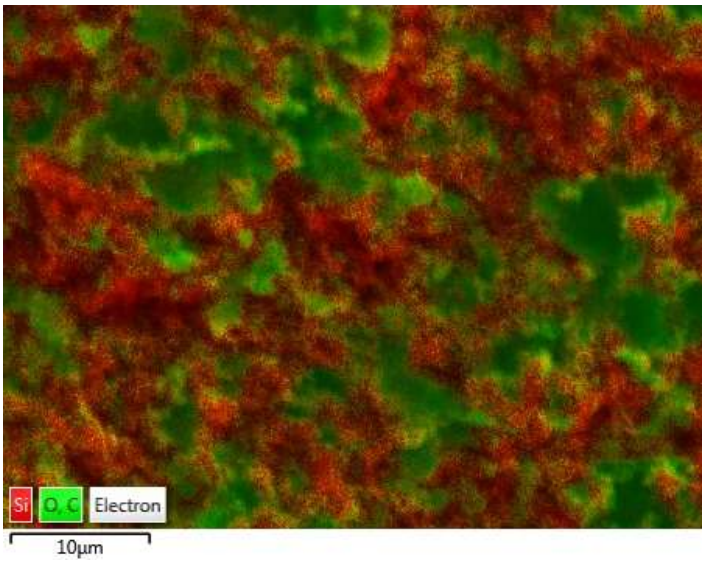

Fig 2.6 Energy Dispersive Spectroscopy (EDS) - Elemental mapping of electrode components of 450k PAA binder system showing the uniform distribution of electrode components

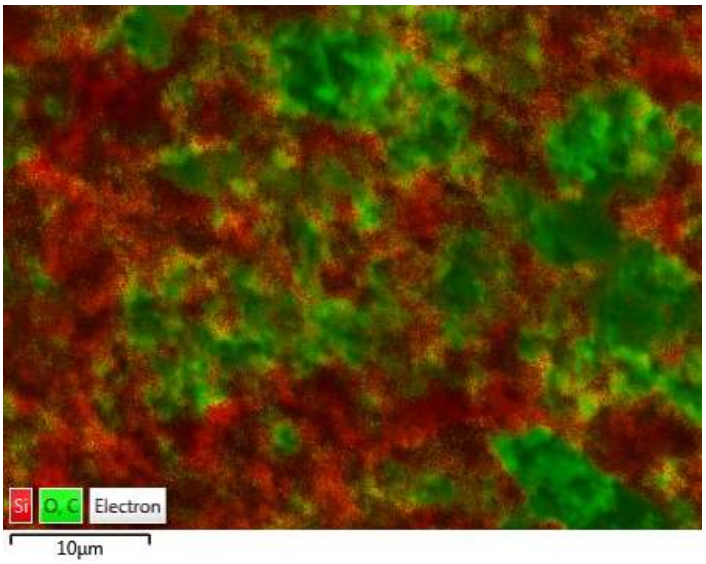

Fig 2.7 Energy Dispersive Spectroscopy (EDS) - Elemental mapping of electrode components of 1.25 mil PAA binder system showing the uneven distribution of electrode components

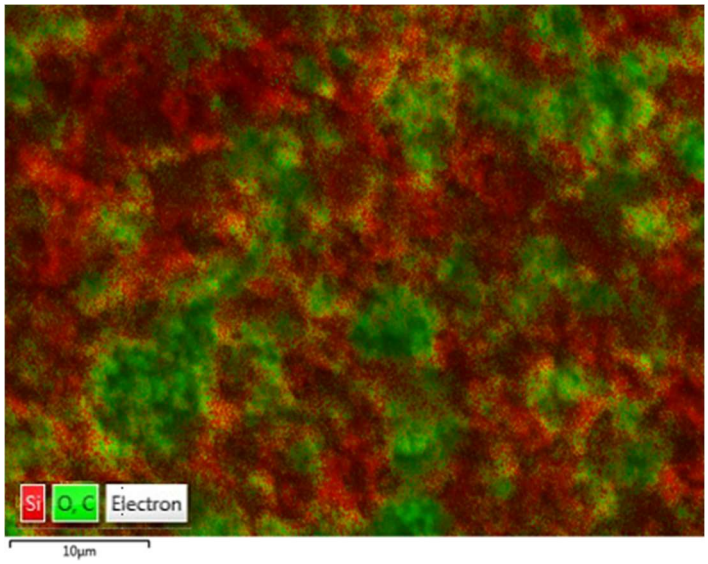

Fig 2.8 Energy Dispersive Spectroscopy (EDS) - Elemental mapping of electrode components of 3 mil PAA binder system showing aggregation of Silicon among the electrode components

Characterization of the polymer binder:

To understand the properties of the binder for the application in our anodes, an evaluation of the strength of the polymers was performed using Dynamical mechanical analysis (DMA). Polymer strips were mold and cut into specific dimensions (15 x 3 x 0.1 mm) and subjected to stress using a moving drive shaft. Based on their strengths, each polymer will have different fracture stress. DMA analysis was performed on polymer films of different M_w (450k, 1.25 mil, and 3 mil) PAA to test their difference in strengths. DMA results revealed that the polymer with a higher molecular weight had a better strength. Fig 2.9 shows the comparison of the stress-strain curve for the 3 different molecular weights of binders used in this system. The polymer with the high molecular weight (3mil) endures more stress and undergoes higher strain % when compared to the remaining two binders (450k and 1.25mil).

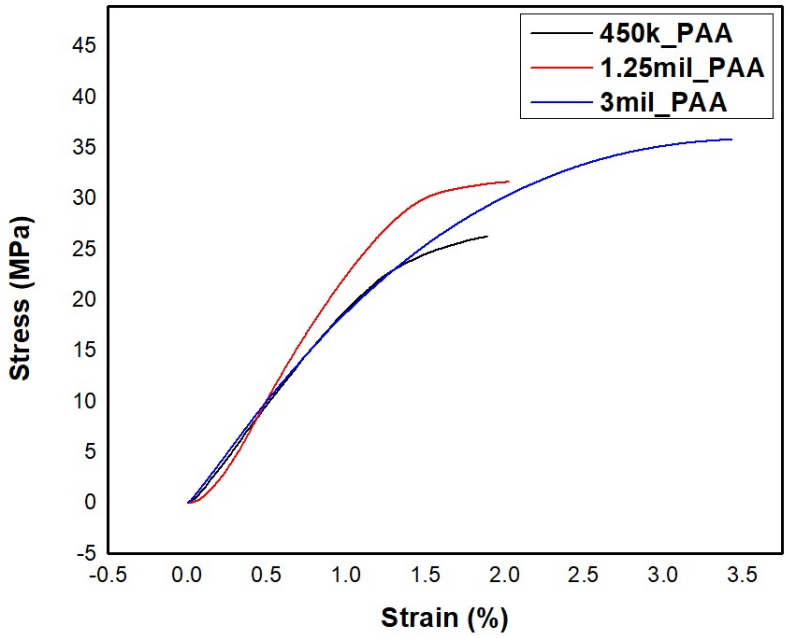

Fig 2.9 Comparison of strengths of binders using Dynamical Mechanical Analysis (DMA)

Table 2.1 Comparison of DMA results for the different molecular weight of PAA

DYNAMICAL MECHANICAL ANALYSIS		
BINDER	**STRESS (MPa)**	**STRAIN (%)**
450k PAA	26	1.85
1.25 mil PAA	31	2.0
3 mil PAA	37	3.5

From Table 2.1, it is evident that there is an increasing trend in the values of stress and strain with increasing molecular weight of the polymer. Higher molecular weight polymer increases the impact resistance of the material. Also, a higher molecular weight indicates the presence of increased chain entanglement. Therefore, to rupture, a higher number of polymer bonds need to be broken, and hence the higher molecular weight polymer can endure/absorb more stress/energy

before failing. Hence, we hypothesize that during the cycling of the electrode, the binder with higher molecular weight can endure more stress caused by Si during volume expansion and will have better capacity retention than lower molecular weights polymers (450k and 1.25 mil).

Electrochemical characterization of Silicon-Graphene-PAA nanocomposite electrode:

The electrodes fabricated in electrospraying were assembled in a 2032 coin-type half cells configuration (shown in Fig 2.2) and were galvanostatically charged and discharged for multiple cycles. Each of these cells was lithiated to a voltage of 1.5V and de-lithiated to a voltage of 0.01V and was made to undergo 5 formation cycles at 0.1C and then were allowed to undergo cycling for 200 cycles post-formation.

Fig 2.10 shows the comparison of capacity-voltage profile for the 3 different molecular weight binders used in the system. All the 3 cases show a very similar profile with a small plateau around 0.8V indicating the formation of SEI and then a larger plateau around 0.25V indicating Li insertion reactions with Si. The 1st cycle delithiation capacity for Si/Gr/450k PAA was 1580 mAh/g while that for Si/Gr/1.25mil PAA was 1330 mAh/g and for Si/Gr/3mil PAA was 1240 mAh/g. The trend was observable, as the molecular weight of the polymer binder increases, the specific capacity reduces. The utilization of silicon is lesser when the molecular weight of the polymer binder increases. The lesser Si is utilized, the lower the capacity of the anode system. This loss in the utilization of Si can be attributed to the formation of aggregates that were visible in the morphological visualization through SEM (Fig 2.4 and Fig 2.5). The 1st cycle coulombic efficiency for 450k, 1.25mil, and 3mil PAA binder systems are 85%, 72%, and 70% respectively (Table 2.2). This decrease in coulombic efficiency is due to the presence of excess silicon on the surface of the electrode visualized through– EDS (Fig 2.8). Additional reaction sites on the surface of Si cause the excess formation of SEI leading to a loss in ICE.

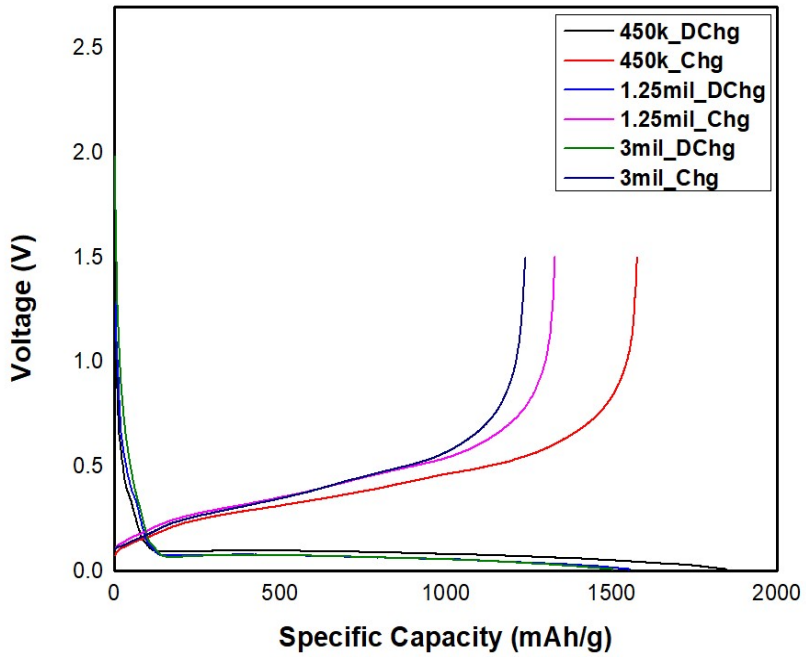

Fig 2.10 Comparison of formation cycles of PAA with 3 different molecular weights

Table 2.2 Comparison of formation cycle of PAA with 3 different molecular weights

FORMATION CYCLE – PAA BINDER COMPARISON			
Binder	**450k**	**1.25mil**	**3mil**
Charge Capacity (mAh/g)	1577	1328	1239
Discharge Capacity (mAh/g)	1847	1554	1503
Initial Coulombic Efficiency (%)	85.5	84	82
Si Utilization (%)	85	72	70

To confirm the effect of aggregation on the capacity of the electrodes, binder solutions with different concentrations were prepared. Two different concentrations of each polymer binder were

tested to determine if the concentration of binder affected the electrochemical performance. In our tests, we used two solutions of 1.25 million PAA, 2% and 1% by wt. and two solutions of 3 million PAA 1% and 0.75% by wt. A similar electrospraying method was used to fabricate the anode and the cells were tested under similar electrochemical conditions. From Fig 2.11, it is seen that 2% wt. (1.25 mil) the solution has a lower capacity when compared to that of 1% wt. (1.25 mil) solution. The binder concentration has a significant effect on the solution characteristics which in turn affect them electrochemically. The higher concentration of the binder makes the electrode slurry thicker thereby causing chunks of electrode material formed during electrospraying. This further leads to a significant loss in capacity. A similar trend is observed in the comparison of 3 million PAA confirming the effect.

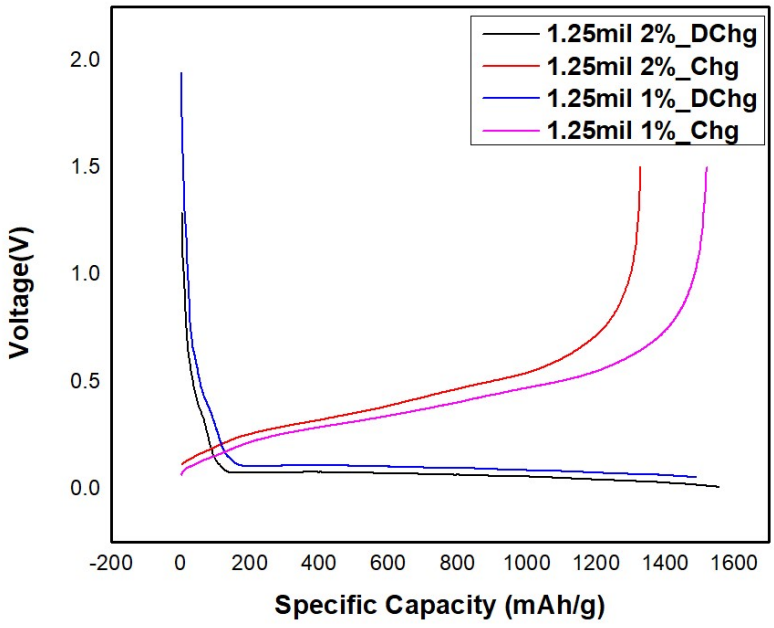

Fig 2.11 Comparison of formation cycle of 1.25 mil PAA with a different binder concentration

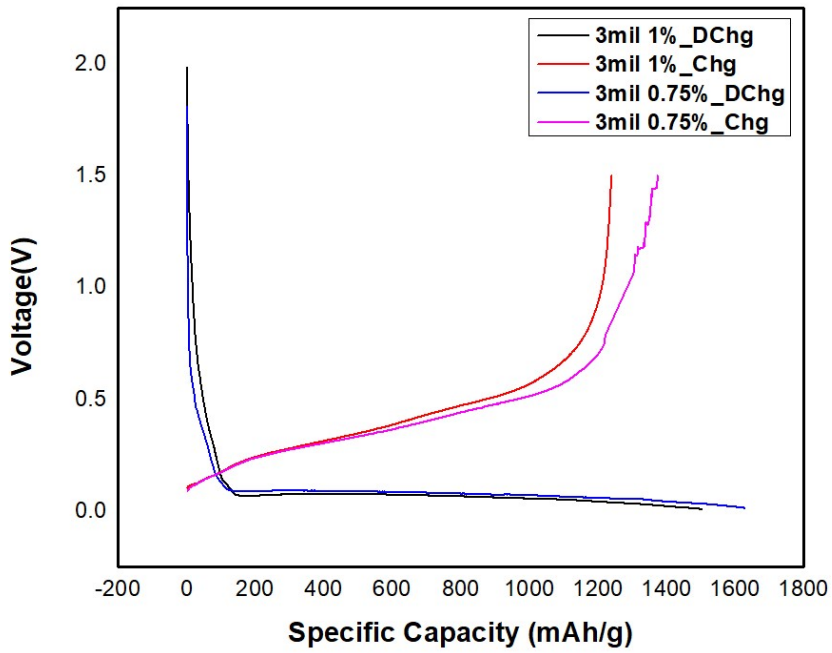

Fig 2.12 Comparison of formation cycle of 3 mil PAA with a different binder concentration

Table 2.3 Comparison of formation cycle of PAA with different concentrations

COMPARISON OF FORMATION CYCLES WITH DIFFERENT CONCENTRATIONS				
Binder used	**1.25 million**		**3 million**	
Binder concentration	**1%**	**2%**	**0.75%**	**1%**
Charge Capacity (mAh/g)	1520	1328	1374	1239
Discharge Capacity (mAh/g)	1836	1554	1627	1503
Initial Coulombic Efficiency (%)	83	84	82	83
Si Utilization (%)	85	72	75	70

The cyclic performance of the 3 binder systems is represented in Fig 2.13. The cells are all cycled at 0.3C for 200 cycles. The 450k binder starts at a higher capacity of 1560mAh/g, whereas the

1.25mil PAA starts at a discharge capacity of 1430 mAh/g, and 3 mil PAA begins at a discharge capacity of 1360 mAh/g. As discussed earlier, this decrease in discharge capacities can be associated with the aggregation issues caused by higher molecular weight binders. Higher molecular weight binders are more viscous when dissolved in a solution and are harder to disperse too. However, the retention capabilities are much better for higher molecular weight binders when compared to the lower molecular weight ones. After 200 cycles, 3 mil PAA binder system retains nearly 62% of its original capacity whereas for 1.25mil PAA the capacity retention is 57% and for 450k PAA the capacity retention is just 46%. Higher molecular weight PAA binder endures more stress during lithiation/de-lithiation and thereby performs better during long term cycling with a capacity retention of 62%. Fig 2.13 shows the comparison of capacity retention curves of the three polymer binder systems.

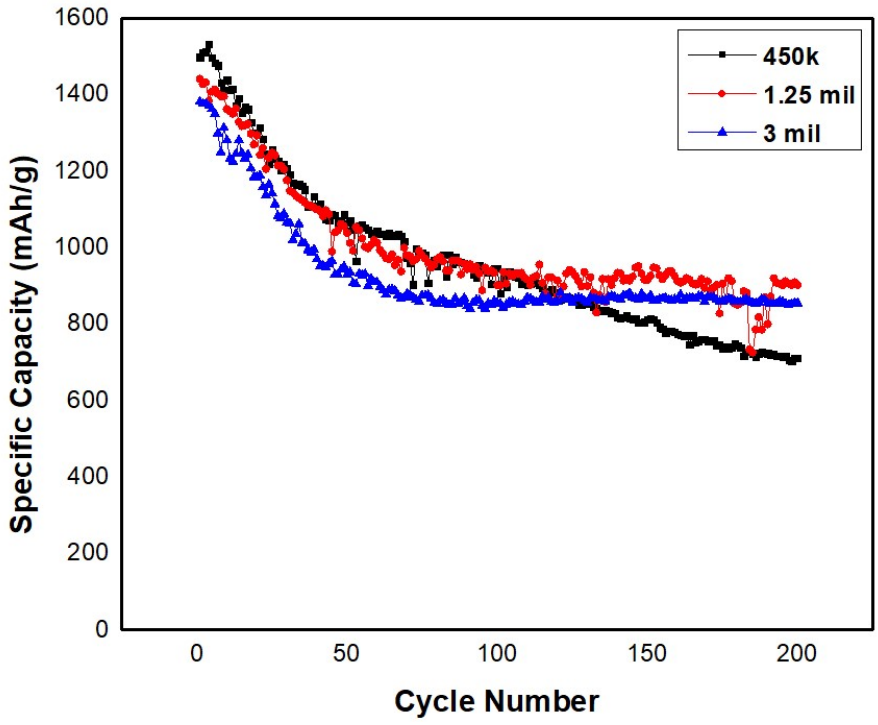

Fig 2.13 Comparison of cycle retention profile of PAA with 3 different molecular weights

The results obtained in cycling are coherent to the results obtained in DMA. In DMA, the polymer with the higher molecular weight endured more stress. Similarly, here the 3 mil PAA endured more stress when compared to the other PAA's. Higher molecular weight polymer increases the impact resistance of the material and has increased chain entanglement. Therefore, to rupture, a higher number of polymer bonds need to be broken, and hence the higher molecular weight polymer endures more stress before failing.

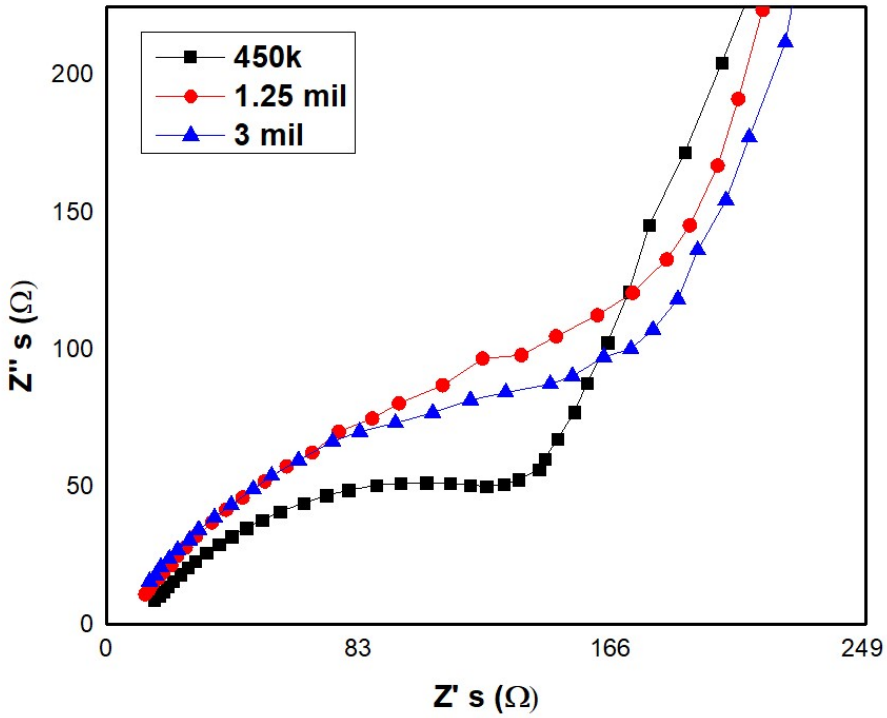

Fig 2.14 Comparison of Nyquist plots of systems containing 3 different molecular weights of Poly (acrylic) acid before formation

Figure 2.14 shows the electrochemical impedance spectroscopy for systems containing 3 different molecular weights of PAA. As seen in the figure 2.14 the charge transfer resistance (R_{ct}) for binder that have low molecular weight is lesser to that of the charge transfer resistance of higher molecular weight polymer binders. Generally, lithium ion transport in polymers progresses *through chain*

hopping. Lower molecular weight binders have smaller chains and hence, lithium ion transport is easier in the case of 450k PAA. Larger molecular weight polymers have much larger chains that makes the transport of lithium ion difficult thereby increasing the charge transfer resistance.

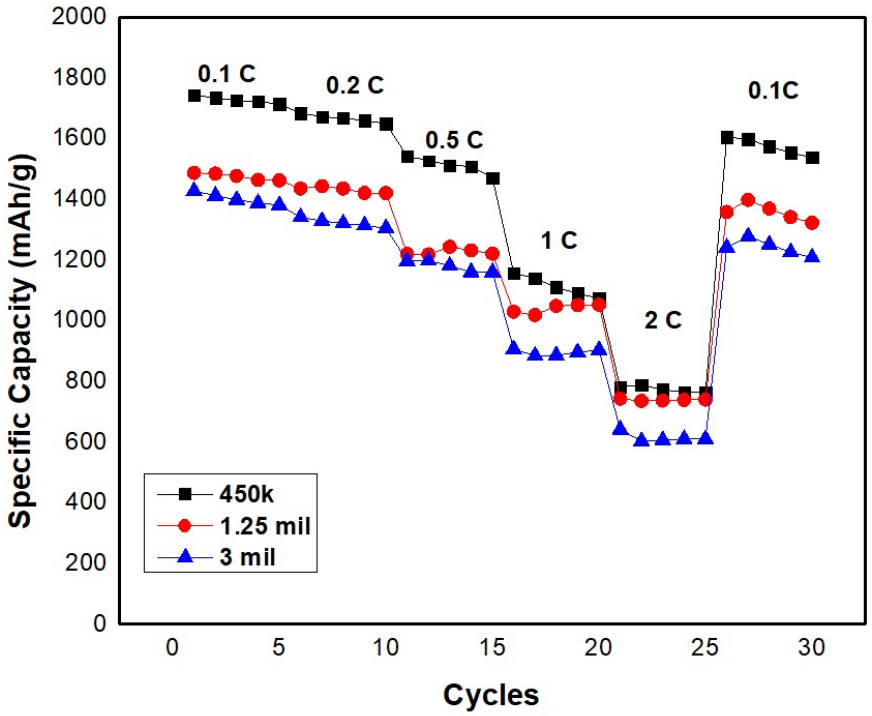

Fig 2.15 Rate capabilities of system involving 3 different molecular weight of PAA

Fig 2.15 shows the rate capability comparison of the 3 systems involving different molecular weight of binders. Results show that 450k PAA binder shows a significant difference in capacity at low charge rates (0.1C, 0.2C and 0.5C). Even at high charge rates, systems containing binders with lesser molecular weight outperforms the one with a higher molecular weight. This is due to the poor transport of Li ions observed in higher molecular weight binders. The uneven distribution of electrode components observed in the electrode morphology (Fig 2.4(c)) deters the rate at which Li ions are transported. Hence, systems involving polymers having lesser molecular weight outperforms those with higher molecular weight.

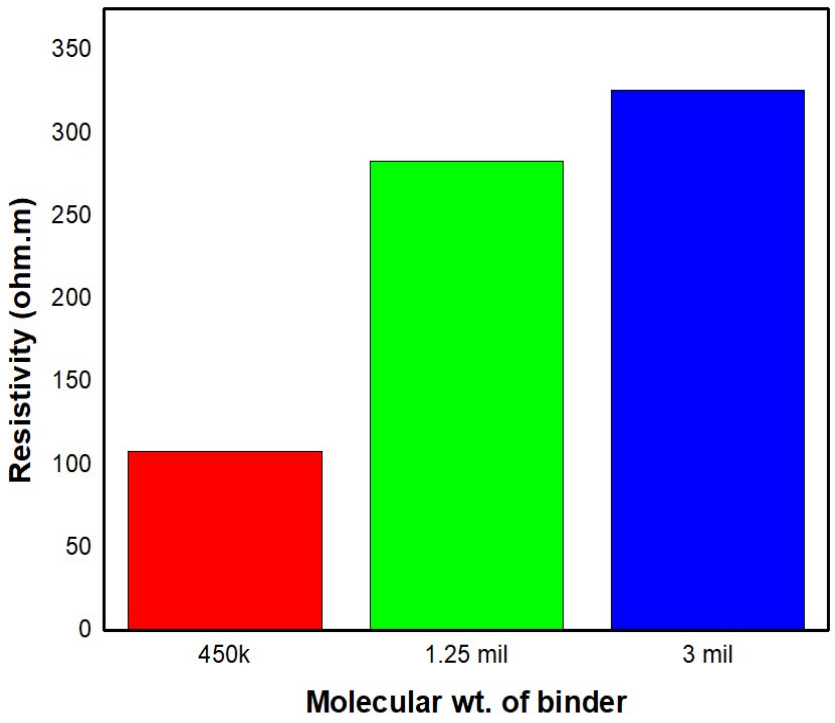

Fig 2.16 Four point probe resistivity measurements of systems involving 3 different molecular weights of PAA binder

Results from four-point probe measurements (Fig 2.16) show that electrodes containing lower molecular weight binder have lesser electrical resistivity. This is synonymous with the results obtained in rate capability and EIS. Binders having lower molecular weight show even distribution of electrode components in EDS (Fig 2.6) depicting good system interconnectivity thereby improving transport properties. Whereas systems involving higher molecular weight binders show an uneven distribution of electrode components in EDS (Fig 2.7 and 2.8) exposing more Si on the surface that contributes to its increased system resistance.

Conclusion:

In summary, this study presents a facile scalable fabrication method of silicon-graphene-PAA complex anodes via air-controlled electrospraying. A thin coating of the electrode material comprising of SiNPs/PAA/Graphene was obtained by directly spraying the active material slurry with the application of high air pressure and voltage. Utilization of PAA, an aqueous binder eliminated the use of toxic solvents. Different molecular weights (450k, 1.25mil, and 3mil) of PAA binders were characterized and their properties were analyzed. The resulting electrodes from the electrospraying showed a significant difference in morphologies (SEM and EDS) with the higher molecular PAA binder (3mil) forming aggregates of silicon. The formation cycles showed a drop in the capacity as the molecular weight of the binder increases. Combining the morphological and the electrochemical results, it is evident that aggregation caused by the increased viscosity in higher molecular weight binder deters the capacity of these electrodes. Dynamical mechanical analysis (DMA) showed that polymers having higher molecular weight endure more stress. Results from cycling showed high capacity retention (62%) for PAA with higher molecular weight, thus analogous to the results from DMA. However, results from electrochemical impedance and rate capability, show a drastic difference in the performance of the system. Electrodes involving lower molecular weight binders perform better at high charge rates and have less charge transfer resistance. Therefore, binders with higher molecular weight have high capacity retention but have dispersion issues that affect their electrochemical performance. Hence, if the dispersion issues (aggregation) are taken care off and the system interconnectivity is improved, the application of high molecular weight binders would provide to be a valuable asset in containing the volume expansion of Silicon in Si-based anodes for lithium-ion batteries.

References:

[1] M. Li, J. Lu, Z. Chen, and K. Amine, "30 Years of Lithium-Ion Batteries," Adv. Mater., vol. 30, no. 33, pp. 1–24, 2018, doi: 10.1002/adma.201800561.

[2] T. Kim, W. Song, D. Y. Son, L. K. Ono, and Y. Qi, "Lithium-ion batteries: outlook on present, future, and hybridized technologies," J. Mater. Chem. A, vol. 7, no. 7, pp. 2942–2964, 2019, doi: 10.1039/C8TA10513H.

[3] N. Rauh, T. Franke, and J. F. Krems, "Understanding the impact of electric vehicle driving experience on range anxiety," Hum. Factors, vol. 57, no. 1, pp. 177–187, 2015, doi: 10.1177/0018720814546372.

[4] H. A. Bonges and A. C. Lusk, "Addressing electric vehicle (EV) sales and range anxiety through parking layout, policy and regulation," Transp. Res. Part A Policy Pract., vol. 83, pp. 63–73, 2016, doi: 10.1016/j.tra.2015.09.011.

[5] Y. Oumellal et al., "The failure mechanism of nano-sized Si-based negative electrodes for lithium ion batteries," J. Mater. Chem., vol. 21, no. 17, pp. 6201–6208, 2011, doi: 10.1039/c1jm10213c.

[6] J. Hou, S. Qu, M. Yang, and J. Zhang, "Materials and electrode engineering of high capacity anodes in lithium ion batteries," J. Power Sources, vol. 450, no. December 2019, p. 227697, 2020, doi: 10.1016/j.jpowsour.2019.227697.

[7] A. Casimir, H. Zhang, O. Ogoke, J. C. Amine, J. Lu, and G. Wu, "Silicon-based anodes for lithium-ion batteries: Effectiveness of materials synthesis and electrode preparation," Nano Energy, vol. 27, pp. 359–376, 2016, doi: 10.1016/j.nanoen.2016.07.023.

[8] N. Yuca and Ü. Çolak, "A facile and functional process to enhance electrochemical performance of silicon anode in lithium ion batteries," Electrochim. Acta, vol. 222, pp. 1538–1544, 2016, doi: 10.1016/j.electacta.2016.11.136.

[9] C. Erk, T. Brezesinski, H. Sommer, R. Schneider, and J. Janek, "Toward silicon anodes for next-generation lithium ion batteries: A comparative performance study of various polymer binders and silicon nanopowders," ACS Appl. Mater. Interfaces, vol. 5, no. 15,

pp. 7299–7307, 2013, doi: 10.1021/am401642c.

[10] C. P. Opsel, B. Graeme, and P. G. Blake, “Silicon based high performance Anode Materials for Next Generation Li-Ion Batteries,” pp. 1–13, [Online]. Available: http://fse.studenttheses.ub.rug.nl/17294/1/mNANO_2018_PopselC.pdf.

[11] Q. Zhang, X. Xiao, W. Zhou, Y. T. Cheng, and M. W. Verbrugge, “Toward high cycle efficiency of silicon-based negative electrodes by designing the solid electrolyte interphase,” Adv. Energy Mater., vol. 5, no. 5, pp. 1–6, 2015, doi: 10.1002/aenm.201401398.

[12] G. G. Eshetu and E. Figgemeier, “Confronting the Challenges of Next-Generation Silicon Anode-Based Lithium-Ion Batteries: Role of Designer Electrolyte Additives and Polymeric Binders,” ChemSusChem, vol. 12, no. 12, pp. 2515–2539, 2019, doi: 10.1002/cssc.201900209.

[13] J. Oh, D. Jin, K. Kim, D. Song, Y. M. Lee, and M. H. Ryou, “Improving the Cycling Performance of Lithium-Ion Battery Si/Graphite Anodes Using a Soluble Polyimide Binder,” ACS Omega, vol. 2, no. 11, pp. 8438–8444, 2017, doi: 10.1021/acsomega.7b01365.

[14] J. Chen, J. Liu, Y. Qi, T. Sun, and X. Li, “Unveiling the Roles of Binder in the Mechanical Integrity of Electrodes for Lithium-Ion Batteries,” J. Electrochem. Soc., vol. 160, no. 9, pp. A1502–A1509, 2013, doi: 10.1149/2.088309jes.

[15] H. Wu, G. Zheng, N. Liu, T. J. Carney, Y. Yang, and Y. Cui, “Engineering empty space between Si nanoparticles for lithium-ion battery anodes,” Nano Lett., vol. 12, no. 2, pp. 904–909, 2012, doi: 10.1021/nl203967r.

[16] J. Y. Li, Q. Xu, G. Li, Y. X. Yin, L. J. Wan, and Y. G. Guo, “Research progress regarding Si-based anode materials towards practical application in high energy density Li-ion batteries,” Mater. Chem. Front., vol. 1, no. 9, pp. 1691–1708, 2017, doi: 10.1039/c6qm00302h.

[17] X. Zuo, J. Zhu, P. Müller-Buschbaum, and Y. J. Cheng, “Silicon based lithium-ion battery anodes: A chronicle perspective review,” Nano Energy, vol. 31, no. October 2016, pp.

113–143, 2017, doi: 10.1016/j.nanoen.2016.11.013.

[18] X. Zhou, Y. X. Yin, L. J. Wan, and Y. G. Guo, “Self-assembled nanocomposite of silicon nanoparticles encapsulated in graphene through electrostatic attraction for lithium-ion batteries,” Adv. Energy Mater., vol. 2, no. 9, pp. 1086–1090, 2012, doi: 10.1002/aenm.201200158.

[19] Y. Shi, X. Zhou, and G. Yu, “Material and Structural Design of Novel Binder Systems for High-Energy, High-Power Lithium-Ion Batteries,” Acc. Chem. Res., vol. 50, no. 11, pp. 2642–2652, 2017, doi: 10.1021/acs.accounts.7b00402.

[20] D. Bresser, D. Buchholz, A. Moretti, A. Varzi, and S. Passerini, “Alternative binders for sustainable electrochemical energy storage-the transition to aqueous electrode processing and bio-derived polymers,” Energy Environ. Sci., vol. 11, no. 11, pp. 3096–3127, 2018, doi: 10.1039/c8ee00640g.

[21] D. Munao, J. W. M. Van Erven, M. Valvo, E. Garcia-Tamayo, and E. M. Kelder, “Role of the binder on the failure mechanism of Si nano-composite electrodes for Li-ion batteries,” J. Power Sources, vol. 196, no. 16, pp. 6695–6702, 2011, doi: 10.1016/j.jpowsour.2010.11.072.

[22] R. Guo, S. Zhang, H. Ying, W. Yang, J. Wang, and W. Han, “Preparation of an Amorphous Cross-Linked Binder for Silicon Anodes,” ChemSusChem, vol. 12, no. 21, pp. 4838–4845, 2019, doi: 10.1002/cssc.201902079.

[23] G. Shoorideh et al., “Harvesting Interconductivity and Intraconductivity of Graphene Nanoribbons for a Directly Deposited, High-Rate Silicon-Based Anode for Li-Ion Batteries,” ACS Appl. Energy Mater., vol. 1, no. 3, pp. 1106–1115, 2018, doi: 10.1021/acsaem.7b00228.

[24] M. K. Datta and P. N. Kumta, “Silicon and carbon based composite anodes for lithium ion batteries,” J. Power Sources, vol. 158, no. 1, pp. 557–563, 2006, doi: 10.1016/j.jpowsour.2005.09.016.

[25] H. Buqa, M. Holzapfel, F. Krumeich, C. Veit, and P. Novák, “Study of styrene butadiene rubber and sodium methyl cellulose as binder for negative electrodes in lithium-ion

batteries," J. Power Sources, vol. 161, no. 1, pp. 617–622, 2006, doi: 10.1016/j.jpowsour.2006.03.073.

[26] A. Miranda et al., "A Comprehensive Study of Hydrolyzed Polyacrylamide as a Binder for Silicon Anodes," ACS Appl. Mater. Interfaces, vol. 11, no. 47, pp. 44090–44100, 2019, doi: 10.1021/acsami.9b13257.

[27] N. Li, S. Jin, Q. Liao, H. Cui, and C. X. Wang, "Encapsulated within graphene shell silicon nanoparticles anchored on vertically aligned graphene trees as lithium ion battery anodes," Nano Energy, vol. 5, pp. 105–115, 2014, doi: 10.1016/j.nanoen.2014.02.011.

[28] H. K. Park, B. S. Kong, and E. S. Oh, "Effect of high adhesive polyvinyl alcohol binder on the anodes of lithium ion batteries," Electrochem. commun., vol. 13, no. 10, pp. 1051–1053, 2011, doi: 10.1016/j.elecom.2011.06.034.

[29] M. Wu et al., "Toward an ideal polymer binder design for high-capacity battery anodes," J. Am. Chem. Soc., vol. 135, no. 32, pp. 12048–12056, 2013, doi: 10.1021/ja4054465.

[30] W. J. Zhang, "A review of the electrochemical performance of alloy anodes for lithium-ion batteries," J. Power Sources, vol. 196, no. 1, pp. 13–24, 2011, doi: 10.1016/j.jpowsour.2010.07.020.

[31] J. T. Li et al., "Water Soluble Binder, an Electrochemical Performance Booster for Electrode Materials with High Energy Density," Adv. Energy Mater., vol. 7, no. 24, pp. 1–30, 2017, doi: 10.1002/aenm.201701185.

[32] L. Qiu, Z. Shao, D. Wang, F. Wang, W. Wang, and J. Wang, "Novel polymer Li-ion binder carboxymethyl cellulose derivative enhanced electrochemical performance for Li-ion batteries," Carbohydr. Polym., vol. 112, pp. 532–538, 2014, doi: 10.1016/j.carbpol.2014.06.034.

[33] J. Li, R. B. Lewis, and J. R. Dahn, "Sodium carboxymethyl cellulose," Electrochem. Solid-State Lett., vol. 10, no. 2, 2007, doi: 10.1149/1.2398725.

[34] N. S. Hochgatterer et al., "Silicon/graphite composite electrodes for high-capacity anodes: Influence of binder chemistry on cycling stability," Electrochem. Solid-State Lett., vol. 11, no. 5, pp. 3–8, 2008, doi: 10.1149/1.2888173.

[35] R. Na et al., “Electrically Conductive Shell-Protective Layer Capping on the Silicon Surface as the Anode Material for High-Performance Lithium-Ion Batteries,” ACS Appl. Mater. Interfaces, vol. 11, no. 43, pp. 40034–40042, 2019, doi: 10.1021/acsami.9b13941.

[36] J. S. Bridel, T. Azaïs, M. Morcrette, J. M. Tarascon, and D. Larcher, “Key parameters governing the reversibility of Si/carbon/CMC electrodes for Li-ion batteries,” Chem. Mater., vol. 22, no. 3, pp. 1229–1241, 2010, doi: 10.1021/cm902688w.

[37] K. L. Browning, R. L. Sacci, M. Doucet, J. F. Browning, J. R. Kim, and G. M. Veith, “The Study of the Binder Poly(acrylic acid) and Its Role in Concomitant Solid-Electrolyte Interphase Formation on Si Anodes,” ACS Appl. Mater. Interfaces, vol. 12, no. 8, pp. 10018–10030, 2020, doi: 10.1021/acsami.9b22382.

[38] K. Min et al., “Grafting Functional Groups in Polymeric Binder toward Enhancing Structural Integrity of Li x SiO2 Anode during Electrochemical Cycling,” J. Phys. Chem. C, vol. 122, no. 30, pp. 17190–17196, 2018, doi: 10.1021/acs.jpcc.8b03625.

[39] S. L. Chou, Y. Pan, J. Z. Wang, H. K. Liu, and S. X. Dou, “Small things make a big difference: Binder effects on the performance of Li and Na batteries,” Phys. Chem. Chem. Phys., vol. 16, no. 38, pp. 20347–20359, 2014, doi: 10.1039/c4cp02475c.

[40] S. Jiang, B. Hu, Z. Shi, W. Chen, Z. Zhang, and L. Zhang, “Re-Engineering Poly(Acrylic Acid) Binder toward Optimized Electrochemical Performance for Silicon Lithium-Ion Batteries: Branching Architecture Leads to Balanced Properties of Polymeric Binders,” Adv. Funct. Mater., vol. 30, no. 10, pp. 1–9, 2020, doi: 10.1002/adfm.201908558.

[41] A. Jaworek and A. T. Sobczyk, “Electrospraying route to nanotechnology: An overview,” J. Electrostat., vol. 66, no. 3–4, pp. 197–219, 2008, doi: 10.1016/j.elstat.2007.10.001.

[42] S. K. Boda, X. Li, and J. Xie, “Electrospraying an enabling technology for pharmaceutical and biomedical applications: A review,” J. Aerosol Sci., vol. 125, no. April, pp. 164–181, 2018, doi: 10.1016/j.jaerosci.2018.04.002.

[43] X. Hao et al., “Effects of the electrospray ionization parameters on the formation and morphology of colloidal microspheres of polyacrylonitrile,” J. Appl. Polym. Sci., vol. 102, no. 3, pp. 2889–2893, 2006, doi: 10.1002/app.24731

CHAPTER 3 : SILICON GRAPHENE ANODES WITH ELECTRODE MODIFICATIONS FOR LITHIUM ION BATTERIES

Introduction:

The demand for high-energy-density lithium (Li) ion batteries (LIBs) is growing tremendously since their applications have been extended beyond electronics (mobiles, laptops, etc.) to long-driving-electric vehicles/battery electric vehicles (BEVs) and even for large-scale storage of renewable energy in smart grids [1], [2]. Although rechargeable LIBs have penetrated through multiple consumer markets, their energy densities with the conventional electrode materials are close to saturation; graphite anodes can store only 1 Li-ion per 6 C atoms (LiC_6) giving a gravimetric capacity of only 372 mAh/g [3]. To increase the capacity further, various anode materials capable of storing more lithium ions per unit mass have been explored. Among the different chemistries explored, the alloying chemistry involving Silicon anodes has gained the most attention[4]. In recent years there has been a surge in the number of publications and research patents involving Si-based anodes for lithium-ion batteries. Silicon has a very high theoretical capacity of 4200 mAh/g, which more than 10 times that of graphite anodes[2]. Si has a relatively low discharge potential of 0.4V vs Li/Li^+ making it very advantageous. Moreover, Si is the 2^{nd} most abundant material on the earth's crust and is environmentally benign. Furthermore, due to the rapid growth of the semiconductor industry, the cost of Si and the growth of its supply chain has made them a more prominent choice anode material to replace graphite material [5]. Despite all the aforementioned advantages, Si has two main challenges that have hindered its wide applications in Si-based anodes. Firstly, the volume inflation; the volume expansion of Silicon during charging/discharging is about 320% irrespective of the particle size, morphology/crystallinity[6]. A large amount of stress and strain are induced due to the rapid

volume changes. These stresses create cracking of active materials thereby exposing fresh surfaces of Si to the electrolyte and also causes delamination of Si particles from the electrode surface. Secondly, an unstable solid-electrolyte interphase (SEI) layer is formed on silicon anodes during electrochemical cycling [7]. SEI is a thin passivating layer formed at the electrode-electrolyte interface at low potentials (> 1V). The SEI layer grows continuously whenever a fresh surface of Si is exposed due to cracking. The SEI on a silicon anode could grow to a thickness of several micrometers after few cycles, therefore forming a thick passivating film increasing the impedance of the cell. Especially in full cells where there is no infinite support of Li, the continuous growth of unstable SEI rapidly consumes the limited lithium and electrolyte, leading to a fast capacity decay. In addition to this volume expansion issue, Si in general has very low intrinsic electrical conductivity. Together, all the above-mentioned problems hinder the application of Si in Li ion based anodes [2], [8]. Researchers have looked at various strategies to mitigate these issues. One of our lab members Yash Joshi, incorporated a porous electrode structure to control the volume expansion in Si anodes. He engineered the electrodes in such a way that the pore space created by the burn off of the binder accommodates the volume expansion of Silicon. Here in, we will see additional strategies like size control and electrode modifications (calendaring and graphene coating) to mitigate the above mentioned issues.

Effect of Silicon particle on electrochemical performance of Si based anodes:

To overcome the volume expansion issues, several approaches have been proposed. In recent times, the application of nanotechnology has greatly encouraged the practicality of Si-based anodes. The electrochemical performance of Si can be greatly enhanced by decreasing the particle size of Si particles from micro to nanoscale [9]. Nanoscale materials have proven to alleviate the volume expansion issue better relative to that of microparticles. Kim et al. and a few other

researchers investigated the critical size of nanosized Si below which cracking does not occur [10], [11]. Several studies have shown electrochemical enhancements using nanoscale silicon, but the commercialization of nanosized Si is very challenging. Some disadvantages accompanied while using nanoscale Si are severe aggregation of Si nanoparticles causing inhomogeneity in slurry resulting in inferior cycling [12], [13]. Secondly, the high specific area in nanoparticles causes massive side reactions leading to more SEI formation and thereby causing lower coulombic efficiencies [9], [14]. Therefore, researchers have proposed various structural designs and modifications of Si nanomaterials involving modifications in their geometries. Some of the commonly performed modifications on Si NPs include having a core-shell solid structure [15], a hollow core-shell, a yolk-shell [6], porous structure, use of nanowires [16] / nanotubes [17], and nanofibers [18]. Recently, there is a surge in the application of carbon-based materials in Si-based anodes. Specifically, Graphene, a 2D carbon material has gained increased interest [19]. Graphene possesses many exceptional properties, like high specific surface area, high electrical conductivity, high strength, and flexibility. Graphene has been explored in Si-based hybrid anodes. Many researchers have successfully used graphene-modified Si hybrid anodes for LIBs [20]. These hybrid electrodes were designed and engineered in several different ways like dispersing Si NPs between graphene sheets, graphene encapsulated Si NPs. These systems yielded better coulombic efficiency and also were more stable during cycling when compared to bare Si NP anodes [21], [22]. Graphene oxides and reduced graphene oxides were also used as supporting carbon materials along with Si. Since graphene is commercially viable, its derivates such as graphene oxide should possess low cost, good quality, and stability [23], [24]. Therefore, the commercialization of graphene-modified silicon anodes hybrids is mainly subject to the scale-up of graphene.

Although various geometries and modifications have been studied, there is no apparent trend or rule that help researchers to design Si nanostructured electrodes that achieve stable electrochemical performance. Kim et.al [25] observed that Si particles with a size less than 150nm (critical size) did not crack under electrochemical cycling. He observed a strong dependence of Si particle fracture with that of Si particle size. Si particles larger than 150 nm generally tend to crack into pieces during cycling and some of these cracked pieces detached from the conductor and stopped participating in an electrochemical reaction resulting in faster deterioration of capacity. Despite multiple research publications, there is still no agreed consensus for the optimal particle size. In this thesis, we aim to study the effect of nanoparticle size on the electrochemical performance of a silicon-graphene-PAA system. Poly(acrylic) acid – (PAA) has been used in this system owing to its strong adhesive nature. Researchers have reported that PAA binder forms a covalent link with Silicon dioxide (SiO_2) layer around the Si particles [26], [27]. This way, Si particles remain linked to the binder despite large volume changes.

In this chapter of the thesis, we aim to study the effect of silicon particle size on electrosprayed silicon-graphene-PAA complex anodes. So far most of the research work relating to the size effect of silicon in Li-ion anodes has been a comparison of micro versus nanoscale. In this chapter, we aim to analyze the effect of particle size of Silicon in the nanoscale regime. Three different silicon nanoparticles of varying sizes (20nm, 40nm, and 50nm) were studied to understand the effect of Si particle size on the electrochemical performance of silicon anodes. We will be using S1, S2, S3 to denote 50nm, 40nm, and 20nm sizes, respectively.

In this thesis, we use a facile air-controlled electrospray [28] method to facilitate a scalable and an economic method of fabricating silicon anodes. Air controlled electrospraying involves the use of a voltage source to atomize a liquid solution in the syringe. These liquid droplets are driven

to the collector by air pressure to quicken the process and remove further drying steps. Fig 1.4 shows the schematic representation of the process. The liquid solution comprising of silicon (20nm, 40nm, and 50nm), graphene, and poly(acrylic) acid (PAA) were pumped through the nozzle under the influence of electric field and high air pressure to obtain the desired silicon anode. High extensional forces imposed on the droplet by application of electric field and the high-pressure airflow ensures the formation of a uniform dispersion of the Si nanoparticles throughout the composite electrode. The resulting electrodes are stored in a dry vacuum over for 3 days until further electrode processing.

Experimental Section:

Preparation of Electrospraying solution:

Preparation of S1 /Graphene /1.25 mil PAA composite via Air-controlled Electrospray:

Initially, 0.2g of 1.25million poly(acrylic) acid (PAA, Sigma Aldrich) was dissolved in 10g of water and this mixture was left for stirring overnight. To a separate vial, 0.2g of Silicon – S1 was added to 3.7g of water and was stirred for 10 minutes. To this mixture, about 1.6g of the prepared PAA solution (2% wt) was added and was allowed to stir under room temperature for 4 hours. This mixture is then sonicated for 30 minutes and 4.8g of Graphene dispersion in water (5% wt, ACS) was added. This mixture was further allowed to stir for 4 hours and sonicated for 30 minutes. Then another 1.6g of PAA solution is added to the mixture and allowed to stir for 30 minutes. The solution was then pumped from the syringe at a flow rate of 0.35ml/minute and sprayed on to a copper disk that was placed at a distance of 22cm away from the tip of the nozzle. To achieve good atomization of droplets and proper dispersion of the solution, a voltage of 25kV was supplied to the outer nozzle by the power supply in addition to the air pressure (25 psi) supplied through the inner nozzle. The resulting droplets from the spray form a uniform dry layer of active material on

the surface of the copper disk. This electrode was dried in a vacuum oven for 3 days before testing them in coin cells.

Preparation of S2 /Graphene /1.25 mil PAA composite via Air-controlled Electrospray:

Initially, 0.2g of 1.25million poly(acrylic) acid (PAA, Sigma Aldrich) was dissolved in 10g of water and this mixture was left for stirring overnight. To a separate vial, 0.2g of Silicon – S2 was added to 3g of water and was stirred for 10 minutes. To this mixture, about 1.2g of the prepared PAA solution (2% wt) was added and was allowed to stir under room temperature for 4 hours. This mixture is then sonicated for 30 minutes and 5g of Graphene dispersion in water (5% wt, ACS) was added. This mixture was further allowed to stir for 4 hours and sonicated for 30 minutes. Then another 1.2g of PAA solution is added to the mixture and allowed to stir for 30 minutes. The solution was then pumped from the syringe at a flow rate of 0.35ml/minute and sprayed on to a copper disk that was placed at a distance of 20cm away from the tip of the nozzle. To achieve good atomization of droplets and proper dispersion of the solution, a voltage of 25kV was supplied to the outer nozzle by the power supply in addition to the air pressure (25 psi) supplied through the inner nozzle. The resulting droplets from the spray form a uniform dry layer of active material on the surface of the copper disk. This electrode was dried in a vacuum oven for 3 days before testing them in coin cells.

Preparation of S3 /Graphene /1.25 mil PAA composite via Air-controlled Electrospray:

Initially, 0.2g of 1.25million poly(acrylic) acid (PAA, Sigma Aldrich) was dissolved in 10g of water and this mixture was left for stirring overnight. To a separate vial, 0.2g of Silicon – S2 was added to 4g of water and was stirred for 10 minutes. To this mixture, about 1.6g of the prepared PAA solution (2% wt) was added and was allowed to stir under room temperature for 4 hours. This mixture is then sonicated for 30 minutes and 4g of Graphene dispersion in water (5% wt,

ACS) was added. This mixture was further allowed to stir for 4 hours and sonicated for 30 minutes. Then another 1.g of PAA so6lution is added to the mixture and allowed to stir for 30 minutes. The solution was then pumped from the syringe at a flow rate of 0.3ml/minute and sprayed on to a copper disk that was placed at a distance of 25cm away from the tip of the nozzle. To achieve good atomization of droplets and proper dispersion of the solution, a voltage of 25kV was supplied to the outer nozzle by the power supply in addition to the air pressure (30 psi) supplied through the inner nozzle. The resulting droplets from the spray form a uniform dry layer of active material on the surface of the copper disk. This electrode was dried in a vacuum oven for 3 days before testing.

Material characterization of electrodes: The prepared composite electrodes were characterized by using Scanning Electron Microscope (SEM, Zeiss Gemini, and Tescan Mira-3) and Energy Dispersive Spectroscopy (Tescan Mira-3) to assess the morphology of the electrode. Thermogravimetric analysis (TGA, TA instruments Q500) was used to characterize the composition of the electrode. Thermogravimetric analysis was carried out over a temperature range from 20°C to 800°C at a ramp rate of 10°C/minute. Nitrogen and air flows are maintained at the flow rate of 40ml/min and 60ml/min, respectively.

Electrical characterization of electrode: Four-point probe was used to analyze the electrical characteristics of the composite electrode film. A four-point probe is a simple apparatus used to measure sheet resistance and bulk (volume) resistivity of materials primarily for semiconductors. The Cascade four-point probe is connected to a Keithley 2400 Source-Meter which is designed for single resistance measurements by sourcing current (50 nA to 1.05 A) and measuring respective voltages (1 μV to 211 V). The probe operates within specifications when the measured voltage is ~5 mV or greater, an appropriate current should be sourced to reach this level. To measure the

resistivity of our samples, we coat (air-assisted electrospraying) our samples as composite films on top of our substrate (silicon wafer).

Battery fabrication and electrochemical measurements electrodes:

2032 type coin cells were made using the electrosprayed Silicon composite disks as the anode and lithium metal disc (MTI) was used as the counter electrode. A polythene material (Celgard) was used as the separator to test the performance of these half cells. A 1M $LiPF_6$ salt in ethylene carbonate, diethyl carbonate, and dimethyl carbonate in the ratio of 4:4:2 with 10% fluoroethylene carbonate were used as solvents inside half cells. All the capacities reported in this chapter were normalized by the total mass of active material (Silicon, Graphene, PAA) on the copper disk. Electrochemical properties of the cells were characterized by electrochemical impedance spectroscopy (PARASAT 4000, Princeton Applied Research) and galvanostatic charge and discharge cycles (MTI). A voltage window of 0.01-1.5V Vs Li/Li^+ were applied to the half cells

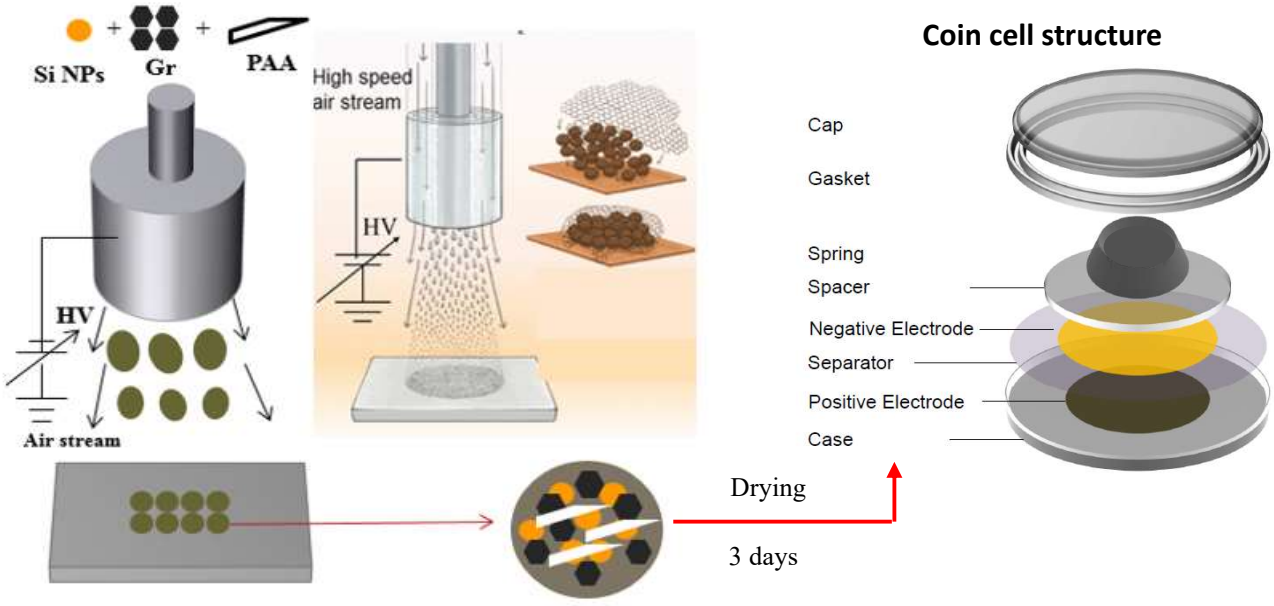

Fig 3.1: Schematic representation of electrode fabrication

Results and discussion:

Characterization of Silicon-Graphene-PAA nanocomposite:

The air-controlled electrospraying process forms a dense coating with a uniform distribution of Silicon (S1, S2, and S3) -Graphene and PAA on the copper surface. The electrodes dry as soon as the droplets come into contact with the copper disk without additional drying steps. Graphene sheets act as conductive agents in our composite system improving the interconnectivity between the active materials in the electrode. To ensure all electrodes had the exact composition of Silicon, Graphene, and PAA, they were subjected to thermogravimetric analysis (TGA). Fig 3.1 shows the comparison of TGA analysis for 450k, 1.25mil, and 3mil poly(acrylic) acid (PAA) with Silicon-Graphene composite. Fig 3.1 shows that all the three mixtures have a similar composition (60% Silicon, 20% Graphene, 20% PAA binder), thereby ruling out the influence of composition when comparing their electrochemical performance.

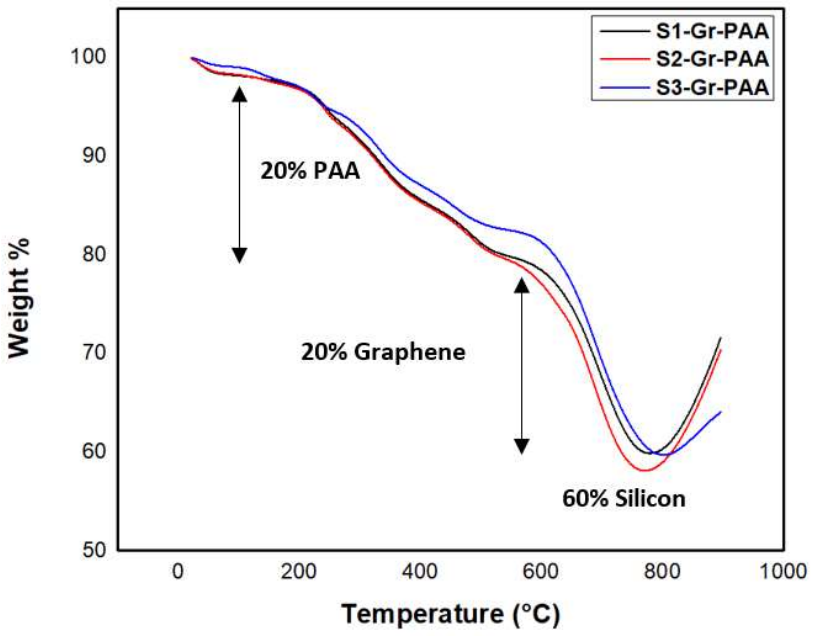

Fig 3.2: Thermogravimetric analysis (TGA) comparison of composites with 3 different silicon

The morphology and the size of the silicon were visually examined using Scanning Electron Microscopy (SEM). Fig 3.3, 3.4, and 3.5 show the top view of the different Silicon nanoparticles (S1, S2, and S3) using in this chapter. All images are taken at the same magnification of 500 nm and were analyzed using Image J to get the size distribution.

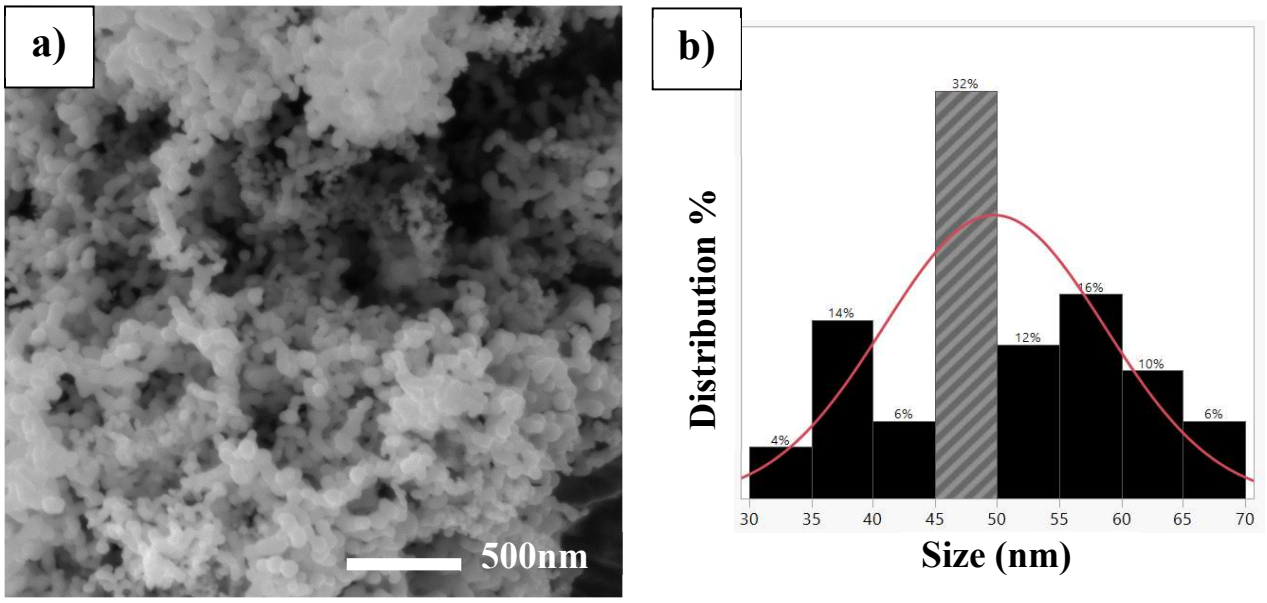

Fig 3.3 a) Morphology of S1- Silicon powder at 500 nm b) Size distribution of S1- Silicon

Fig 3.3 a) and b) shows the morphology and size distribution of S1-Silicon. It can be seen from 3.3 b), that the size of S1 silicon is around 50 nm with almost 50% of the Si nanoparticles lying around the 45-55 nm range. The average particle size of S1 silicon was found to be 50nm.

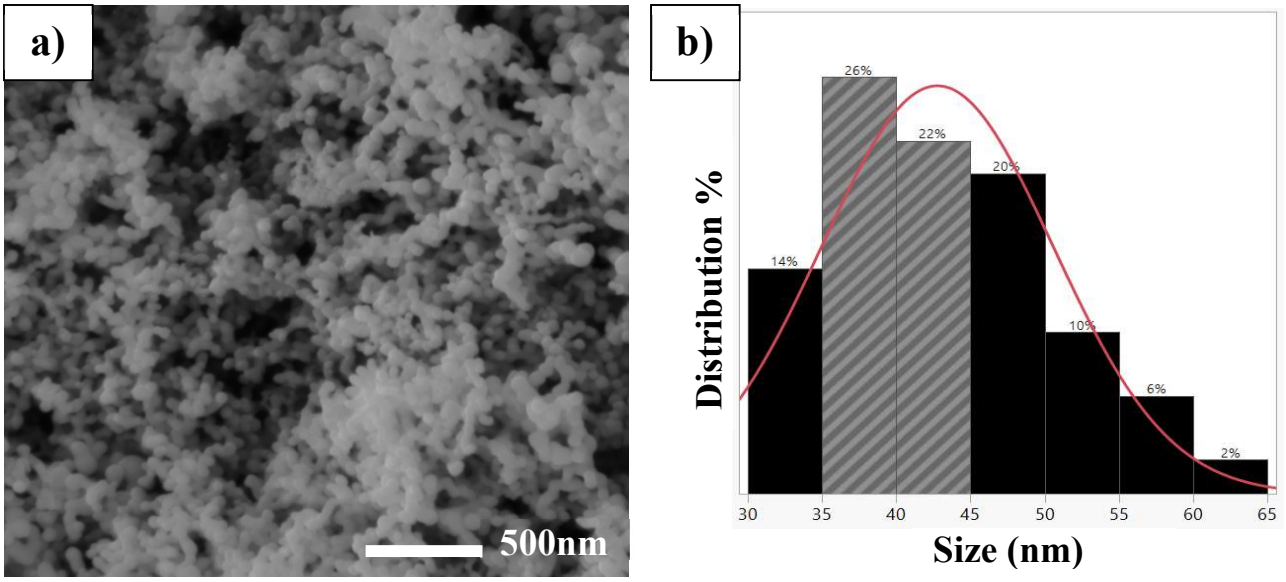

Fig 3.4 a) Morphology of S2- Silicon powder at 500 nm b) Size distribution of S2- Silicon

Fig 3.4 a) and b) show the morphology and size distribution of S2-Silicon. It can be seen from 3.4 b), that the size of S2 silicon is around 40 nm with almost 50% of the Si nanoparticles lying around the 35-45 nm range. The average particle size of S2 silicon was found to be 41nm.

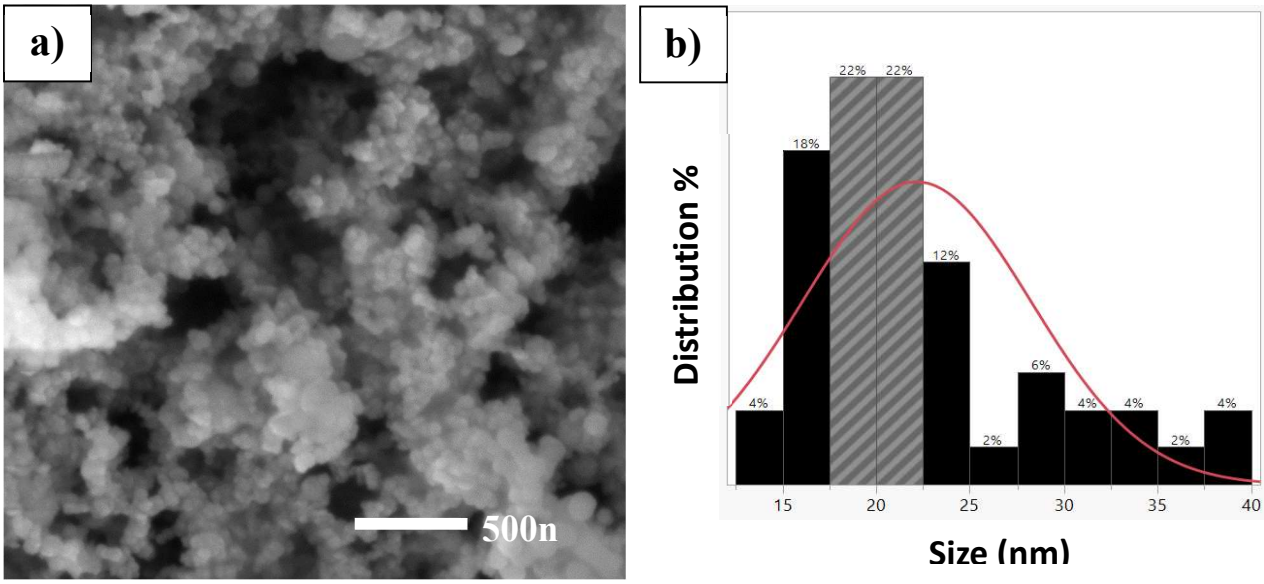

Fig 3.5 a) Morphology of S3- Silicon powder at 500 nm b) Size distribution of S3- Silicon

Fig 3.5 a) and b) shows the morphology and size distribution of S3-Silicon. It can be seen from 3.5 b), that the size of S3 silicon is around 20 nm with almost 70% of the Si nanoparticles lying around the 15-25 nm range. The average particle size of S3 silicon was found to be 20nm. It is established that we have silicon nanoparticles of different sizes (20nm, 40nm, and 50 nm) through scanning electron microscopy (SEM). From here on S1 refers to 50nm, S2 refers to 40nm and S3 refers to 20nm sized Si NPs.

Once the sizes of Si NPs have been established, we move on to examine the morphology of the electrodes using different Si NPs through scanning electron microscopy (SEM). Electrospraying was used to fabricate the composite electrodes (Si NPs, Graphene, PAA). All the 3 electrodes containing combinations of different Si NPs (S1, S2, S3), graphene and PAA binder were visually examined at a magnification of 200 nm. Fig 3.6 a), b) and c) show the top view of composite anodes with S1, S2, and S3 Silicon, respectively. Fig 3.6 a) and b) shows as even distribution of silicon, graphene, and binder by visual inspection. In the case of 3.6 c) silicon NPs exhibit aggregation with the formation of clusters of Si NPs. This is due to the instability caused by Silicon nanoparticles of smaller size (20nm). S3 silicon NPs almost have half the size of the other two NPs (S1 and S2) used in this chapter. Researchers have shown that smaller nanoparticles make it all the more difficult to disperse in a slurry. The aggregation was seen in Fig 3.6c) is associated with the smaller size of Silicon. This lumpy behavior of silicon could cause hindrance in the electrochemical performance of the electrode.

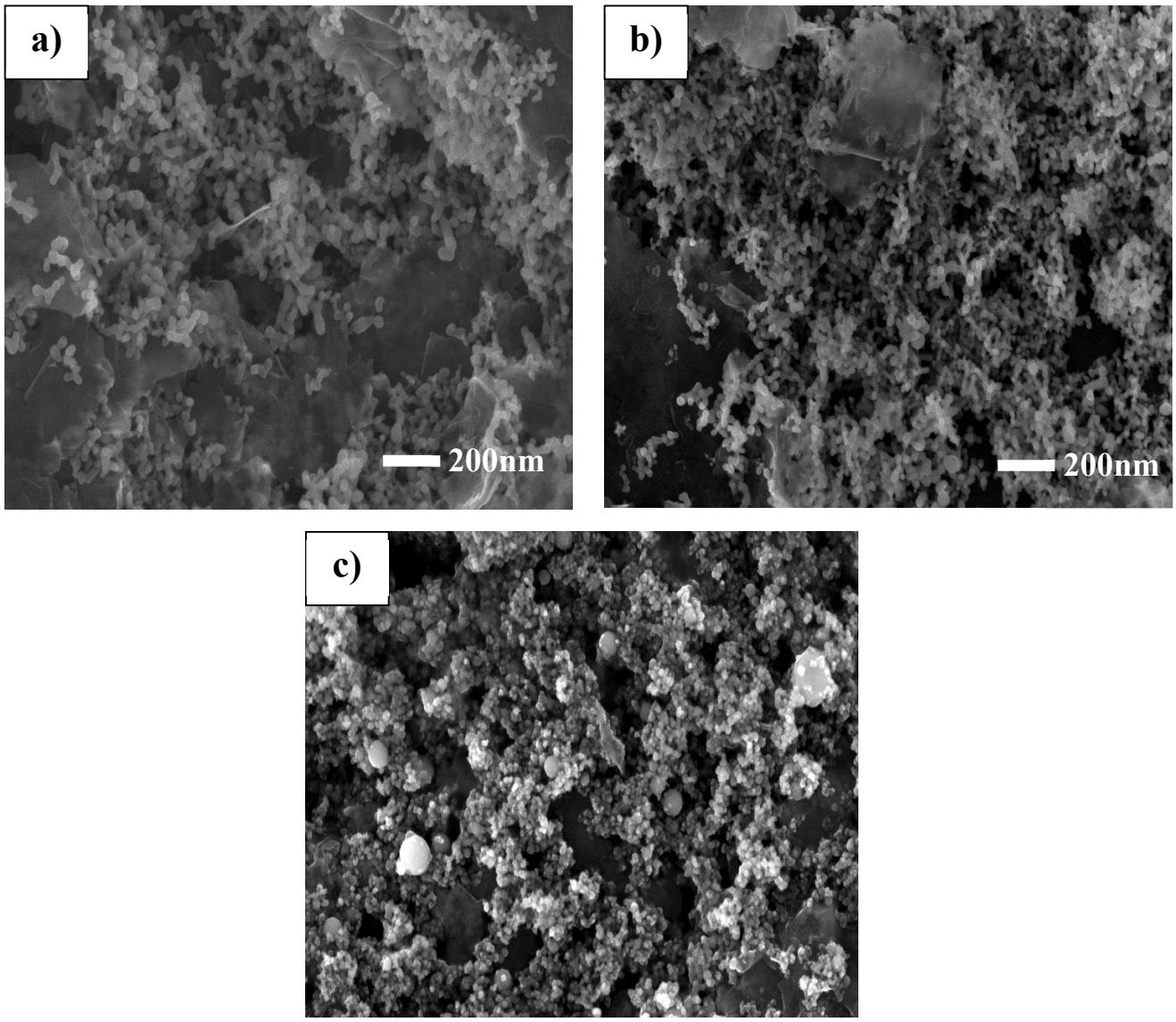

Fig 3.6 a) Morphology of S1- Gr- PAA composite electrode showing even distribution of electrode components b) Morphology of S2-Gr-PAA composite electrode showing even distribution of electrode components c) Morphology of S3-Gr-PAA composite electrode showing lumpy behavior and aggregation of Si NPs

It is important to note that the flow characteristics of the prepared slurry will affect how they settle post electrospraying. This will have a significant impact on the quality of the electrode coatings and the resulting performance of anodes. Inhomogeneity in the distribution of the particles in the coating could result in isolated active material particles in the final electrode structure. Therefore, during cycling, the inhomogeneous particle distribution could render high tensions and stress in parts with high loadings of active material eventually leading to cell failure. Fig 3.7 shows the difference between a homogeneous and an inhomogeneous slurry. Fig 3.7a) shows an even distribution of the components of the electrode in a solution, whereas Fig 3.7 b) shows a clear phase separation (the settling of graphene on the bottom of the vial).

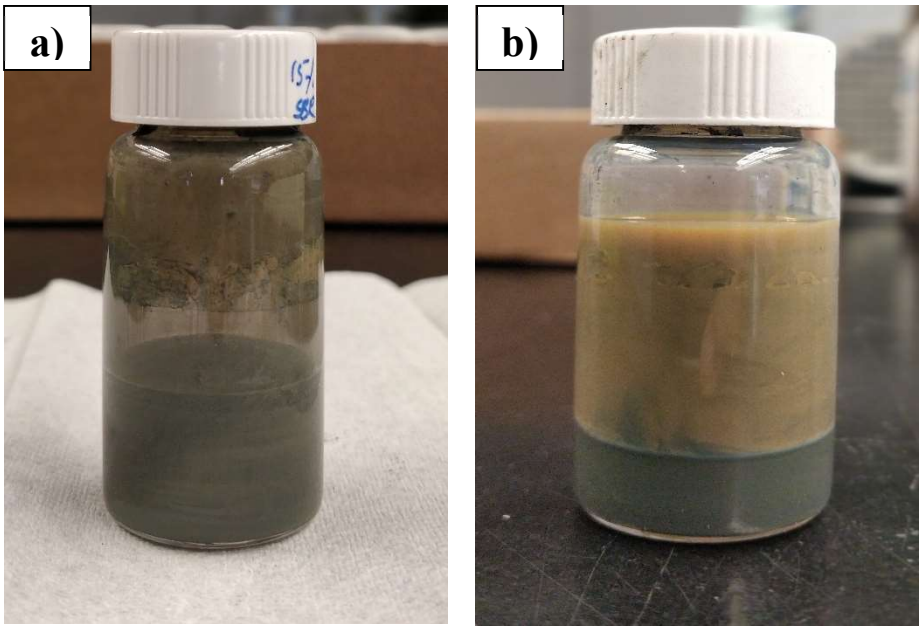

Fig 3.7 Comparison of homogeneous and inhomogeneous slurry before electrode fabrication (electrospraying)

Researchers used surfactants like Sodium dodecyl benzyl Sulphonate (SDBS), ammonium poly(acrylic) acid (PAA-NH_4) to enhance the dispersion and to prevent inhomogeneity in anode slurries. Similarly, we employ Sodium dodecyl benzyl Sulphonate (SDBS) surfactant to enhance the dispersion of our slurry.

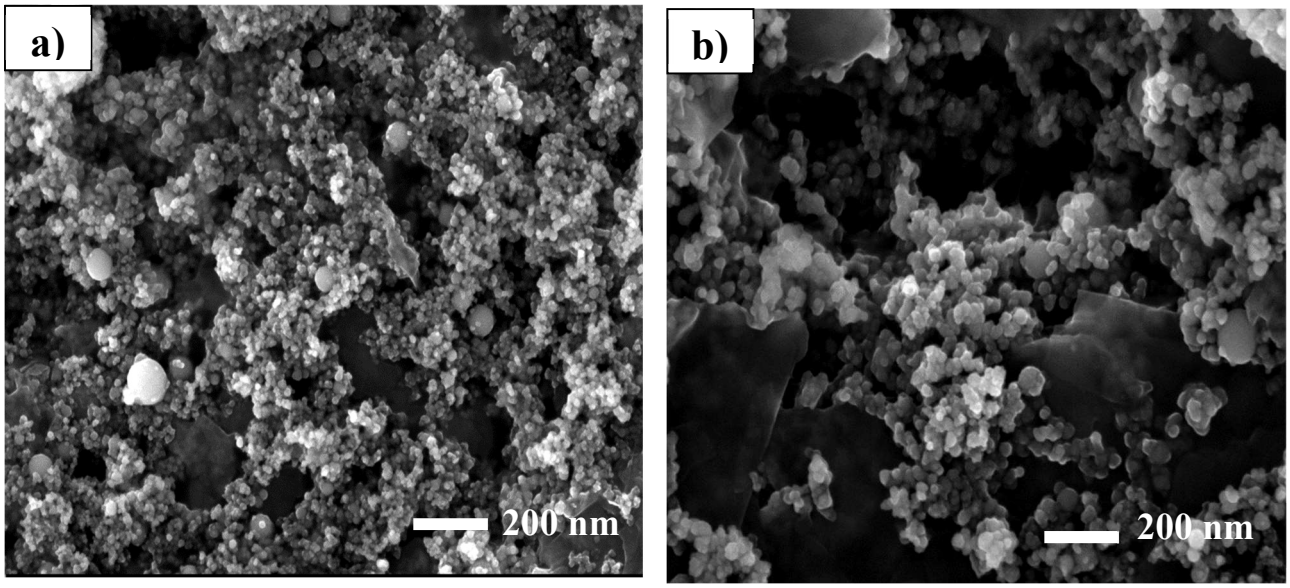

Fig 3.8 a) Morphology of S3- Gr- PAA composite electrode – Before addition of SDBS

b) Morphology of S3-Gr-PAA composite electrode – After addition of SDBS

Fig 3.8 shows the morphology of the electrode containing S3 Silicon-Graphene and PAA with and without the addition of SDBS. From the image, it is evident that the presence of SDBS improves the dispersion. There is a stark improvement in the distribution of the electrode components and also a decrease in the aggregation of Silicon. However, Fig 3.8 b) showed a clear height difference between graphene and silicon materials in the electrodes. It is very important to ensure the proper packing of electrode materials. Improper packing will lead to loss of conductive pathways and also results in capacity loss.

To calculate the packing density of the electrode, measurements of loading and thickness of the electrodes were made. The thickness of the electrodes was measured using a micrometer. Multiple readings of thickness were measured to ensure the reliability of thickness data. Loading of the electrodes was calculated by measuring the weight of the electrode before and after electrospraying.

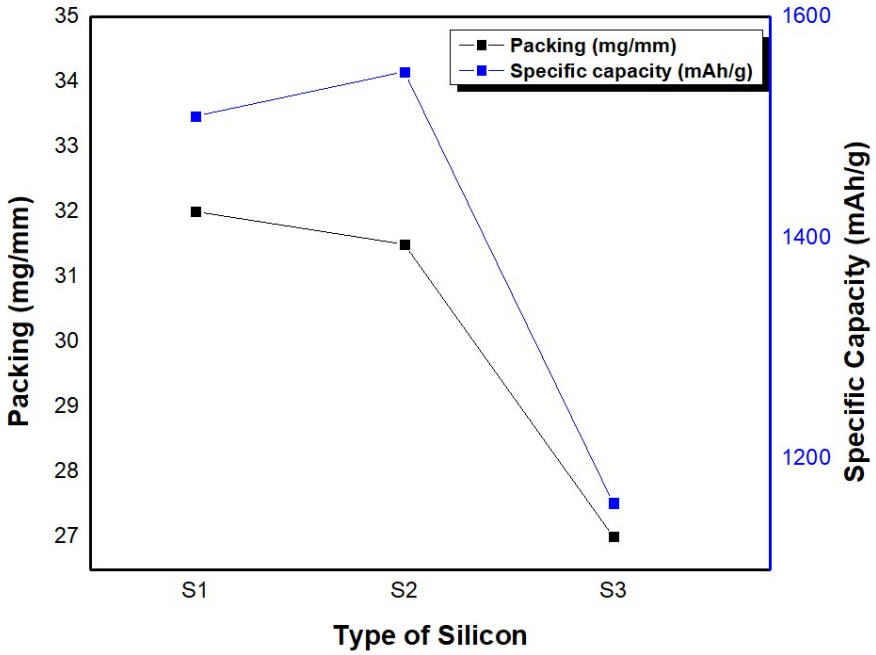

Fig 3.9 Comparison of Silicon - Packing (mg/mm) and their respective capacities (mAh/g)

Fig 3.9 shows that electrodes fabricated with S1and S2 silicon have a better packing density/ better distribution of electrode components when compared to that of S3 silicon. This packing density of the electrodes can also be related to their respective capacities. Poor packing leads to a lack of conductive pathways between the electrode components. We hypothesize that the poor interconnectivity among the electrode components leads to reduced utilization of silicon which further leads to a reduction in capacity.

Cross-sectional images of the electrodes were examined through Scanning electron microscopy (SEM). Fig 3.10 clearly showed significant multiple layers in the electrode structure. The arrangement of silicon and graphene was irregular, thereby leading to a poor electrode structure. As mentioned earlier, this could lead to loss of electrical contact between the electrode materials and affect the cell performance.

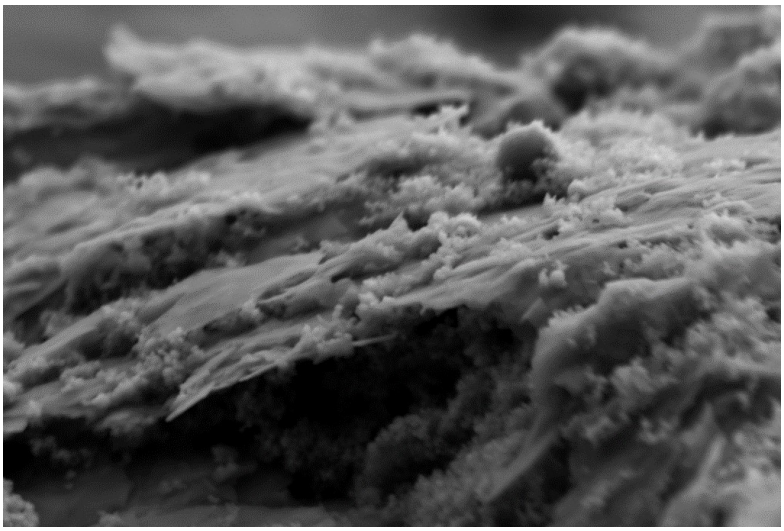

Fig 3.10 Cross-section image of electrode exhibiting poor packing of the electrode

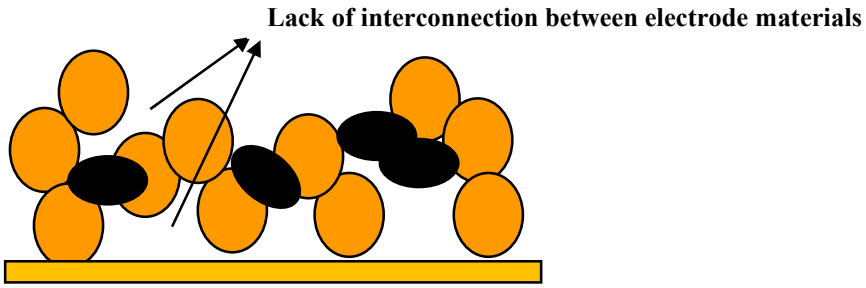

Fig 3.11 Electrode structure showing a significant loss of conductive pathways and poor interconnectivity between electrode materials

Si nanoparticle's inherent low conductivity leads to its dependence on conductive agents like graphene to improve the interconnectivity and conductivity of the system. To improve the packing of the system, additional steps need to be performed to ensure the improvement of electrode density and reducing void spaces. Calendaring could alleviate the above-mentioned problem and provides a better packing density of the electrode.

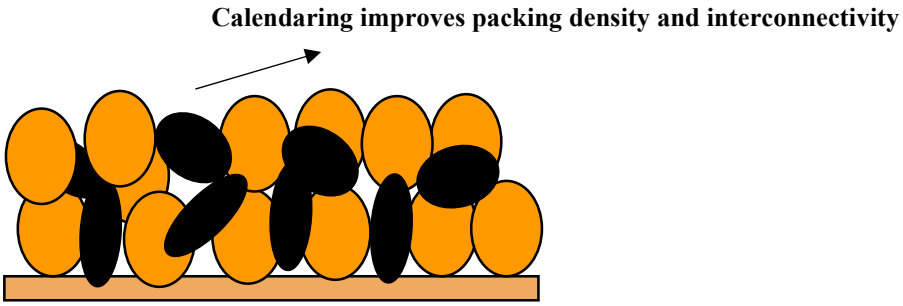

Fig 3.12 Schematic representation of electrode structure – post calendaring showing improved packing density and interconnectivity

Besides the decrease in the inner conductive pathways caused by the poor electrode structure, the poor packing of electrode structure leads to excess exposure of silicon to the electrolyte solution. Si NPs settled on the electrode surface are exposed more to the electrolyte and trigger excess side reactions. Besides, Si NPs expand and contract without limitations at the electrode surface and leads to additional cracks. These cracks tend to form additional SEI layers thereby blocking Li^+ transport and leading to the formation of unstable SEI. Therefore, we come up with the idea of coating an additional sheath layer of graphene over the calendared electrode to cover the whole electrode surface. This creates a stable SEI layer between the electrolyte and graphene instead of

the silicon. Therefore, this graphene layer acts as a protection layer both physically and electrochemically above the electrode structure.

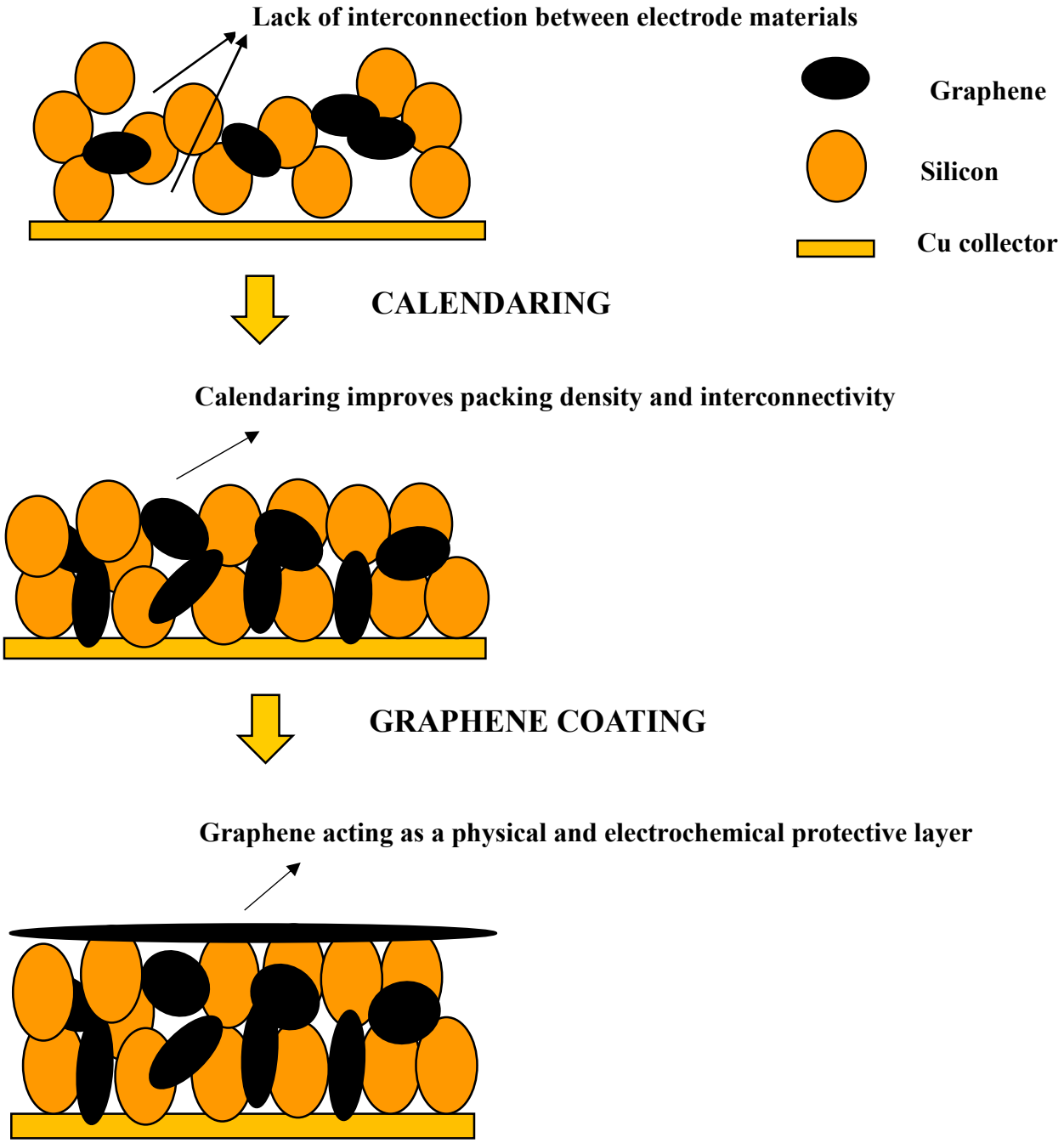

Fig 3.13 Schematic representation of step-by-step electrode modifications

Fig 3.13 shows the schematic representation of step-by-step modifications performed on the electrode to render good packing of electrode materials and also preventing the formation of unstable solid electrolyte interphase (SEI). Calendaring alleviates the problems related to electrode packing and coating the electrode with an additional sheath layer of graphene ensures a stable SEI layer between the electrolyte and graphene.

Electrical characterization of electrodes: Four-point probe:

A four-point probe was used to analyze the electrical characteristics of the composite electrode film. To measure the resistivity of our samples, we coat (air-assisted electrospraying) our samples as composite films on top of the substrate (silicon wafer).

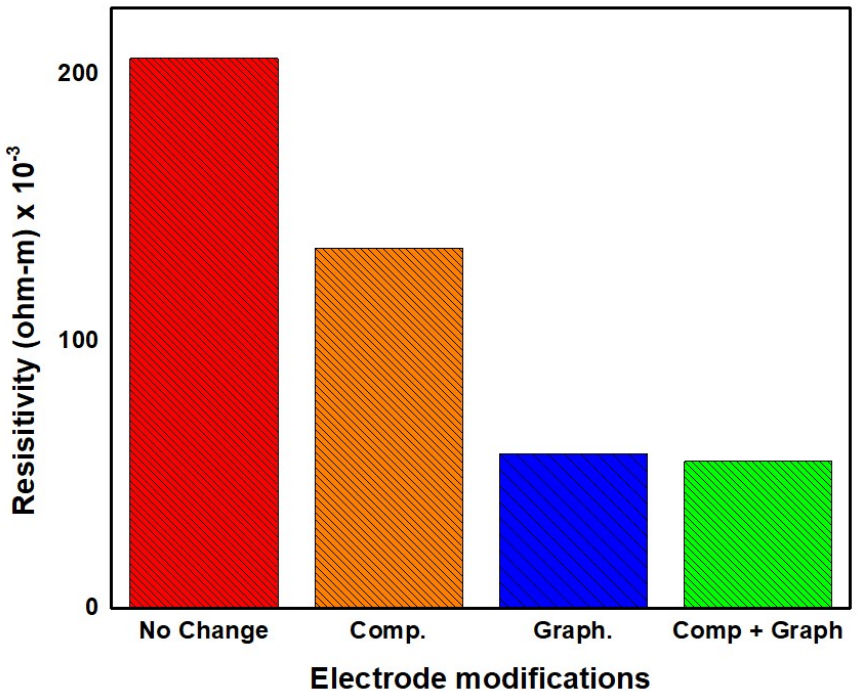

Fig 3.14 Four-point probe resistivity measurements with electrode modifications indicating improvement electrode interconnectivity after calendaring and graphene coating

Four-point probe conductivity measurements in Fig 3.14 reveals that with additional electrode modifications like calendaring (compression) and coating an additional layer of graphene, reduces the system resistivity. This means the interconnectivity produced by the proper packing of electrode components has enabled a better conductive pathway leading to reduce resistivity. Also, the additional sheath layer of graphene provides a better conductive pathway leading to a reduction in the overall resistance of the system. Therefore, electrode modifications like calendaring and coating render a better conductivity within the system which could lead to improved electrochemical performance.

Electrochemical characterization of Silicon-Graphene-PAA nanocomposite electrode:

The electrodes fabricated in electrospraying were assembled in a 2032 coin-type half cells configuration and were galvanostatically charged and discharged for multiple cycles. Each of these cells was lithiated to a voltage of 1.5V and de-lithiated to a voltage of 0.01V and was made to undergo 5 formation cycles at 0.1C and then were allowed to undergo cycling for 200 cycles post-formation.

Fig 3.15 shows the comparison of capacity-voltage profiles of the 3 different Si (S1, S2, and S3) used in the system. All the 3 cases show a very similar profile with a small plateau around 0.8V indicating the formation of SEI and then a larger plateau around 0.25V indicating Li insertion reactions with Si. All the Si were used as obtained and no additional modifications were performed to the electrodes. To our surprise, the Si which had the least size (S3 – 20nm) performed the worst with a delithiation capacity of 830 mAh/g with a silicon utilization of 53% and the silicon with the largest size (S1 – 50nm) performed the second best with a capacity of 1270 mAh/g with a-Si utilization of 70%. Whereas the silicon with the second least size (S2 – 40nm) performed the best with a delithiation capacity of 1330 mAh/g with a-Si utilization of 74%. Technically, the

performance of Si does remain similar in the nanoscale range. S1 and S2 silicon (40nm and 50nm respectively) have similar capacities. However, there is a stark difference in the delithiation capacity of systems involving S3 silicon (20nm). This can be explained by the inhomogeneity observed in the scanning electron microscopy (SEM) images (Fig 3.6) and also by visual inspection of vials before electrospraying (Fig 3.7). Both these figures demonstrate the inhomogeneity in the distribution of the active materials that result in isolated active material particles in the final electrode structure. This isolation of active material and aggregation causes poor activation of Si and hence causes a reduction in capacity.

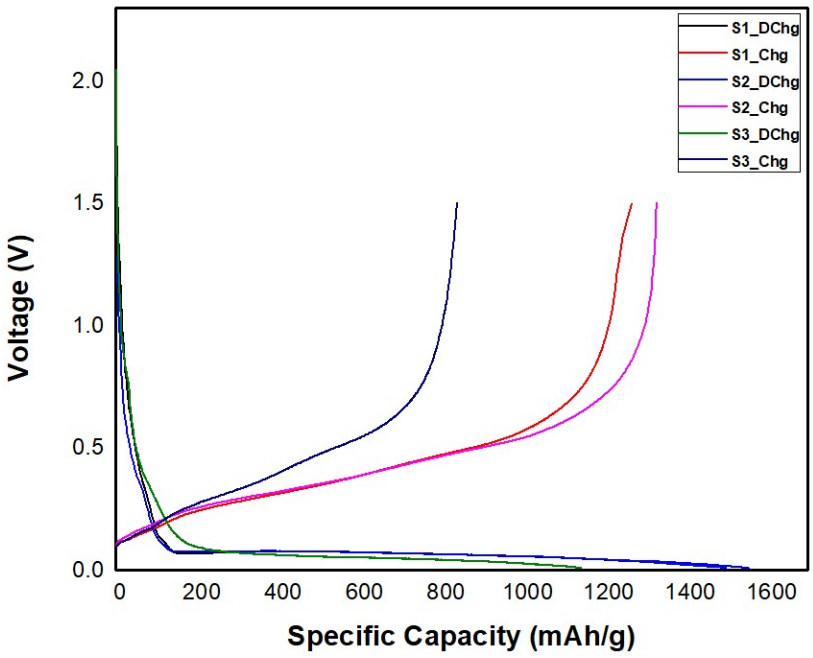

Fig 3.15 Comparison of formation cycles with different Silicon (S1, S2, and S3)

To eliminate the problem of aggregation in slurry solution (containing S3), Sodium dodecyl benzyl Sulphonate (SDBS) surfactant was employed to enhance the dispersion of our slurry. About 1% of SDBS was substituted in place of the binder (PAA) and used in the system to enhance the dispersion. SEM results (Fig 3.8 a and b) show the significant difference in the morphology of the

coating before and after the addition of SDBS. The addition of SDBS showed enhancement in the distribution of active materials in the electrode (Fig 3.8 b)).

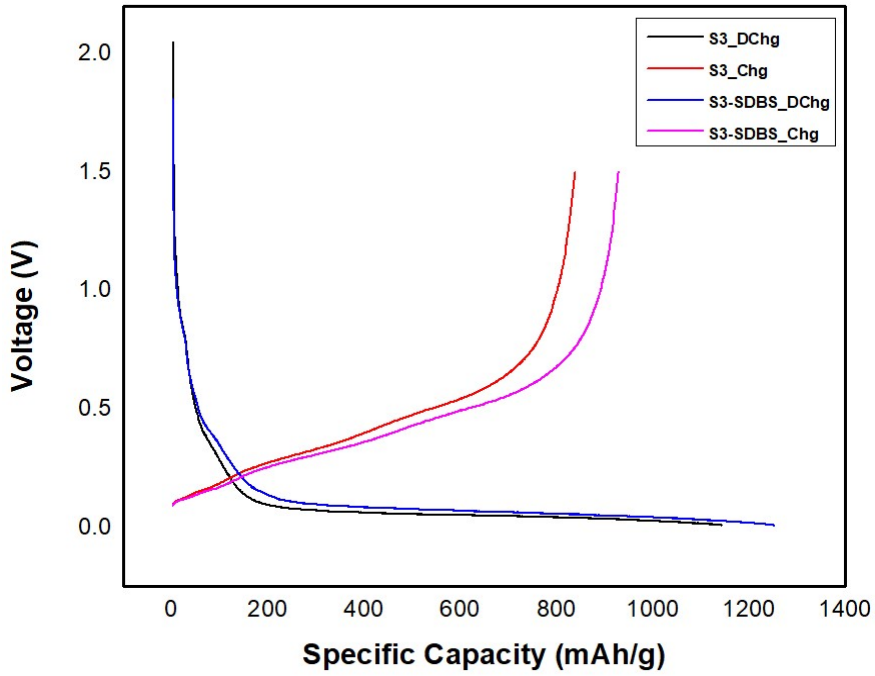

Fig 3.16 Comparison of formation cycles of Silicon (S3) before and after addition of SDBS

However, despite the addition of surfactant agents like SDBS the performance enhancement was not drastic. Silicon (S3) with SDBS showed only a 10% enhancement in capacity. It had a delithiation capacity of 930 mAh/g with an only Si utilization of 58%. Further addition of SDBS (2-5%) deteriorated the capacity and produced lesser coulombic efficiency and hence the amount of SDBS was limited to 1% of the total electrode composition.

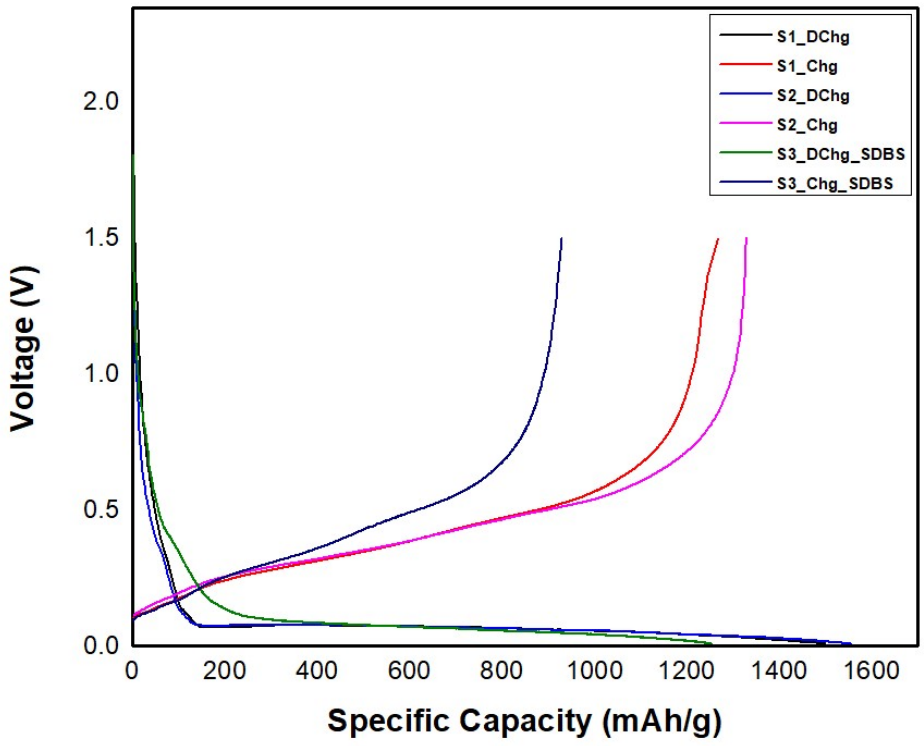

Fig 3.17 Comparison of formation cycles of different Silicon (S1, S2) and S3 with SDBS

Fig 3.17 shows that despite the addition of SDBS surfactant to improve the dispersion of active materials, the capacity of the system containing S3 (20nm) is lower than S1 (50nm) and S2 (40nm). The coulombic efficiency of S3 is 74% when compared to that of S1 and S3 particles having close to 85%. The significant reduction in coulombic efficiency of smaller sized particles is attributed to their size. Since smaller size particles have a larger surface area, there are additional reaction sites that thereby reduces the initial coulombic efficiencies. Table 3.1 shows the lithiation, delithiation capacities, the initial coulombic efficiency, and the silicon utilization percentages of the silicon used.

Table 3.1 Comparison of formation cycles of different Si systems used in this chapter

Property	Silicon used and their respective sizes			
	S1 (50nm)	**S2 (40nm)**	**S3 (20nm)**	**S3 (20nm) with SDBS**
Discharge Capacity (mAh/g)	1500	1554	1142	1251
Charge Capacity (mAh/g)	1266	1328	841	928
Initial coulombic efficiency (ICE) (%)	85	84	74	73
Si utilization (%)	70	74	53	58

Additional structural examination (cross-sectional imaging- Fig 3,10), revealed that S3 silicon had a poor packing density when compared to that of other silicon used in the system. The poor packing density of the electrode could potentially be the reason for the inferior performance of the S3 electrode. Improper packing of the electrode leads to loss of electrical contact between the active materials that cause a significant reduction in the utilization of Si. Hence, additional modifications like calendaring and coating additional graphene sheath layers were done to enhance the performance of the electrode (Fig 3.13). Calendaring alleviates the aforementioned issues related to packing and renders better interconnectivity of the active materials within the electrode system, whereas coating the electrode with an additional sheath layer of graphene ensures that a stable SEI layer between the electrolyte and graphene. The electrodes were electrochemically tested under the same conditions with the current electrode modifications.

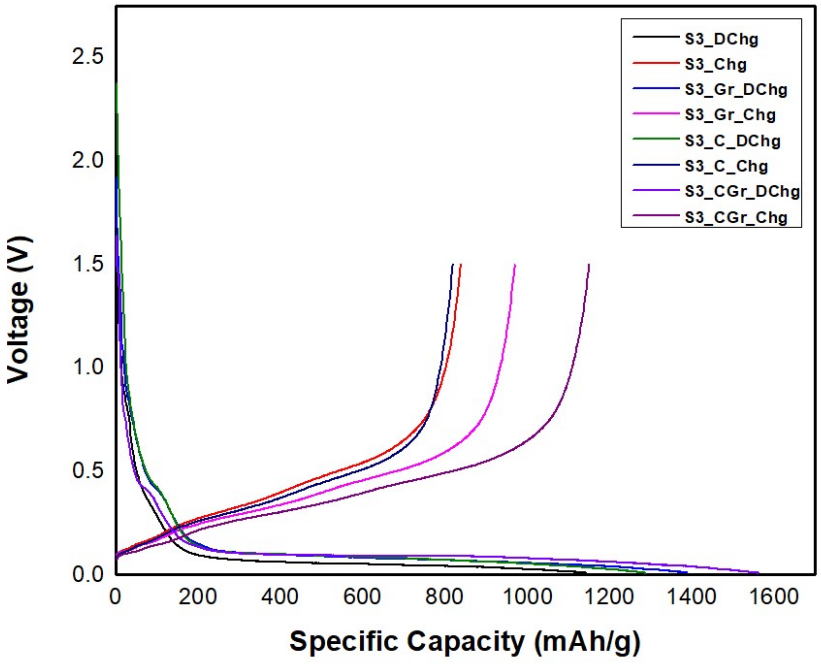

Fig 3.18 Comparison of formation cycles of Silicon (S3) with modifications

(Comp – Compression, Gr- Graphene coating, CGr – Compression & Graphene coating)

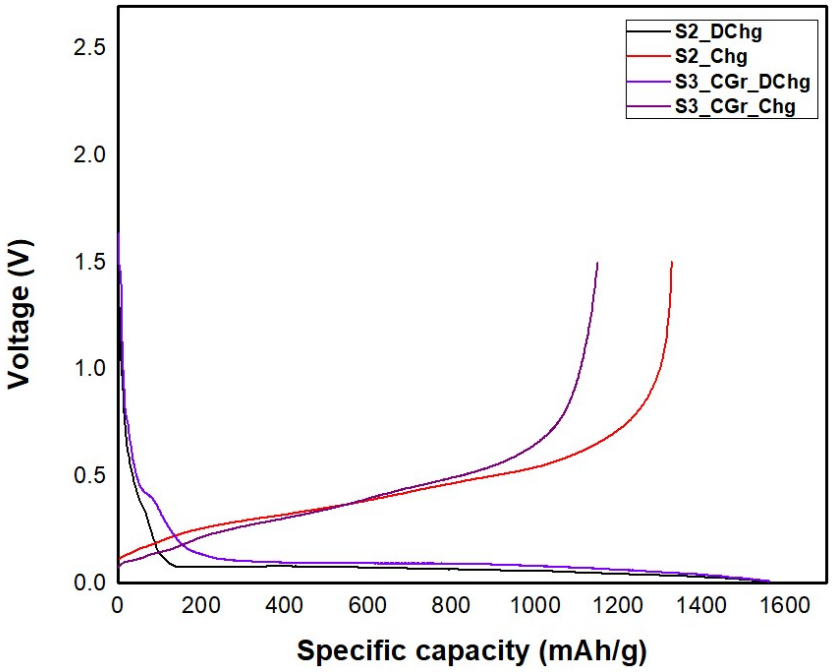

Fig 3.19 Comparison of formation cycles of S2 and S3 with modifications

Fig 3.18 shows the comparison of formation cycles of electrodes with electrode modifications. As discussed earlier, the combined effect of calendaring and graphene coating outperforms the other modifications. The disc with no electrode modifications shows the least coulombic efficiency, due to its highly open structure. The electrolyte decomposition starts the leading to more Li+ waste for irreversible SEI formation (Fig 3.17). It also has the lowest specific capacity, which shows the lack of inner conductive pathways for Li ions transport due to the presence of loose structure (Fig 3.11) The second largest irreversible capacity loss is found in the system containing the anode that goes through compression but does not have a graphene protective layer. The coulombic efficiency has vastly improved in the case of additional graphene coating, showing the presence of additional graphene layer prevents the contact of Si and electrolyte thereby avoiding the formation of SEI (Si-electrolyte) that inhibits the coulombic efficiency. The system containing a combination of calendaring and graphene coating not only shows a densely packed geometry but also shows better coulombic efficiency due to the presence of graphene layers on top that reduces inner resistance effectively. The electrochemical reactions between graphene and electrolyte prevents those between silicon nanoparticles and electrolytes, preserving the reversible capacity. Fig 3.19 shows that the discharge capacity of S3_CGr is the same as that of S1 providing a similar amount of Si utilization. S3 silicon achieves a discharge capacity of 1570 mAh/g with a-Si utilization of 75%. However, the first cycle coulombic efficiency of S3 is only 75% compared to the 84% observed in S2. This is largely attributed to the size of the silicon. S3 silicon has a larger surface area due to its smaller size thereby having additional reaction sites. These additional reaction sites cause decrease in coulombic efficiencies. This continues to be a major hindrance for the application of smaller sized silicon particles. Table 3.2 shows the comparison data of capacities and efficiencies of S3 silicon with the modifications.

Table 3.2 Comparison of formation cycles of S2 and S3 with modifications

Property	Silicon used and their respective sizes			
	S2	S3_Gr	S3_Comp	S3_CGr
Discharge Capacity (mAh/g)	1554	1388	1286	1570
Charge Capacity (mAh/g)	1328	992	823	1130
Initial coulombic efficiency (ICE) (%)	84	75	64	77
Si utilization (%)	74	70	64	75

The electrodes fabricated in electrospraying were assembled in a 2032 coin-type half cells configuration and were galvanostatically charged and discharged for multiple cycles. Each of these cells was lithiated to a voltage of 1.5V and de-lithiated to a voltage of 0.01V and were made to undergo 5 formation cycles at 0.1C and then were allowed to undergo cycling for 200 cycles post-formation.

Cycle retention profiles (Fig 3.20) illustrate systems' ability to maintain geometric integrity and provide Li ion conductive pathways in long-term charge/discharge process Fig 3.20 shows the comparison of cycle-life characteristics of S2 and S3 silicon with modifications. S3 with modifications outperforms S2 and has a retention capacity of nearly 71% over 100 cycles, whereas S2 silicon only has a retention capacity of 61%. The smaller size of silicon along with additional electrode modifications render a much stable electrochemical performance over a long time when compared to that of S2 silicon.

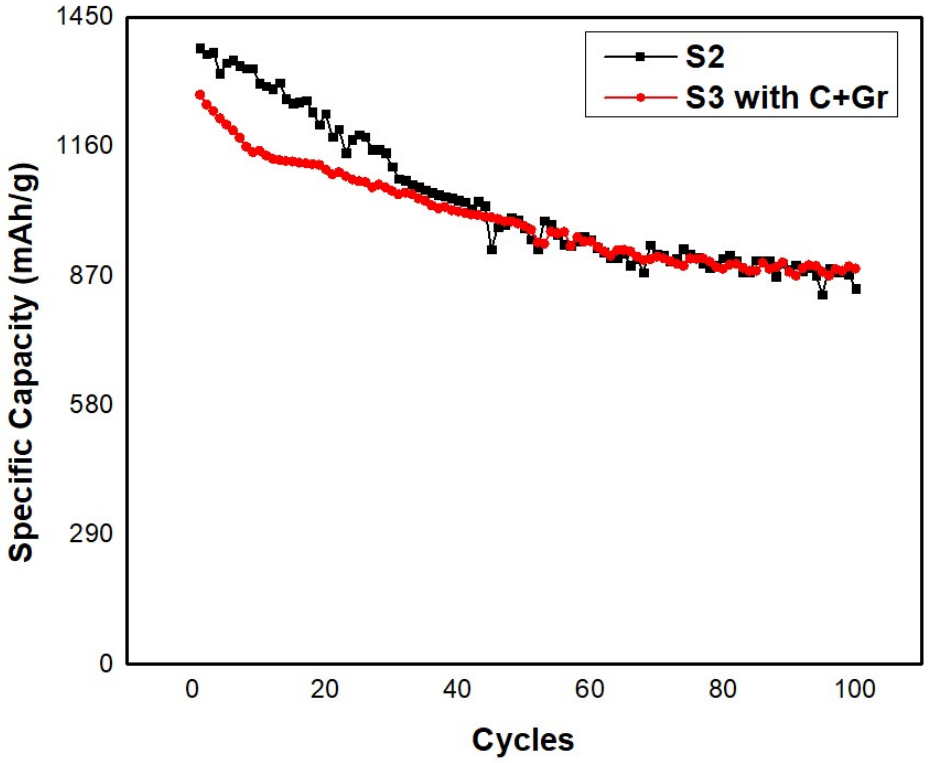

Fig 3.20 Comparison of cycling characteristics of S2 and S3 with modifications exhibiting better cycle retention characteristics in S3

Improvements in the electrochemical performance's post modifications have been confirmed through electrochemical impedance spectroscopy (Fig 3.21and 3.22) (EIS). EIS was performed on cells with modification (calendaring, graphene coating and a combination of both). Semicircle in the EIS curve depicts the charge transfer resistance and the sloped line is a measurement of Li ion diffusivity. Calendaring reduces the resistance by nearly 30% without hindering the Li ion diffusivity. By calendaring, more inner conductive pathways are created due to the reconnection between the active materials (Si and graphene). The addition of a graphene layer (0.06 mg cm^{-2}) also reduces the charge transfer resistance owing to graphene's superior conductivity. The electrode with the combination of both calendaring and graphene coating renders a better interconnectivity and also improves the system conductivity and thereby has the least resistance.

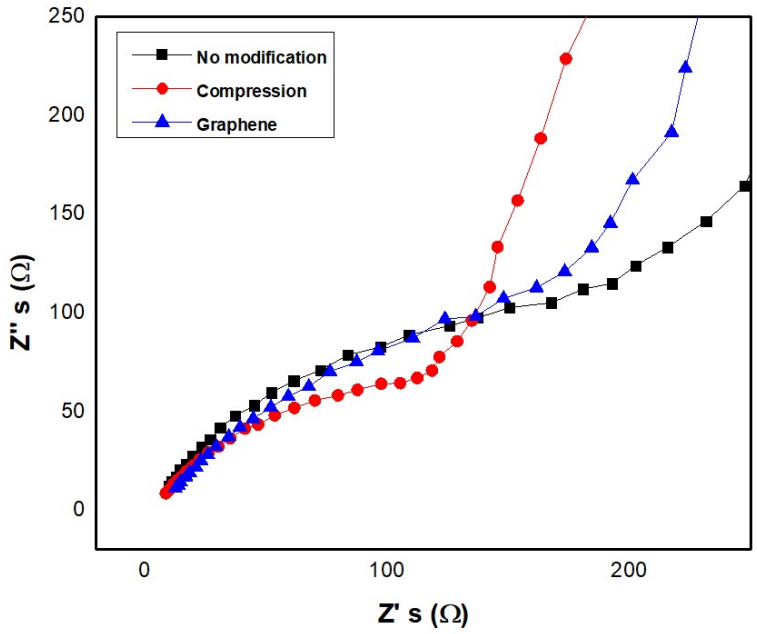

Fig 3.21 Nyquist plot comparing electrodes with no modification and modifications like calendaring and graphene coating

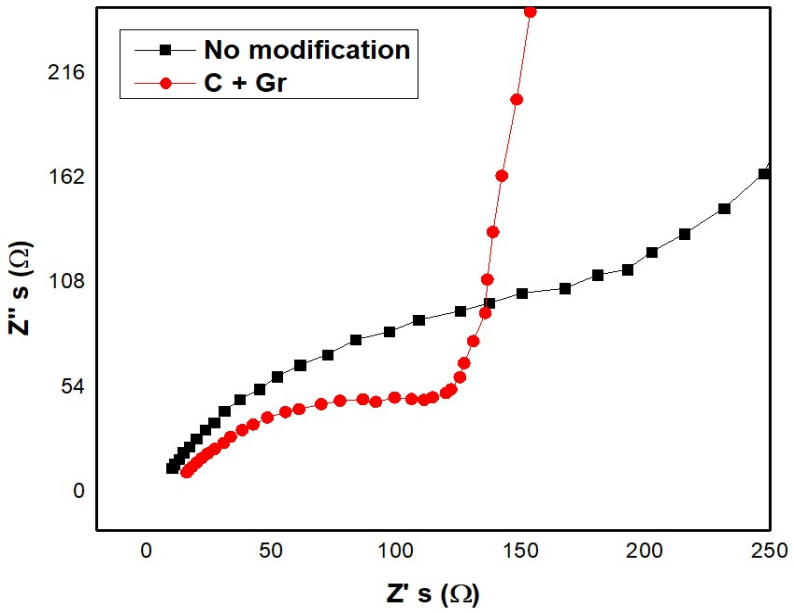

Fig 3.22 Nyquist plot comparing electrodes with no modification and combined modification of calendaring and graphene coating

To further distinguish the effect of additional modifications, rate capability tests were conducted on the systems with and without modifications to see their performance at higher charge rates. Fig 3.23 shows the rate capability comparison with different electrode modifications. All additional modifications perform much better than the system without modifications. Calendaring (compression) enables better contact between active materials and thereby improving the interconnectivity of the system. Graphene coating improves the overall conductivity of the system and thereby aiding quicker transport of Li ions. The combination of compression and graphene together improves both system interconnectivity and also enhance the overall conductivity of the system thereby facilitating quicker Li ion transport. All these properties render the electrode with the combination of compression and graphene, a significantly higher capacity compared to the rest.

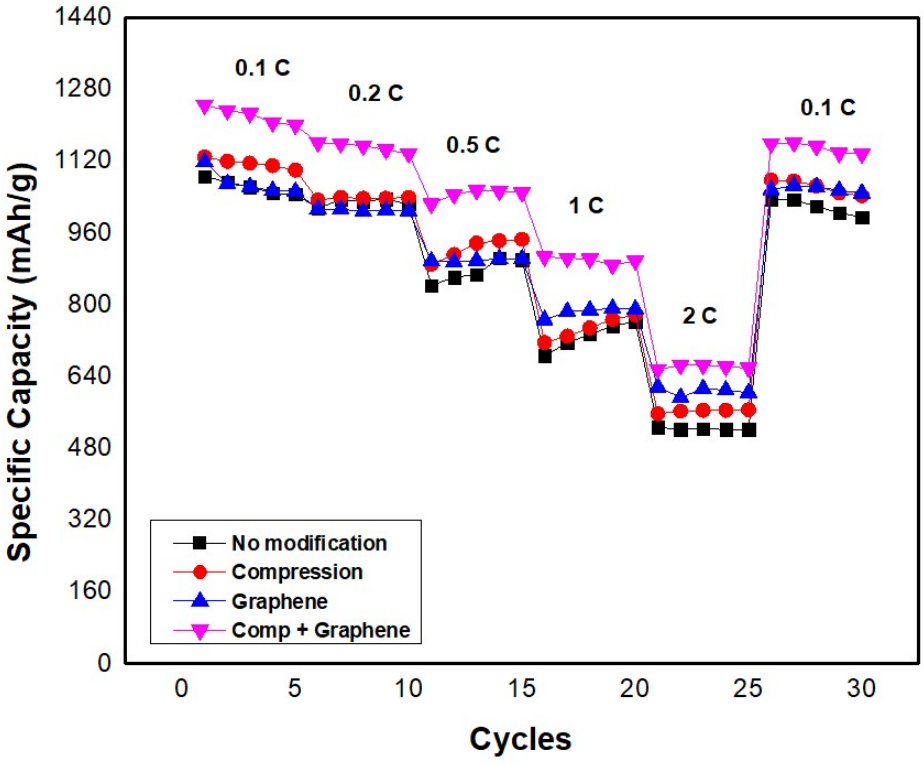

Fig 3.23 Rate capability comparison with different electrode modifications

Four point probe conductivity measurements confirm our earlier results. Fig 3.24 shows that the system containing a modification of compression clearly has lesser resistivity compared to that of the one with no modification. This is owing to the fact that system interconnectivity is improved in the compressed electrode. Graphene coating outperforms both the previous electrodes mainly owing to the significant conductivity of graphene. The disk with both the modifications has the least resistivity, thus coherent with previous results of rate capability and EIS. Hence, electrodes containing additional modifications like calendaring and additional sheath layer of graphene perform better overall when compared to electrodes without modifications (Fig 3.14).

Conclusion:

In summary, this study presents a facile scalable fabrication method of silicon-graphene-PAA complex anodes via air-controlled electrospraying. A thin coating of the electrode material comprising of SiNPs/PAA/Graphene was obtained by directly spraying the active material slurry with the application of high air pressure and voltage. Different sizes of silicon (S1- 50m, S2- 40nm, S3- 20nm) were characterized and their electrochemical performance were analyzed. Electrochemical comparison showed that electrodes containing S3 silicon showed lower capacity (low utilization of Si – 53%) owing to its dispersion issues and poor electrode structure (poor packing). Additional electrode modifications like calendaring and graphene coating were performed to enhance their electrochemical performance (by offering more activation sites and conductive pathways). Calendaring and graphene coating on its own delivers significantly higher specific capacity and provide better capacity retention characteristics than that of electrode containing no modifications. However, the combination of compression and graphene layer with loading of 0.06 mg cm^{-2} delivers the best result. The combination of electrode modification along with the smaller size of silicon renders a better capacity retention over a long time. We engineer silicon/graphene/PAA electrode with additional modifications and prove that with the enhanced structure post modifications, a much better electrochemical performance can be achieved. In conclusion, this study is achieved with simple and non-toxic process and suitable for scaling up in future. Smaller sized silicon (~20nm) with appropriate modifications (calendaring and graphene coating) has a much more stable performance and supports the development of next-generation, high-capacity, long-cycle and portable Li-ion battery.

References:

[1] T. Kim, W. Song, D. Y. Son, L. K. Ono, and Y. Qi, "Lithium-ion batteries: outlook on present, future, and hybridized technologies," J. Mater. Chem. A, vol. 7, no. 7, pp. 2942–2964, 2019, doi: 10.1039/C8TA10513H.

[2] C. P. Opsel, B. Graeme, and P. G. Blake, "Silicon based high performance Anode Materials for Next Generation Li-Ion Batteries," pp. 1–13, [Online]. Available: http://fse.studenttheses.ub.rug.nl/17294/1/mNANO_2018_PopselC.pdf.

[3] N. Yuca and Ü. Çolak, "A facile and functional process to enhance electrochemical performance of silicon anode in lithium ion batteries," Electrochim. Acta, vol. 222, pp. 1538–1544, 2016, doi: 10.1016/j.electacta.2016.11.136.

[4] J. Y. Li, Q. Xu, G. Li, Y. X. Yin, L. J. Wan, and Y. G. Guo, "Research progress regarding Si-based anode materials towards practical application in high energy density Li-ion batteries," Mater. Chem. Front., vol. 1, no. 9, pp. 1691–1708, 2017, doi: 10.1039/c6qm00302h.

[5] V. Etacheri, R. Marom, R. Elazari, G. Salitra, and D. Aurbach, "Challenges in the development of advanced Li-ion batteries: A review," Energy Environ. Sci., vol. 4, no. 9, pp. 3243–3262, 2011, doi: 10.1039/c1ee01598b.

[6] M. Ashuri, Q. He, and L. L. Shaw, "Silicon as a potential anode material for Li-ion batteries: Where size, geometry and structure matter," Nanoscale, vol. 8, no. 1, pp. 74–103, 2016, doi: 10.1039/c5nr05116a.

[7] Y. Sun, K. Liu, and Y. Zhu, "Recent Progress in Synthesis and Application of Low-

Dimensional Silicon Based Anode Material for Lithium Ion Battery," J. Nanomater., vol. 2017, 2017, doi: 10.1155/2017/4780905.

[8] X. Zuo, J. Zhu, P. Müller-Buschbaum, and Y. J. Cheng, "Silicon based lithium-ion battery anodes: A chronicle perspective review," Nano Energy, vol. 31, no. October 2016, pp. 113–143, 2017, doi: 10.1016/j.nanoen.2016.11.013.

[9] R. Andersson, G. Hernández, K. Edström, and J. Mindemark, "Micro versus Nano: Impact of Particle Size on the Flow Characteristics of Silicon Anode Slurries," Energy Technol., vol. 2000056, pp. 1–7, 2020, doi: 10.1002/ente.202000056.

[10] B. Liu et al., "Size effect of Si particles on the electrochemical performances of Si/C composite anodes," Chinese Phys. B, vol. 27, no. 8, 2018, doi: 10.1088/1674-1056/27/8/088201.

[11] X. H. Liu, L. Zhong, S. Huang, S. X. Mao, T. Zhu, and J. Y. Huang, "Size-dependent fracture of silicon nanoparticles during lithiation," ACS Nano, vol. 6, no. 2, pp. 1522–1531, 2012, doi: 10.1021/nn204476h.

[12] M. Gu, Y. He, J. Zheng, and C. Wang, "Nanoscale silicon as anode for Li-ion batteries: The fundamentals, promises, and challenges," Nano Energy, vol. 17, pp. 366–383, 2015, doi: 10.1016/j.nanoen.2015.08.025.

[13] W. R. Liu et al., "Effect of electrode structure on performance of Si anode in Li-ion batteries: Si particle size and conductive additive," J. Power Sources, vol. 140, no. 1, pp. 139–144, 2005, doi: 10.1016/j.jpowsour.2004.07.032.

[14] Y. Cen, Q. Qin, R. D. Sisson, and J. Liang, "Effect of Particle Size and Surface Treatment

on Si/Graphene Nanocomposite Lithium-Ion Battery Anodes," Electrochim. Acta, vol. 251, pp. 690–698, 2017, doi: 10.1016/j.electacta.2017.08.139.

[15] L. F. Cui, Y. Yang, C. M. Hsu, and C. Yi, "Carbon-silicon Core-shell nanowires as high capacity electrode for lithium lon batteries," Nano Lett., vol. 9, no. 9, pp. 3370–3374, 2009, doi: 10.1021/nl901670t.

[16] A. M. Chockla et al., "Silicon nanowire fabric as a lithium ion battery electrode material," J. Am. Chem. Soc., vol. 133, no. 51, pp. 20914–20921, 2011, doi: 10.1021/ja208232h.

[17] Z. Wen et al., "Silicon nanotube anode for lithium-ion batteries," Electrochem. commun., vol. 29, pp. 67–70, 2013, doi: 10.1016/j.elecom.2013.01.015.

[18] G. Zhu, Y. Wang, S. Yang, Q. Qu, and H. Zheng, "Correlation between the physical parameters and the electrochemical performance of a silicon anode in lithium-ion batteries," J. Mater., vol. 5, no. 2, pp. 164–175, 2019, doi: 10.1016/j.jmat.2019.03.005.

[19] H. Xiang et al., "Graphene/nanosized silicon composites for lithium battery anodes with improved cycling stability," Carbon N. Y., vol. 49, no. 5, pp. 1787–1796, 2011, doi: 10.1016/j.carbon.2011.01.002.

[20] Y. Qi, G. Wang, S. Li, T. Liu, J. Qiu, and H. Li, "Recent progress of structural designs of silicon for performance-enhanced lithium-ion batteries," Chem. Eng. J., vol. 397, p. 125380, 2020, doi: 10.1016/j.cej.2020.125380.

[21] J. K. Lee, K. B. Smith, C. M. Hayner, and H. H. Kung, "Silicon nanoparticles-graphene paper composites for Li ion battery anodes," Chem. Commun., vol. 46, no. 12, pp. 2025–2027, 2010, doi: 10.1039/b919738a.

[22] J. Luo, X. Zhao, J. Wu, H. D. Jang, H. H. Kung, and J. Huang, "Crumpled graphene-encapsulated Si nanoparticles for lithium ion battery anodes," J. Phys. Chem. Lett., vol. 3, no. 13, pp. 1824–1829, 2012, doi: 10.1021/jz3006892.

[23] F. Li, X. Jiang, J. Zhao, and S. Zhang, "Graphene oxide: A promising nanomaterial for energy and environmental applications," Nano Energy, vol. 16, pp. 488–515, 2015, doi: 10.1016/j.nanoen.2015.07.014.

[24] H. Tang et al., "Porous reduced graphene oxide sheet wrapped silicon composite fabricated by steam etching for lithium-ion battery application," J. Power Sources, vol. 286, pp. 431–437, 2015, doi: 10.1016/j.jpowsour.2015.03.185.

[25] H. Kim, M. Seo, M. H. Park, and J. Cho, "A critical size of silicon nano-anodes for lithium rechargeable batteries," Angew. Chemie - Int. Ed., vol. 49, no. 12, pp. 2146–2149, 2010, doi: 10.1002/anie.200906287.

[26] Z. Karkar, D. Guyomard, L. Roué, and B. Lestriez, "A comparative study of polyacrylic acid (PAA) and carboxymethyl cellulose (CMC) binders for Si-based electrodes," Electrochim. Acta, vol. 258, pp. 453–466, 2017, doi: 10.1016/j.electacta.2017.11.082.

[27] K. L. Browning, R. L. Sacci, M. Doucet, J. F. Browning, J. R. Kim, and G. M. Veith, "The Study of the Binder Poly(acrylic acid) and Its Role in Concomitant Solid-Electrolyte Interphase Formation on Si Anodes," ACS Appl. Mater. Interfaces, vol. 12, no. 8, pp. 10018–10030, 2020, doi: 10.1021/acsami.9b22382.

[28] A. Jaworek and A. T. Sobczyk, "Electrospraying route to nanotechnology: An overview," J. Electrostat., vol. 66, no. 3–4, pp. 197–219, 2008, doi: 10.1016/j.elstat.2007.10.001.

CHAPTER 4: FUTURE WORK

Chapter 2:

In chapter 2, we discussed about the potential of Poly (acrylic) acid (PAA) binders and its electrochemical performance over large number of cycles. Carboxymethyl cellulose (CMC) just like PAA possess carboxylic functional groups that enable then to strongly bond with the native hydroxyl functional groups present on the Silicon particle surface. Secondly, CMC does not swell in electrolyte and is also mechanically robust. CMC is a linear derivative of cellulose with commonly 0.5 – 1.5 monomeric units of carboxymethyl groups ($-CH_2COO^-$). However, CMC is a rigid polymer and is not elastic enough to contain the volume expansion of Si. In recent years, researchers have witnessed an increasing interest towards designing high strength polymers with cross-linking architecture in various fields ranging from drug delivery to batteries. This is due to the fascinating mechanical properties that allow these polymers to be stretched more than 5-10 times their original volume. This is in stark contrast which we observed in PAA binders and could act as a promising multifunctional binder for constructing Si anodes. Styrene butadiene (SBR) is a binder that possess a high flexibility, stronger binding force and is highly elastic. All these properties make SBR a very good combination with to CMC. Dynamical mechanical analysis (DMA) was done as a comparison to visualize how much stress these binders can endure. Results (Fig 4.1) from DMA show that CMC endures more stress and has higher strain than that of 3 mil PAA (binder molecular weight that had highest strength in Chapter 2). CMC-SBR system on the other hand exhibits low stress but are very elastic. The strain % of CMC-SBR is nearly 50 times that of other binders and this elasticity of CMC-SBR binder could be very useful in containing the volume expansion in Si based anodes.

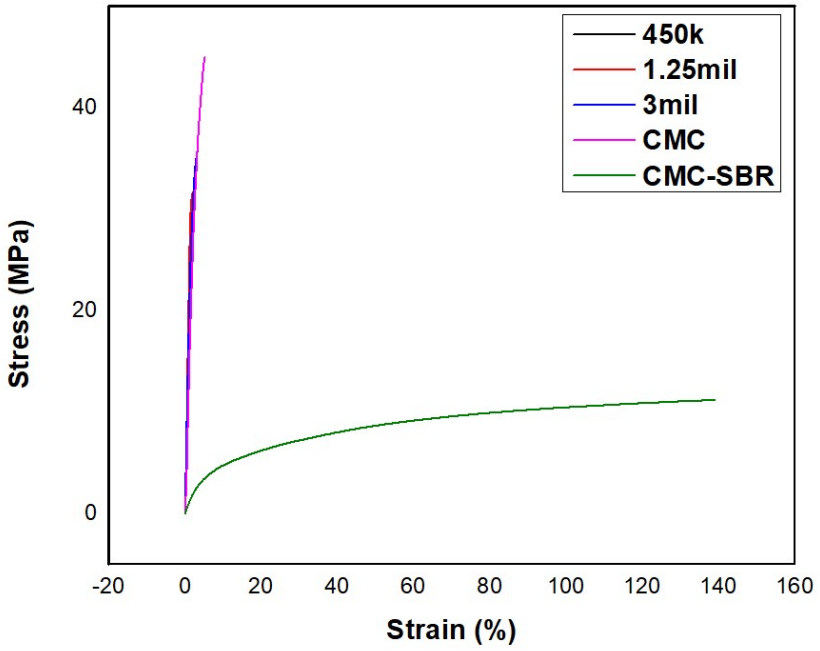

Fig 4.1 DMA comparison of binders showing the extremely high strain of CMC-SBR

Table 4.1 Dynamic mechanical analysis (DMA) results for various binder

Dynamic mechanical analysis (DMA) results for various binder		
Binders	**Stress (MPa)**	**Strain (%)**
450k	26	1.89
1.25 mil	32	2.03
3 mil	36	3.43
CMC	44	5.17
CMC-SBR	14	139

Therefore, CMC-SBR crosslinked binder has a significant potential to mitigate issues related to volume expansion in silicon based anodes for lithium ion batteries.

Chapter 3:

In chapter 3, issues related to the size of silicon were addressed. It was seen that S3 Silicon which had the smallest size (~20nm) with electrode modifications had a much better retention capacity than that of S2 silicon. The smaller size of S3 silicon and the additional electrode modifications rendered good capacity as well as rate capability. Researchers have looked at other properties of silicon like its shape and morphology (solid core-shell, a yolk-shell, hollow core-shell, nanotubes, nanowires etc.). Surface oxidation of Si particles readily occurs during their preparation, transportation, and storage. The role of oxygen element in the electrochemical properties of Si still remains unclear and hence would be an interesting property to study. Si particle size and oxygen content; surface conditions, morphology and major electrochemical properties are key physical parameters that have a significant effect on electrochemical performance is of great significance for the selection and optimization of Si materials in the LIB industry. Therefore, it would be a good follow up study to understand the effects of these key physical properties.